



**TRANSITION METAL DICHALCOGENIDE
MONOLAYERS FOR GAS SENSOR
APPLICATIONS**

Master of Science Thesis

Gonca USLU ÖZKÜÇÜK

Eskişehir 2019

**TRANSITION METAL DICHALCOGENIDE MONOLAYERS FOR GAS SENSOR
APPLICATIONS**

Gonca USLU ÖZKÜÇÜK

MASTER OF SCIENCE THESIS

Institute of Graduate Programs

Department of Electrical and Electronics Engineering

Supervisor: Assoc. Prof. Dr. Nihan KOSKU PERKGÖZ

Eskisehir

Eskisehir Technical University

Institute of Graduate Programs

June 2019

FINAL APPROVAL FOR THESIS

This thesis titled “Transition Metal Dichalcogenide Monolayers for Gas Sensor Applications” has been prepared and submitted by GONCA USLU ÖZKÜÇÜK in partial fulfillment of the requirements in “Eskişehir Technical University Directive on Graduate Education and Examination” for the Degree of Master of Science in Electrical and Electronics Engineering Department has been examined and approved on 19/06/2019.

<u>Committee Members</u>	<u>Title, Name and Surname</u>	<u>Signature</u>
Member (Supervisor)	: Assoc. Prof. Dr. Nihan KOSKU PERKGÖZ
Member	: Assoc. Prof. Dr. Feridun AY
Member	: Assoc. Prof. Dr. Evren MUTLUGÜN

Prof. Dr. Murat TANIŞLI

Director of Institute of Graduate Programs

ABSTRACT

TRANSITION METAL DICHALCOGENIDE MONOLAYERS FOR GAS SENSOR APPLICATIONS

Gonca USLU ÖZKÜÇÜK

Department of Electrical and Electronics Engineering

Eskişehir Technical University, Institute of Graduate Programs, June 2019

Supervisor: Assoc. Prof. Dr. Nihan KOSKU PERKÖZ

Recently, transition metal dichalcogenide materials (TMDC) have drawn interest because of their layer dependent electronic and chemical features to use in various device applications. 2D TMDC materials have large interaction capacity with gases as a result of their large surface areas. Purpose of using gas sensors is to identify and quantify features of detected gases in an environment. This type of devices is essential in many different areas for example, in emission control, military and medical diagnosis. These two dimensional TMDC materials are showing properties of semiconductor with a layer-dependent bandgap. In transistor, semiconductor TMDC materials can be used as a channel material and this type of FET devices can be used as gas sensing devices. For using in gas sensor applications, it is necessary to produce large scale monolayer TMDC flake growth. In this thesis, by using a piece of glass as catalytic in CVD experiments monolayer and large scale growth of TMDC materials was carried out. The growth TMDC flakes were analyzed by optical microscopy, Raman and photoluminescence spectroscopy and atomic force microscopy. The growth was realized on the Si/SiO₂ substrate, so FET device was able to produce without transferring of the flakes.

Keywords: CVD, FET, MoS₂, MoSe₂, WS₂

ÖZET

GAZ SENSÖRÜ UYGULAMALARI İÇİN TEK KATMANLI GEÇİŞ METAL DİKALKOJENİTLERİ

Gonca USLU ÖZKÜÇÜK

Elektrik-Elektronik Mühendisliği Anabilim Dalı

Eskişehir Teknik Üniversitesi, Lisansüstü Eğitim Enstitüsü, Haziran 2019

Danışman: Doç. Dr. Nihan KOSKU PERKGÖZ

Son zamanlarda, geçiş metali dikalkojenit (GMK) yapıları kalınlığa bağlı elektronik ve kimyasal özelliklerinden dolayı çeşitli cihaz uygulamaları ile dikkat çekiyor. 2B GMK malzemeleri, büyük bir yüzey/hacim oranları sayesinde gaz molekülleri ile yüksek oranda etkileşime girebiliyorlar. Bir ortamda tespit edilen gazların özelliklerini tanımlamak ve ölçmek için gaz sensörleri kullanılabilir. Bu tür bir cihaz, askeri ve tıbbi teşhis gibi birçok farklı alanda gereklidir. Bu iki boyutlu TMDC materyalleri, katmana bağlı bir bant aralığına sahip yarı iletken özelliklerini göstermektedir. Transistörlerde yarı iletken GMK malzemeleri kanal malzemesi olarak kullanılabilir ve bu tip FET cihazları gaz algılama cihazları olarak kullanılabilir. Gaz sensörü uygulamalarında kullanmak için, büyük ölçekli, tek katmanlı GMK yaprak yapıları üretmek gereklidir. Bu tez çalışmasında, KBB deneylerinde katalitik olarak bir cam parçası kullanılarak, tek tabakalı ve büyük boyutlu GMK malzemelerinin büyümesi gerçekleştirilmiştir. Büyüyen örnekleri analiz ve karakterize etmek için optik mikroskop, Raman spektroskopisi, PL ölçümü ve AFM kullanılmıştır. Büyüme, Si/SiO₂ alt taşı üzerinde gerçekleşmiştir, böylece FET cihazı, yaprakları transfer etmeden üretebilmiştir.

Anahtar Sözcükler: KBB, FET, MoS₂, MoSe₂, WS₂

ACKNOWLEDGEMENT

Firstly, I would like to thank my advisor, Assoc. Prof. Dr. Nihan KOSKU PERKGÖZ for all her encouragement, guidance and patience.

I would also like to thank to Assoc. Prof. Dr. Feridun AY for all his guidance and advices.

Lastly, I would like to thank to my family for the infinity love and support.

STATEMENT OF COMPLIANCE WITH ETHICAL PRINCIPLES AND RULES

I hereby truthfully declare that this thesis is an original work prepared by me; that I have behaved in accordance with the scientific ethical principles and rules throughout the stages of preparation, data collection, analysis and presentation of my work; that I have cited the sources of all the data and information that could be obtained within the scope of this study, and included these sources in the references section; and that this study has been scanned for plagiarism with “scientific plagiarism detection program” used by Eskişehir Technical University, and that “it does not have any plagiarism” whatsoever. I also declare that, if a case contrary to my declaration is detected in my work at any time, I hereby express my consent to all the ethical and legal consequences that are involved.

.....

Gonca USLU ÖZKÜÇÜK

TABLE OF CONTENTS

	<u>Page</u>
TITLE PAGE.....	i
FINAL APPROVAL FOR THESIS.....	iii
ABSTRACT.....	iv
ÖZET	v
ACKNOWLEDGEMENT.....	vi
STATEMENT OF COMPLIANCE WITH ETHICAL PRINCIPLES AND RULES	vii
TABLE OF CONTENTS	viii
LIST OF FIGURES.....	xi
LIST OF TABLES.....	xiv
LIST OF ABBREVIATIONS AND SYMBOLS	xv
1. INTRODUCTION	1
1.1. Basic Properties of TMDC Materials.....	1
1.2. Synthesis Methods of TMDC Materials.....	2
1.2.1. Top-down methods	3
1.2.1.1. <i>Mechanical exfoliation</i>.....	3
1.2.1.2. <i>Liquid exfoliation</i>	3
1.2.1.3. <i>Electrochemical exfoliation</i>	4
1.2.2. Bottom-up methods.....	4
1.2.2.1. <i>Chemical vapor deposition</i>	4
1.3. TMDC Materials Characterization Techniques	7
1.3.1. Optical microscopy.....	7
1.3.2. Raman spectroscopy.....	8

	<u>Page</u>
1.3.3. Photoluminescence spectroscopy	11
1.3.4. Atomic force microscopy	14
1.4. Electronic and Optoelectronic Applications of 2D TMDC Materials.....	17
1.4.1. Transistors.....	18
1.4.2. Integrated circuits	19
1.4.3. Optoelectronic devices.....	20
1.4.4. Energy applications	20
1.4.5. Sensors	21
1.4.5.1. 2D TMDC based gas sensors.....	21
<i>Gas sensing mechanism</i>	22
<i>Types of gas sensing devices</i>	22
<i>Performance parameters of the gas sensing devices</i>	23
<i>The improvement of the performance of the gas sensors</i>	24
<i>Gas sensing applications of graphene and other layered TMDCs</i>	25
1.5. Motivation of the Thesis	26
1.6. Thesis Structure	27
2. CVD GROWTH AND CHARACTERIZATION OF TMDC MATERIALS ..	28
2.1. MoS ₂	30
2.1.1. Experimental details.....	30
2.1.1.1. Optimization of MoS ₂ growth parameters by CVD	32
2.1.2. Results and discussions for MoS ₂ structures.....	33
2.2. WS ₂	40
2.2.1. Experimental details.....	40
2.2.1.1. Optimization of WS ₂ growth parameters by CVD	42

	<u>Page</u>
2.2.2. Results and discussions for WS ₂ structures	43
2.3. MoSe ₂	50
2.3.1. Experimental details.....	50
2.3.1.1. <i>Optimization of MoSe₂ growth parameters by CVD</i>	51
2.3.2. Results and discussions for MoSe ₂ structures.....	52
3. DEVICE FABRICATION	60
3.1. Mask Design for Gas Sensor Applications	62
3.2. Transfer of the TMDC Flakes	68
3.3. Photolithography	69
3.4. Metal Coating and Lift-off Processes.....	70
3.5. Measurement of FET Devices	71
4. CONCLUSIONS AND SUGGESTIONS FOR FUTURE WORK.....	74
4.1. Conclusions.....	74
4.2. Suggestions for Future Work.....	75
REFERENCES.....	77
CURRICULUM VITAE	

LIST OF FIGURES

	<u>Page</u>
Figure 1.1 Schematic drawing of a general CVD system.....	6
Figure 1.2 (a) Bright field image (b) dark field image of MoSe ₂ flake.....	8
Figure 1.3 Energy transition schema for Rayleigh and Raman scattering.....	9
Figure 1.4 Schematic drawing of Raman spectroscopy.....	10
Figure 1.5 Raman spectroscopy analysis of monolayer WS ₂ structure.....	11
Figure 1.6 PL spectrum results of monolayer MoS ₂ structure.....	13
Figure 1.7 Schematic drawing of AFM.....	15
Figure 1.8 (a) AFM image of MoS ₂ (b) height profile of green line on(a).....	17
Figure 1.9 The schematic representation of the applications of 2D TMDC materials.....	18
Figure 1.10 Illustration of (a) top gated (b) back gated TMDC based FET.....	19
Figure 2.1 Schematic illustration of MoS ₂ growth experiment by CVD.....	31
Figure 2.2 OM images of MoS ₂ with Glass-1 (a) as bright (b) dark Field.....	33
Figure 2.3 OM images of MoS ₂ with Glass-2 (a) as bright (b) dark field.....	34
Figure 2.4 Raman spectra of MoS ₂ with Glass-1.....	35
Figure 2.5 Raman spectra of MoS ₂ with Glass-2.....	36
Figure 2.6 PL spectra of MoS ₂ with Glass-1.....	37
Figure 2.7 PL spectra of MoS ₂ with Glass-2.....	38

Figure 2.8 (a) AFM image of MoS₂ by Glass-1 (b)height profile of green line on(a)39

Figure 2.9 (a) AFM image of MoS₂ by Glass-2 (b)height profile of green line on(a)39

Figure 2.10 Schematic illustration of WS₂ growth experiment by CVD.....40

Figure 2.11 OM images of WS₂ with Glass-1 (a)as bright and (b)dark Field.....43

Figure 2.12 OM images of WS₂ with Glass-2 (a)as bright and (b)dark field.....44

Figure 2.13 Raman spectra of WS₂ with Glass-145

Figure 2.14 Raman spectra of WS₂ with Glass-246

Figure 2.15 PL spectra of WS₂ with Glass-147

Figure 2.16 PL spectra of WS₂ with Glass-248

Figure 2.17 (a)AFM image of WS₂ by Glass-1 (b)height profile of green line on(a)49

Figure 2.18 (a)AFM image of WS₂ by Glass-2 (b)height profile of green line on(a)49

Figure 2.19 Schematic illustration of MoSe₂ growth experiment by CVD50

Figure 2.20 OM images of MoSe₂ with Glass-1 (a)as bright and (b)dark field53

Figure 2.21 OM images of MoSe₂ with Glass-2 (a)as bright and (b)dark field53

Figure 2.22 Raman spectra of MoSe₂ with Glass-154

Figure 2.23 Raman spectra of MoSe₂ with Glass-255

Figure 2.24 PL spectra of MoSe₂ with Glass-1.....56

Figure 2.25 PL spectra of MoSe₂ with Glass-2.....57

Figure 2.26 (a)AFM image of MoSe₂ by Glass-1 (b)height profile of green line on(a)58

	<u>Page</u>
Figure 2.27 (a) AFM image of MoSe ₂ by Glass-2 (b) height profile of green line on(a)	58
Figure 3.1 Flow chart of the FET device fabrication processes	61
Figure 3.2 IDE patterned (a) MoS ₂ (b) MoS ₂ (c) WS ₂ based devices for gas detection	63
Figure 3.3 Overall view of the designed gas sensor device mask	64
Figure 3.4 Designed IDE patterns of the metal mask for gas sensor applications.....	66
Figure 3.5 Designed etching layout patterns.....	67
Figure 3.6 Alignment marks of the (a) metal (b) etching (c) resolution test patterns	68
Figure 3.7 Schematic view of the mechanism of positive photo resist.....	70
Figure 3.8 Schematic view of the metal coating and lift-off process	71
Figure 3.9 (a) The cross-sectional view (b) the optical image of the device.....	72
Figure 3.10 Transfer Curve of the MoSe ₂ with Glass-2 Based FET Device	73

LIST OF TABLES

	<u>Page</u>
Table 1.1 Electronic properties of various TMDC materials	2
Table 1.2 Gas sensing applications of graphene and TMDC materials	25
Table 2.1 EDS analysis results of the Glass-1 and Glass-2	29
Table 2.2 MoS ₂ growth parameters.....	31
Table 2.3 Experimental parameters for MoS ₂ growth	32
Table 2.4 WS ₂ growth parameters	41
Table 2.5 Experimental parameters for WS ₂ Growth	42
Table 2.6 MoSe ₂ growth parameters	51
Table 2.7 Experimental parameters for MoSe ₂ growth.....	52
Table 3.1 Dimensions of IDE patterns used in the design	65

LIST OF ABBREVIATIONS AND SYMBOLS

2D	: Two dimensional
AFM	: Atomic force microscopy
Al ₂ O ₃	: Aluminum oxide
ALD	: Atomic layer deposition
APCVD	: Atmosphere pressure chemical vapor deposition
Ar	: Argon
CBM	: Conduction band minimum
CCD	: Charged couple device
Cl ₂	: Chlorine gas
CO	: Carbon monoxide
CVD	: Chemical vapor deposition
DC	: Direct current
DF	: Dark field
DFT	: Density functional theory
DI water	: Deionized water
DNA	: Deoxyribonucleic Acid
EBPVD	: Electron-beam physical vapor deposition
EDS	: Energy Dispersive X-ray Spectrometry
eV	: Electro-volts
FET	: Field effect transistors
FWHM	: Full width half maximum

H ₂	: Hydrogen
H ₂ O	: Water
hBN	: Hexagonal boron nitride
HCN	: Hydrogen cyanide
HfO ₂	: Hafnium dioxide
HPCVD	: Hybrid physical chemical vapor deposition
IDE	: Interdigitated electrode
LED	: Light emitting diode
LPCVD	: Low-pressure chemical vapor deposition
MFC	: Mass flow controllers
MOCVD	: Metal organic chemical vapor deposition
MoO ₃	: Molybdenum trioxide
MoS ₂	: Molybdenum disulfide
MoSe ₂	: Molybdenum diselenide
N ₂	: Nitrogen
NA	: Numerical aperture
Na ₂ SO ₄	: Sodium sulfate
NaCl	: Sodium chloride
NH ₃	: Ammonia
nm	: Nanometer
NO	: Nitric oxide
NO ₂	: Nitrogen dioxide

O ₂	: Oxygen gas
OM	: Optical microscopy
PECVD	: Plasma-enhanced chemical vapor deposition
PMMA	: Poly (methyl methacrylate)
PL	: Photoluminescence
ppb	: Parts-per-billion
ppm	: Parts-per-million
Pt	: Platinum
rpm	: Revolutions per minute
sccm	: Standard cubic centimeters per minute
Si	: Silicon
SiO ₂	: Silicon dioxide
SO ₂	: Sulfur dioxide
TMDC	: Transition metal dichalcogenide materials
UHV-CVD	: Ultra-high vacuum chemical vapor deposition
UV	: Ultraviolet
VBM	: Valance band maximum
vdW	: van der Waals
WO ₃	: Tungsten trioxide
WS ₂	: Tungsten disulfide
WSe ₂	: Tungsten diselenide

1. INTRODUCTION

In this chapter, an overall description about the structure and features of the two dimensional (2D) transition metal dichalcogenide materials (TMDCs) and a general information about 2D TMDCs characterization techniques studied in this thesis is giving. Firstly, basic properties of 2D TMDCs are presented in sections 1.1. Secondly, synthesis methods of 2D TMDCs are explained in sections 1.2. Thirdly, the TMDC materials characterization techniques are presented in section 1.3. After that section, in section 1.4, given information about electronic and optoelectronic applications of 2D TMDC materials. In section 1.5, explained the motivation of the thesis. Finally, section 1.6 gives the structure of this thesis.

1.1. Basic Properties of TMDC Materials

2D TMDCs are nowadays being intensely studied due to having unexampled optical and electronic properties (Q. H. Wang et al., 2012). Graphene was the first obtained as 2D material form graphite by using micro mechanical exfoliation technique in 2004 and thanks to their discoveries they have won the Nobel Prize. Having zero bandgap restricts the usage area of graphene in semiconductor industry. Following the discovery of the graphene, other monolayer or few layer materials have developed. These developed materials are; dielectric hexagonal boron nitride (hBN), transition metal trichalcogenides, transition metal dichalcogenides and transition metal oxides (Geim and Grigorieva, 2013; Rao et al., 2013).

TMDC materials can be formed from bulk to 2D form. These materials have interesting physical and electrical features. TMDCs are having a formula MX_2 , M represent transition metal atom (Mo, W, etc.) and X represent chalcogenide elements (S, Se, etc.). Metal atom layers are sandwiched between two chalcogenide atom layers. TMDCs consist of covalently bonded transition metal and chalcogenide atoms. Between metal atom layers and chalcogenide atom layers there are van der Waals (vdW) forces. Their physical and electronic properties change as TMDC materials change from bulk to two-dimensional form. For example, these semiconductor TMDCs, MoS_2 , MoSe_2 and WS_2 , band gap's change from indirect to direct when their form is changed from bulk to two-dimensional. Due to these

features TMDCs can be used in light-emitters, transistors, photodetectors and electroluminescent devices applications (Kuc et al., 2011). Comparing the properties of bulk and monolayer forms of TMDC materials, monolayer semiconductors show more advantageous. Monolayer TMDCs surfaces have smaller roughness, dangling bonds and defects than bulk TMDC materials. Monolayer TMDC materials have high surface and no volume but the bulk form of the TMDCs does not have high surface to volume ratio. Considering all these facts, monolayer TMDCs are potential candidate for sensor application (Xi et al., 2014). The various electronic properties of TMDC materials are listed in Table 1.2 (Roldán et al., 2014; Sorkin et al., 2014; Tian et al., 2016; Xu et al., 2016).

Table 1.1 *Electronic properties of various TMDC materials*

Material	Electronic Property	Bandgap
MoS ₂	Semiconductor	Monolayer:1.8 eV Bulk:1.2 eV
MoSe ₂	Semiconductor	Monolayer:1.5 eV Bulk:1.1 eV
WS ₂	Semiconductor	Monolayer:1.9-2.1 eV Bulk:1.4 eV
WSe ₂	Semiconductor	Monolayer:1.7 eV Bulk:1.2 eV

1.2. Synthesis Methods of TMDC Materials

2D TMDC materials can be produced by using two types of methods: top-down methods where the few layer or monolayer form of materials exfoliated from bulk form of the materials and bottom-up method. The main objective is obtaining 2D TMDCs with large area, homogenous structure and clean surfaces. The following part describes these methods.

1.3. Top-down methods

Top-down methods involve separation in micromechanical size domain. Mechanical exfoliation, liquid exfoliation and electrochemical exfoliation are types of the top down method. After producing Graphene by mechanical exfoliation method (K. S. Novoselov et al., 2004), this method has been applied to other inorganic material (K. Novoselov et al., 2005; Braga et al., 2012; Hui Fang et al., 2012).

1.3.1.1. Mechanical exfoliation

Up to now, mechanical exfoliation has been thought as the most efficient method for producing homogeneous 2D materials. In this method firstly, thin TMDC materials are cleave from the bulk materials by using a sticky tape. Secondly, that separated TMDCs on the sticky tape are putted on a target substrate and rubbed to stick them. Finally, the sticky tape is removed and monolayer or multilayer TMDC materials are left on the substrate. By using this method flakes with high homogeneity can be produced, but drawbacks of this method is it is not possible to produce scalable flakes and it is not possible to control the thickness and size of the produced flakes.

1.3.1.2. Liquid exfoliation

Liquid exfoliation by direct ultra-sonication method, was used to produce graphene and proven its success, after that the method was used to fabricate single layer or multilayer of TMDC materials (Coleman et al., 2011; Nicolosi et al., 2013). In this process various kinds of organic solvents are used as dispersing solvents, with respect to bulk layered materials to produce 2D micro flakes (O'Neill et al., 2012; Srivastava et al., 2014). The sonication energy as external power to generate 2D materials should be carefully adjusted to an appropriate level to exfoliate the bulk layered materials to a monolayer or few layered materials. Coleman et al. reported that the sonication power and timing are the key factors to control the quality of the 2D materials obtained by liquid exfoliation (Coleman et al., 2011). Liquid-phase exfoliation has some drawbacks. The flake sizes of the production TMDCs are limited (Brent et al., 2017).

1.3.1.3. Electrochemical exfoliation

Electrochemical exfoliation is another method to obtain 2D monolayer TMDC flakes (N. Liu et al., 2014). Before starting the process bulk MoS₂ crystals are held by Platinum (Pt) clamps and dipped into sodium sulfate (Na₂SO₄) solution. A direct current (DC) voltage applied between bulk MoS₂ crystals and Pt wire. As a result, MoS₂ flakes are separated from the bulk crystals and dispersed in solution. The problem with this method is the bulk MoS₂ is oxidizing during electrochemical exfoliation process so MoS₂ Nano sheets may effect from this oxidation.

1.4. Bottom-up methods

Bottom-up methods involve CVD method. By using CVD graphene and other layered materials can be produced (Losurdo et al., 2011).

1.4.1.1. Chemical vapor deposition

For the large scaled manufacturing of various devices, large area, homogeneous 2D materials have significant role. To produce large area and monolayer TMDC materials, methods are developing. Chemical vapor deposition (CVD) is an effective chemical reaction advance to grow flakes having large-area and thin films (Bilgin et al., 2015). Fabrication of graphene having large area sheets production by CVD was carried out previously (Li et al., 2009), and for other layered materials such as TMDC materials CVD is another production technique which is commonly thought as an efficient chemical process to produce large area thin films and flakes. There are various types of CVD, such as ultra-high vacuum chemical vapor deposition (UHV-CVD) (Kuzminykh et al., 2013), metal organic chemical vapor deposition (MOCVD) (S. Lee et al., 2008), plasma-enhanced chemical vapor deposition (PECVD) (Meyyappan et al., 2003), hybrid physical chemical vapor deposition (HPCVD) (Seong et al., 2007), etc. The types of CVD systems is depending on the types of reactants, the range of the pressure or the use of equipment with an enhanced activation system. CVD

method has advantageous in some subjects, for example, the growth reaction can selectively occur in certain regions of the substrate, the CVD method provides the possibility of covering different types of surfaces or vertical side walls of the substrate with high coverage and CVD usually does not require high vacuum system.

In CVD system there are different methods used to produce TMDC from vapor phase.

- As metal and chalcogenide sources they can be used in powder form in CVD chamber and the carrier gases can carry them they react to produce TMDC thin films or flakes in appropriate temperature (Özden et al., 2017).
- Metal or metal oxides can be deposited on substrate and chalcogenide powders can be used in CVD system. It is a two-step process. Firstly, metal/metal oxide layer deposited onto Si/SiO₂ substrate by using atomic layer deposition (ALD) and then in CVD chamber vapor phase sulphurized (Y. Zhan et al., 2012) or selenium used (Kong et al., 2013). The size and thickness of the final product TMDC is depend on the thickness of the pre-deposited metal/metal oxide.
- In CVD chamber the metal and chalcogenide compounds can be supplied by gases precursors (Bosi, 2015). In CVD system onto the substrate the TMDC structures are occurred as a result of the reactions of the gases.

In CVD, source materials are carried by carrier gases which is known as precursors, to reaction region for producing thin films or flakes after a series of chemical reactions of different precursors and gases on substrate. The chemical reactions can occur in reaction chamber and on the substrate. In CVD process nitrogen (N₂), hydrogen (H₂) and argon (Ar) and mixtures of these gases can be used as carrier gas. The temperature of CVD process ranges from room temperature to 2000°C.

There are series of reactions in a CVD process (Vossen et al., 1991). The reaction of the CVD process determine the growth rate which makes the mass transport mechanism and design of the CVD system principally important. The gases pass through a pipe and valves to the reaction chambers. The amount of gases is set using mass flow controllers (MFC) and valves. In the reaction chamber the precursors react to form TMDC structures onto the

substrate at a specific temperature and under a specific amount of pressure. The steps in the CVD process are summarized as follows (Simpkins et al., 1979; H Fang et al., 2008):

- The metal and chalcogenide sources, in gaseous phase, are brought to the reaction zone by the carrier gases,
- The source materials, metal and chalcogenide, diffuse through the boundary layer,
- The reactant materials, metal and chalcogenide, carry to the substrate,
- On the substrate, physical absorption and chemical reactions occurs,
- Surface reactions occurs to produce thin films or flakes,
- Gaseous by products diffuse away from the reaction zone by help of vacuum pump system.

All these CVD process steps take place in order and all these steps affect the growth rate. In a typical CVD system, there are gas flow controllers, a reaction tube, heating system, and pumping system, shown in Figure 1.1. According to the pressure system there are two types of CVD system which are low-pressure chemical vapor deposition (LPCVD) (Gardeniers et al., 1996) and atmosphere pressure chemical vapor deposition (APCVD) (Ketchum, 1995). APCVD does not need a vacuum system. In APCVD systems there are high reactant consideration at low temperatures so in APCVD systems there are high growth rate. In CVD systems generally there are a resistive heating system to reach the temperature that activate the chemical reaction.

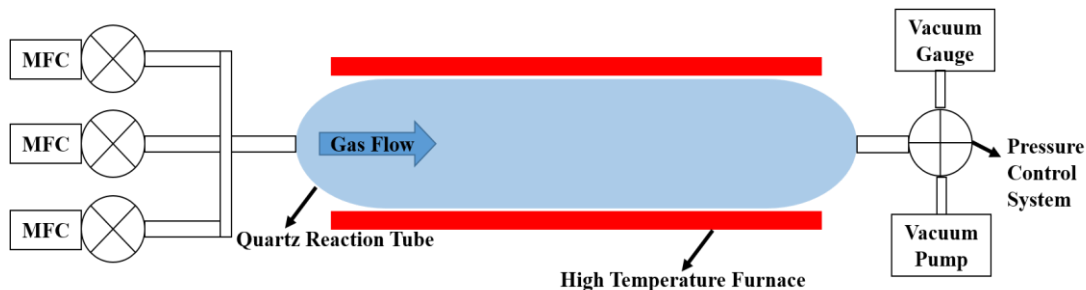


Figure 1.1 Schematic drawing of a general CVD system

In the CVD method, the main challenge is realizing large-area monolayers with horizontal growth configuration due to the lack of sufficient vapor pressure reaching onto the substrates. These difficulties have been overcome by using different methods such as, using glass in CVD chamber as substrate (Chen et al., 2017), using Sodium chloride (NaCl) salt solutions as catalyzer (P. Yang et al., 2018) and etc.

1.5. TMDC Materials Characterization Techniques

To determine number of layer, surface structure and size of the growth TMDC materials some measurement techniques are used. In the following sections some of these measurement techniques are explaining briefly.

1.5.1. Optical microscopy

In Optical microscopy light and lenses are used to zoom in the small objects. For nanometer or micrometer sized TMDC flakes or thin films, optical microscopy gives information about their sizes and cleanness of their surfaces. Dark field microscopy method excludes the unscattered beam from the image then, the field around the specimen is getting dark. An example of bright field image and dark field image of monolayer MoSe₂ flake given in Figure 1.2. The dark field microscopy method gives information about grain boundaries, surface defectivity and overlap of TMDC materials (Özden et al., 2017). The grain boundary areas are seen brighter in dark field image.

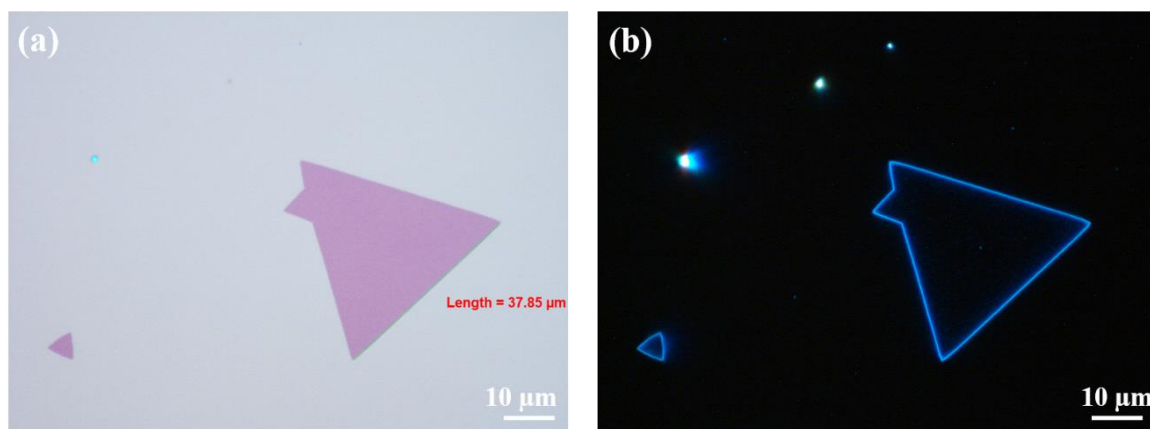


Figure 1.2 (a) *Bright field image* (b) *dark field image of MoSe₂ flake*

1.5.2. Raman spectroscopy

Raman spectroscopy is an efficient, noncontact, nondestructive and a widely used technique for the fingerprinting layered materials without having to conduct. For layered materials Raman spectrum can be used to extract out a range of other information like internal stresses, impurities, thermal conductivity, crystalline quality, crystal domain size etc.

Rotational and vibrational spectra of atoms or molecules inside a material can be investigated by using Raman Spectroscopy technique. This method was developed using the Raman effect, the inelastic scattering of incident light by atom or molecules, observed by C.V. Raman in 1928 (Long, 1977). When a sample is irradiated with a laser, the re-emitted light has the same wavelength as the incident laser, which is termed as Rayleigh scattering. On the other hand, a small amount of the scattered light has the frequency shifted from the incident laser because of the vibrations and rotation of the atoms or molecules. This frequency shifted scattering process is known as Raman scattering. In the Rayleigh scattering process, the excited molecules or atoms relax from virtual state to the initial state and a photon is generated with the same frequency value of the incident light, with a frequency of ν_0 . Rayleigh scattering shows elastic property but on the other hand stokes and anti-stokes scattering which referred to as Raman scattering shows in-elastic property, that means in the stokes and anti-stokes scattering process the excited molecules relax from the virtual state with higher or lower frequency of incident light ($\nu_0 \pm \nu_{\text{vib}}$) to the initial state and a photon

is generated with higher or lower frequency of the incident light. In the Raman spectrum the frequency shifts to the lower energy referred as Stokes line and the frequency shifts to higher energy referred as anti-stokes line. Atoms and molecules have their particular Stokes and anti-Stokes lines and the particular Stokes and anti-Stokes lines are not dependent to the incident light. The Stokes and anti-Stokes lines, in another saying Raman spectrum is used for identification of the materials which means that the Raman spectrum is the fingerprint spectrum of the materials. In Figure 1.3, the energy transformation schema of the Raman and Rayleigh scattering are shown.

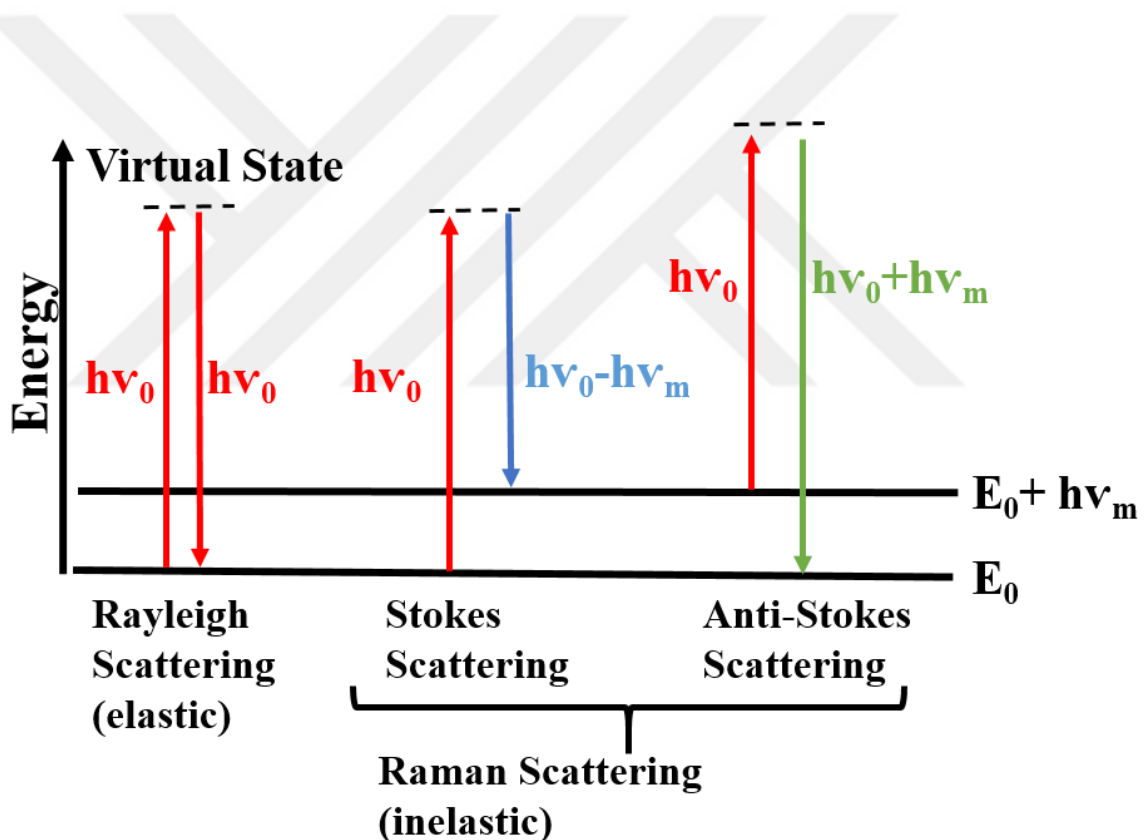


Figure 1.3 Energy transition schema for Rayleigh and Raman scattering

In Raman spectroscopy system usually laser with wavelengths of 473 nanometer (nm), 532 nm 633 nm and 780 nm is used as excitation source. The wavelength of the laser and the intensity of the Raman scattering are inversely proportional, so to obtain strong Raman signal short laser wavelength is used (Nie and Emory, 1997). Raman scattering's

frequency shift is quite small (in the order of 1 cm^{-1}) so to detect the inelastic scattering for obtaining Raman spectrum of the materials a double or triple monochromator is required. In Raman systems as incident light laser is used as its line width of frequency is narrow in order to distinguish weak Raman scattering light from the high-intensity elastic scattering light (Haynes et al., 2005). A schematic drawing of Raman Spectroscopy is shown in Figure 1.4.

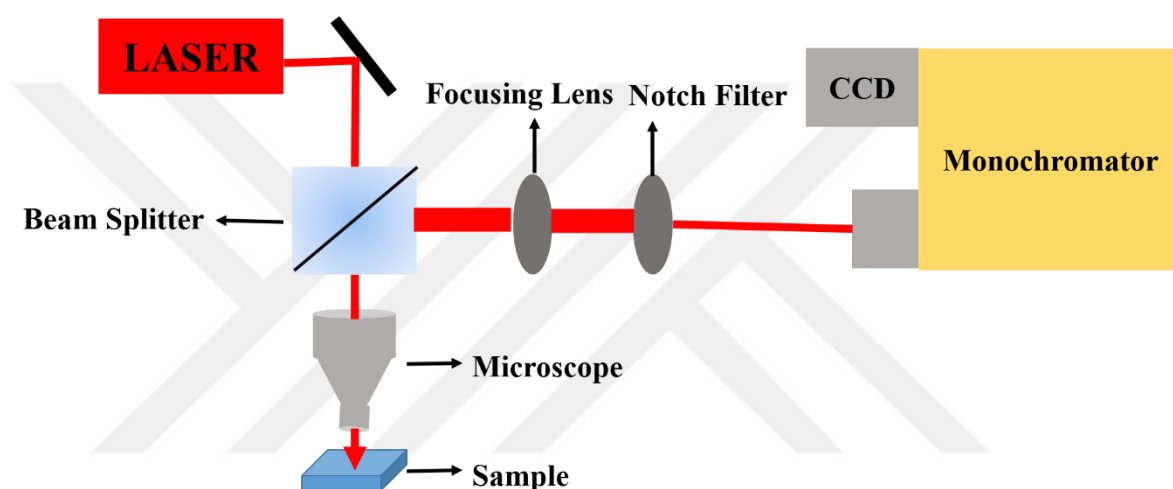


Figure 1.4 Schematic drawing of Raman spectroscopy

Raman spectrum consists some features, in the form of strong peaks. The features are unique to a material. The features also fingerprint of the material and can be used to identify the material. Variations observed in the features can range from changes in the Raman intensity, full width half maximum (FWHM), or the frequency shifts of the peaks with respect to the ideal material's Raman spectrum. Traditionally, these changes can be attributed to the change in amount of material, crystallinity or internal stresses in the sample. As an example of Raman analysis of monolayer WS_2 structure is given in Figure 1.5.

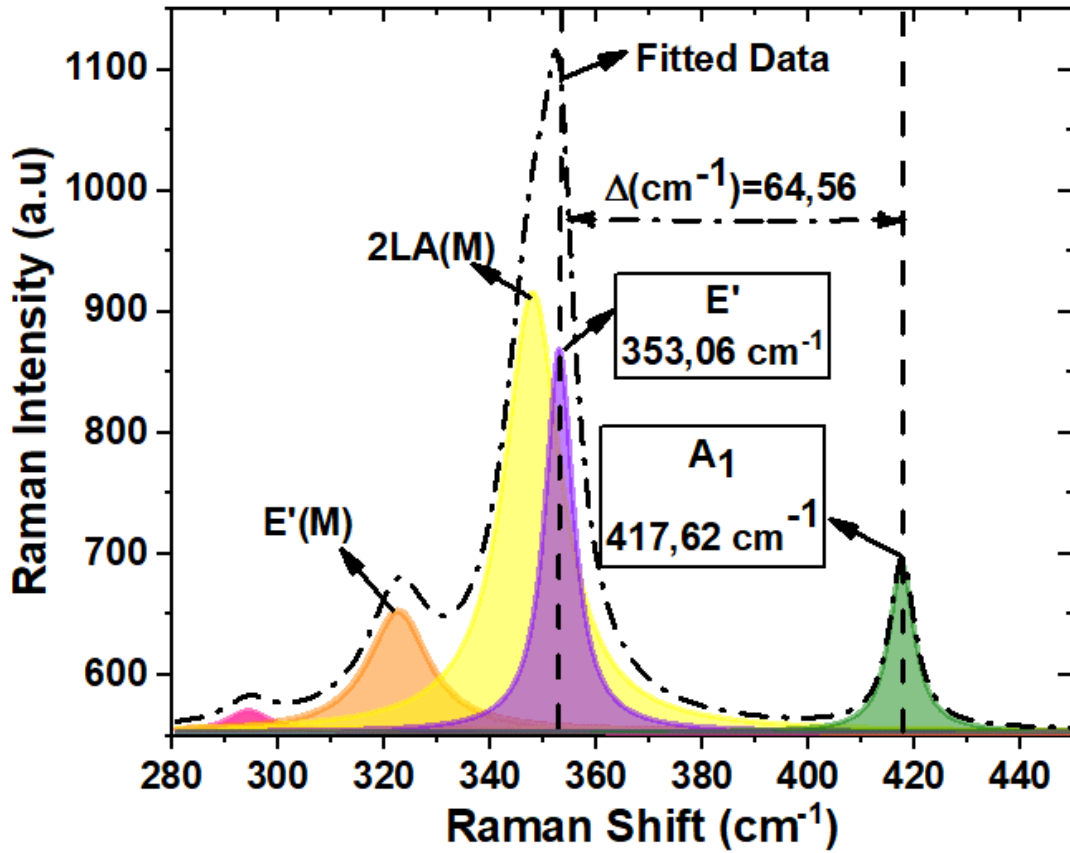


Figure 1.5 Raman spectroscopy analysis of monolayer WS₂ structure

1.5.3. Photoluminescence spectroscopy

Both Raman scattering and photoluminescence (PL) spectroscopy can occur when a material is excited with a laser. PL spectroscopy is an efficient, non-contact, non-destructive and a mostly utilized technique for the analysis of semiconductors with stimulating optoelectronic properties.

Photoluminescence is defined as the natural emission of light from a material under optical excitation. Photoluminescence in certain photo luminescent material can be observed by exciting the material using an incident laser beam which has an energy larger than the material's bandgap and enough to excite carriers. The resulting photons reemitted materials are then captured using a charged couple device (CCD) detector. The emission recorded from the material is then used to extract out a variety of information detailing the discrete

electronic states involving the material's intrinsic optical processes. Besides, PL spectra can also be used to understand the transitions associated with endemic defects in semiconductor materials. This energy of the emitted photons is measured in energy and a unit of electronvolts (eV) is suitably used. The spectra are graphically depicted in measurements as PL spectra. In this spectra, the intensity (photon count) of the scattered light (y-axis) is plotted for energy (eV) on the x-axis. PL studying on materials with indirect bandgap is very hard because PL spectra is favorable to radiative process but the indirect bandgap materials have weak radiative activity. PL spectra is used for determining the intrinsic optical bandgap of a semiconductor. The recombination in a direct bandgap semiconductor, which has intrinsic valence band maximum (VBM) and conduction band minimum (CBM) at the same momentum value, is very efficient process. Thus they are very photo luminescent and will show a large peak at an x-axis value E_G . The peak position of the PL spectra obtained in a defect free direct band gap semiconductor can be said to be its optical bandgap. The material quality of a material can be assessed by comparison of the PL yield of the sample with an ideal direct bandgap material with maximum yield. The radiative yield (PL) for a defective sample would be a smaller because of the presence of a significant amount of non-radiative recombination, which is often associated with localized defects in the sample. Low temperature PL studies has its own advantages too. Underlying contributions to the main PL peak at room temperature can be deconvoluted into components from various transitions at low temperature. For further obtaining the underlying reason for emission at different energies, PL spectra obtained by varying the power of the excitation laser can be crucial. In literature there is some studies focus on this feature such as, with increase in the laser excitation power, PL intensities from bound exciton (from defects) tends to saturate towards higher powers. This happens as defects get fully populated with exciton. Whereas the integrated intensity of the PL peak associated with free exciton shows no saturation and scales almost linearly with power. Thus, at lower powers the PL spectrum is dominated by the bound exciton and at higher powers the PL peak from free exciton dominates (Tongay et al., 2013). As an example in Figure 1.6, photoluminescence spectrum results of a monolayer MoS₂ flake is shown.

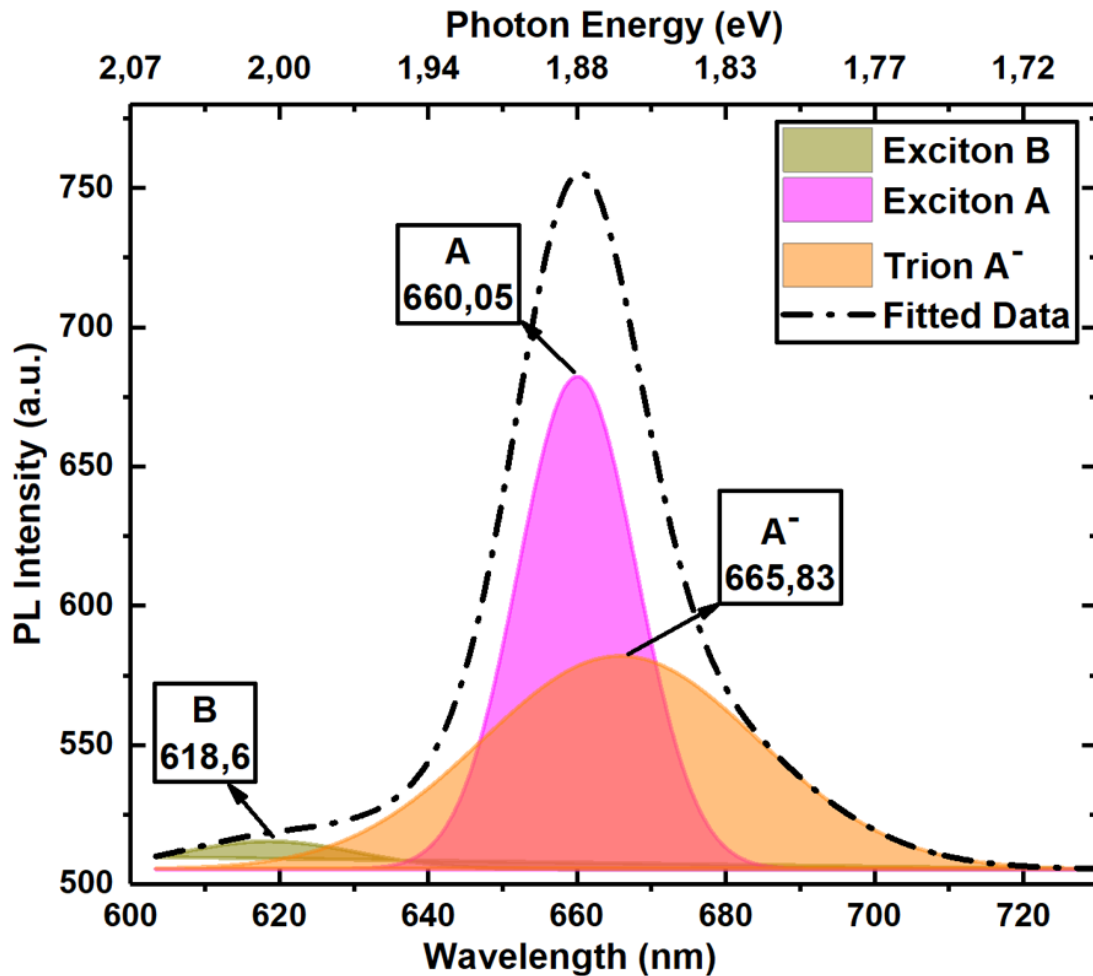


Figure 1.6 PL spectrum results of monolayer MoS_2 structure

The direct to indirect bandgap transition accompanying thickness change of the 2D TMDC materials can be determined by observation of the PL peaks of these materials (Mak et al., 2010; Splendiani et al., 2010). When a materials thickness is decreased to monolayer the PL intensity of this material is increased which is related to the formation of the direct bandgap. But the change in the PL intensity of the material may be a result of extrinsic or intrinsic factors such as; annealing (Eda et al., 2011), the interlayer coupling between the two layers (Huang et al., 2014), defect of the material (Chow et al., 2015), pressure (Nayak et al., 2014), electrical gating (Newaz et al., 2013), doping (Mouri et al., 2013), etc.

1.5.4. Atomic force microscopy

Thickness of single-layer and few-layer TMDC can dramatically change and because of this feature, accurate thickness measurement is important. The main problem about TMDC materials is intricate due to the thickness of the samples is sometimes not homogeneous, because of domain boundaries. For such a complicated materials using atomic force microscopy (AFM) is a method to measure thickness of the nanoscale 2D TMDC materials in three-dimensional view. By using AFM the thickness of the materials can be measured directly.

AFM was invented by Binnig et. al. in 1986 (Binnig et al., 1986). The surface of the sample is scanned by a probe to measure the changes in the interaction force between the AFM cantilever and the sample. On material sample surface a AFM cantilever is applying and the separation distance determines the dominant interaction force. Bending on the cantilever, positive or negative, can be detected by a laser beam targeted to the cantilever and reflected onto a photodetector. According to the deflection the surface morphology, adhesion, friction, hardness and elasticity can be determined (Eaton and West, 2010). AFM is used to investigate not only TMDC materials but also conducting or non-conducting materials, biological species, molecules in air, in liquid or in vacuum. AFM and the sample must be in within an interactive force field to operate. AFM uses different kinds of forces operate such as, contact region, non-contact region and tapping region (Eaton and West, 2010). In Figure 1.7, schematic of the AFM is shown.

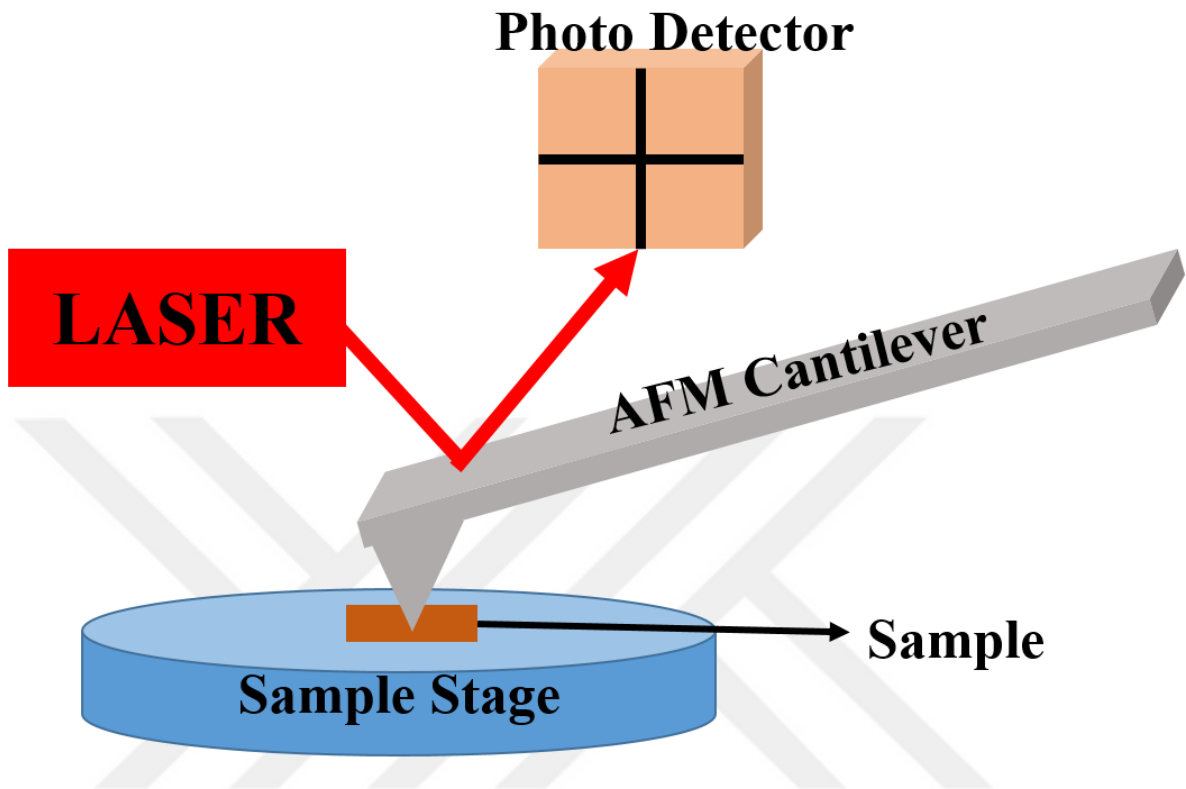


Figure 1.7 Schematic drawing of AFM

In the contact region, distance between sample surface and the AFM cantilever is only a few angstroms and there is a repelling force between sample and AFM cantilever. This repelling force comes from the electrostatic repelling interaction between the electron clouds and the sample surface and the force is reduced as the distance between sample and AFM cantilever is increased.

In the non-contact region, distance between sample surface and the AFM cantilever is hundreds angstroms and there is a long range attractive force, known as van der Waals force between sample surface and AFM cantilever. When the AFM cantilever is getting nearer to the sample surface, the attractive force is increasing to induce the cantilever to deflect towards the sample. However, at a distance lower than angstroms, the repelling force becomes dominant to induce positive deflection of the cantilever. The AFM cantilever can be affected by not only Coulomb force and van der Waals force but also various other interactions.

AFM has three operation modes, contact mode which the distance between the sample and the AFM cantilever is less than 0.5 nm, intermittent contact mode in another saying tapping mode which the distance between the sample and the AFM cantilever is less than 2 nm and more than 0.5 nm and non-contact mode which the distance between sample and the AFM cantilever is less than 10 nm and more than 1 nm (Saint Jean et al., 1999; Bruch, 2005).

During contact mode scanning process the AFM cantilever is in a gentle contact with the sample surface and the contact mode is the most used mode. The distance between the AFM cantilever and the surface of the sample is small and constant and called as constant distance mode. The cantilever inhibits a constant force for a constant cantilever deflection by using feedback loop which is called as constant force mode. By using the contact mode of AFM high-resolution images of the sample surface at nanometer scale can be obtained. For hard surface samples contact mode is preferred and by using the contact mode manipulations of the sample surface are enabled. But the contaminations on the surface sample is affected the AFM cantilever badly and there is an extreme force between applied to the sample by AFM cantilever and this force may cause damage of the AFM cantilever.

The intermittent mode or another saying tapping mode is similar to the contact mode but in the tapping mode scanning process the cantilever has a constant resonant frequency which is nearly hundreds of kilohertz (kHz). For producing a constant oscillation, the AFM cantilever is tightly tapping on the surface of the sample. The tapping is rapid because of the oscillation time so the additional forces are reduced. For high-resolution imaging of soft, easily damaged and the structures bonded to a surface as loosely, the tapping mode is used.

In non-contact mode, the cantilever oscillates while scanning process of the sample and the distance between the AFM cantilever and the sample is increasing by the attractive force regime dominated by van der Waals interaction. In non-contact mode, if the AFM cantilever is too close to the surface of the sample capillary force will bring the AFM cantilever down to contact the sample surface, which is named as jump-to-contact. The feedback loop is used to monitor the amplitude of the cantilever to measure the attractive

force of the surface. The AFM cantilever may be affected by the contamination of the surface (Eaton and West, 2010). In Figure 1.8. AFM result of monolayer MoS₂ structure is shown.

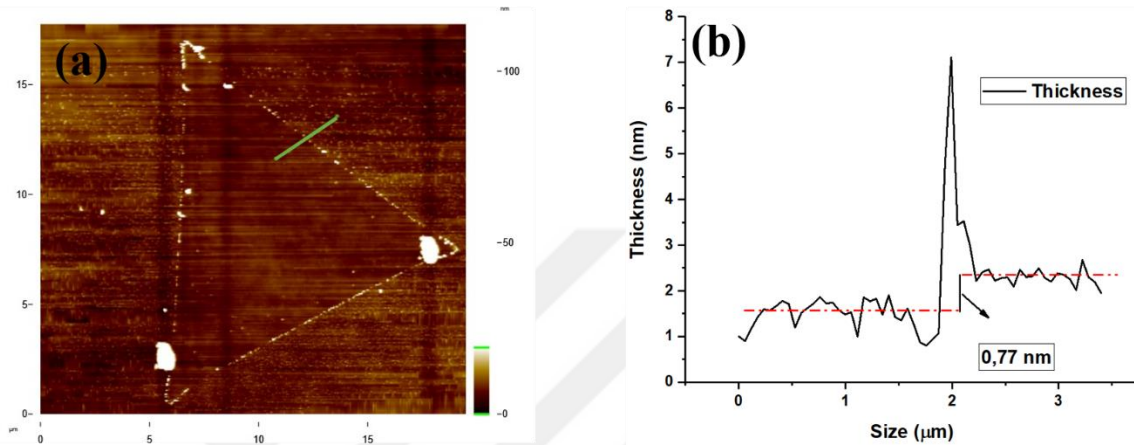


Figure 1.8 (a)AFM image of MoS₂ (b)height profile of green line on(a)

1.6. Electronic and Optoelectronic Applications of 2D TMDC Materials

Graphene was the first and most important material for a multifarious applications (K. Novoselov et al., 2005), owing to its attractive features (Geim and Novoselov, 2010), but on the other hand, graphene has zero band gap, difficulty of controlling number of layers and intrinsic defects and all these features makes graphene a challenging material for future semiconductor device applications. Thus 2D semiconductor TMDC materials are attracting a huge attention in various applications because of their small bandgap, minor dangling bond, stability feature, high surface area and high mobility. The possible applications of 2D TMDCs are shown in Figure 1.9.

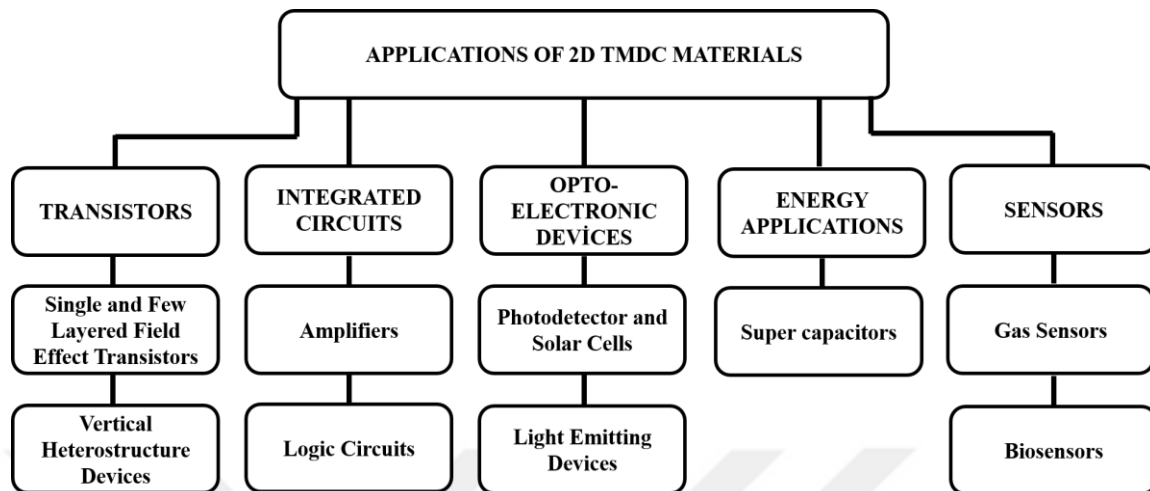


Figure 1.9 The schematic representation of the applications of 2D TMDC materials

1.6.1. Transistors

Transistor can be defined as a semiconductor device which have three terminals for connection to an external circuit. The invention of transistors revolutionized in the electronics (Brinkman et al., 1997). A transistor can be used to obtain intense output signal, in the form of current or voltage, from a small input signal. The ratio of the output signal-to-input signal is named as gain. A transistor also can be used as a switch which turn the current ON or OFF in a circuit. A modern version of the transistors is field effect transistors (FET). A typical FET has three terminals, named as gate, drain and source. The drain and source terminals of the FET is contacts for the thin area connecting them, named channel. The gate terminal of the FET device could be a covered thin dielectric material, named as gate dielectric. This terminal is used to control the conductivity of the channel by changing the charge carrier concentration.

In literature there are FET device applications used single and few layered TMDC materials. 2D semiconducting TMDC materials has fewer dangling bonds, stable structure, high mobility and these features make 2D TMDCs suitable for the channel layers of thin-film field effect transistors (Radisavljevic, Radenovic, et al., 2011). In 2004, tungsten diselenide (WSe_2) was the first of the TMDC materials to be used in a FET as semiconducting channel layer (Podzorov et al., 2004). After this developments, a MoS_2 thin film was used in

FET device as semiconducting layer in back gated FET device construction and the mobility of the device was measured as $10 \text{ cm}^2\text{V}^{-1}\text{s}^{-1}$ (Ayari et al., 2007). A top gated MoS_2 FET was also indicated and the mobility of the FET device was reached at $200 \text{ cm}^2\text{V}^{-1}\text{s}^{-1}$ (Radisavljevic, Radenovic, et al., 2011). After the development of the synthesis large area 2D TMDCs by CVD method, production of the FET device in wafer scale was possible (Tarasov et al., 2014). Vertical heterostructure devices also fabricated (Yu et al., 2013). In the study of vertical heterostructure FET device, MoS_2 and graphene were used. The ON/OFF ratio of the device was reported over 10^3 at room temperature. The illustration of the top gated and back gated TMDC based FET devices are shown in Figure 1.10. The top gated FET devices allow of a decreased gate voltage and integrates different types of devices on a single substrate. Hafnium dioxide (HfO_2) and Aluminum oxide (Al_2O_3) are used as dielectric material in the single-layer MoS_2 and WS_2 devices (Zou et al., 2014; Ganapathi et al., 2016).

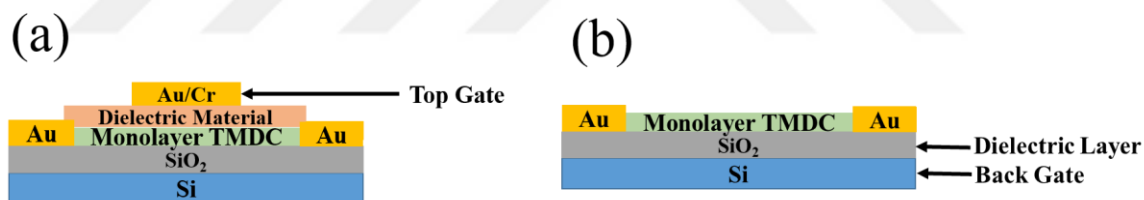


Figure 1.10 Illustration of (a)top gated (b)back gated TMDC based FET

1.6.2. Integrated circuits

After the fabrication of the FET devices based on mono-layer TMDC materials, mono-layer TMDC based analog small signal amplifier operations evinced (Radisavljevic et al., 2012). In this study, monolayer MoS_2 based, two transistors were connected in series. One of the transistor was acted as a switch and the other transistor as an active load and the transistor circuit as a linear amplifier. After amplifiers demonstration, which are simple integrated circuits using mono layer or few layer TMDC based FETs, more complicated devices for logic circuits were designed (Radisavljevic, Whitwick, et al., 2011; H. Wang et al., 2012; Jariwala et al., 2014). An example of a such circuit, a NOR gate logic circuit by

connecting two monolayer MoS₂ based transistor in parallel and using an external resistor as load (Radisavljevic, Whitwick, et al., 2011).

1.6.3. Optoelectronic devices

Optoelectronic devices have interaction with light such as, generation of light, detection of light and controlling the light. For fabrication of solar array devices, wearable electronic devices and transparent display devices such as, wearable displays, solar cells, transparent and flexible materials including semiconductors, dielectrics and conductors are used as functional part such as, optical absorbers, window layers and light emitter. Monolayer TMDC materials have direct band gap and this feature makes monolayer TMDC materials suitable for optoelectronic applications. Few or mono layer TMDC materials were used in several applications of optoelectronic devices. When photons which have higher energy than the band gap of semiconductor material are incident on the semiconductor material, the photons create bound electron-hole pairs (excitons) or free carriers which is depend on the exciton binding energy in the semiconductor. The bound excitons generate a current, named as photocurrent. There are studies that few or mono layered TMDC semiconductor materials are used in fabrication of phototransistor to use as photodetector (Yin et al., 2011; Perea-López et al., 2013; W. Zhang et al., 2013). Photovoltaic cells are another important application of the few or mono layered TMDC materials due to their tunable band gaps for visible light absorptions (Shanmugam et al., 2012b; 2012a; Fontana et al., 2013).

Light emitting diode (LED) is two-lead semiconductor light source. When an electrical stimulus, voltage, applies on the LED photons are emitted. Few or mono layered TMDC materials which have direct band gaps are suitable materials for active light emitting layers in LED devices (Carladous et al., 2001).

1.6.4. Energy applications

In energy applications such as energy storage and conversion nanostructured TMDC materials have potential for use as lithium-ion battery electrodes (Stephenson et al., 2014).

Few layered TMDC materials were used as an advanced electrode material for super capacitors (Balasingam et al., 2015).

1.6.5. Sensors

2D TMDC materials have high surface area and this feature makes 2D TMDC materials unique for sensor applications where chemical particles affect the properties of TMDC material by adhering to the surface of 2D TMDC materials. Mono-layer MoS₂ Nano sheets was used for Deoxyribonucleic Acid (DNA) detection (C. Zhu et al., 2013). 2D monolayer MoS₂ based FET biosensor was also used for detection of pH and biomolecules (Sarkar et al., 2014). The sensitivity of this FET based biosensor is defined as the ratio of the difference in the current before and after biomolecule binding to the surface of the MoS₂. In biosensor applications not only MoS₂ but also WS₂ Nano sheets were used. WS₂ biosensors were used for detection of oligonucleotides, proteins (Y. Yuan et al., 2014) and micro Ribonucleic acids (Xi et al., 2014). 2D TMDC based gas sensors are described in detail in the following section.

1.6.5.1. 2D TMDC based gas sensors

2D TMDC nanomaterials are appropriate materials for gas sensor devices applications because of having high surface area and strong surface activities. Gas sensors can be used for detecting or characterizing harmful gases in environment (Drobek et al., 2016). Gas sensors can be used for various purposes such as, emission control, safety, military, medical diagnoses. As gas sensing material graphene, MoS₂, MoSe₂ and WS₂ can be utilized. Graphene also can be used in gas sensor applications (W. Yuan and Shi, 2013). A few amount of gas adsorption on graphene surface may cause a change in its resistance (Lin and Avouris, 2008). Because of this feature of graphene for gas sensing applications graphene, graphene oxide, reduced graphene oxide are mostly used as gas sensor. TMDC materials have thickness dependent physical and chemical properties, high surface area as graphene and also semiconducting property which enhance the sensing performance, all these features of TMDC materials make them fascinating for gas sensor applications (Late et al., 2013).

Gas sensing mechanism

There are different mechanism types for gas sensing. Metal oxides (ZnO, SnO₂, etc.) based gas sensors work with the surface adsorbed oxygen ion mechanism. The operating temperature of these sensors are between 200°C-500°C. Negative ions of oxygen (O⁻, O²⁻ and O₂⁻) adsorbed on the surface of the metal oxides and the ions charge the metals negatively (Barsan and Weimar, 2001). Different types of gases adsorbing on metal oxides are interacting with oxygen negative ions the interaction between gases and oxygen negative ions change the conductivity of the metal oxides. In the charge transfer mechanism the sensing surface acts as acceptor or donor of charge. Charge transfer reaction occurs between sensing surface and adsorbed gases in this sensing mechanism. Depending on the material of the sensing layer and the exposing gases, the transfer directions and quantities of charges can be change. The changes in direction and quantities of the charges effect the material resistance. When the sensing material re-exposed to air, the sensing material desorb the gas molecules and the resistance of the sensing material return to initial state. For example, a n-type monolayer MoS₂ based gas sensor tested under different gases such as, O₂, water vapor (H₂O), ammonia (NH₃), nitric oxide (NO), nitrogen dioxide (NO₂) and carbon monoxide (CO) etc. and it was seen that the types of the gases was affecting the charge transfer mechanism (Yue et al., 2013). According to density functional theory (DFT) results used in this study, before adsorption of the gas molecules there were some electrons in the conduction band of the monolayer MoS₂. After adsorption of the gases, the electron charges transferred from MoS₂ to electron-accepted gases, so carrier density in MoS₂ decreased and resistance of the MoS₂ increased; on the other hand, the electron charges transferred from electron donor gases such as, NH₃, to monolayer MoS₂ as a result of this reaction carrier density in MoS₂ increased and reducing its resistance.

Types of gas sensing devices

There are various types of graphene and TMDC based gas sensors. Chemiresistors are a type of the gas detecting devices. Chemiresistors operation mechanism can be defined

as, the adsorbing gas molecules on the surface of gas sensing layer and leads to a change in the electrical resistance of the sensing layer material (Hubble et al., 2015). The chemiresistor type devices have some advantages. It is easy to fabricate the devices, simple to operate and they are cost effective devices (Davis et al., 2005; Raguse et al., 2007). Chemiresistors have sensing material, two metallic electrodes or interdigitated electrodes. This type of devices can be used to detect O₂, H₂, CO, NO, NO₂, chlorine gas (Cl₂) and organic vapors (Joseph et al., 2008; Ammu et al., 2012; Y. Liu et al., 2014; Nallon et al., 2015).

Field effect transistors (FET) can be used as gas sensor device which is easy to manufacture, sensitive to gas molecules and can be produced in nanoscale (Schedin et al., 2007; Pu et al., 2014; B. Zhan et al., 2014). A FET based gas sensor have two metal electrodes as drain and source electrodes, a sensing layer with semiconducting property as channel material (He et al., 2012). The gas sensing is occurred under a constant bias voltage by measuring the change of the drain current before and after the exposing to the gas molecules. After absorbing the gas molecules, the electronic structure of the semiconducting sensing layer change as a result of this change the conductance of the material change also (Pu et al., 2014). FET based gas sensor device is used to detect many kind of gases such as, CO, NO, NH₃, NO₂, sulfur dioxide (SO₂), H₂, hydrogen cyanide (HCN), ethanol, and 2,4-dinitrotoluene (Dan et al., 2009; Du et al., 2009; Johnson et al., 2010; B. Chen et al., 2012; Yavari and Koratkar, 2012; B. Zhan et al., 2014).

Performance parameters of the gas sensing devices

The performance of a gas sensor can evaluate by various parameters such as, sensor response, sensitivity, selectivity, response time and recovery time. Sensor response, S (%) can be defined as the ratio between the difference of resistance before and after exposing the gas molecules and the resistance value before exposing the gas molecules (Kannan et al., 2015). Selectivity is another performance parameter of gas sensor devices. Selectivity is defined as the capability of a gas sensor responding to a specific group of gases. So selectivity can be evaluated by comparing the sensor response to different gases. Ethanol, carbon monoxide, and methane have appreciable cross-sensitivity, which makes them difficult to

distinguish (Korotcenkov and Cho, 2013). The response time is defined as the time that sensor show a response to the gas molecules and the recovery time defined as the time that sensor return its initial state (Di Francia et al., 2009).

The improvement of the performance of the gas sensors

The performance of the gas sensor can be affected by many different factors, such as properties of the used materials, temperature, humidity, gas flow rate, dimensions of the sensing areas, length-to-width ratio of the sensing material etc. Temperature is an important factor for gas sensors. Increasing the temperature increasing the adsorption/desorption processes of gases and increases the reactivity between sensing materials and sensitive gases (Morrison, 1987; Yamazoe and Shimano, 2011). But in some applications, room temperature is required such as, explosive environments (Korotcenkov and Cho, 2013). Humidity is another influence factor for gas sensor devices. The water vapor adversely affects the detection of gas by the gas sensors. So minimizing the impact of water vapor is developing the gas sensor performance (Korotcenkov and Cho, 2013). On the other hand, TMDC based humidity sensors have been developed (Late et al., 2013; S.-L. Zhang et al., 2014). Humidity sensing mechanism depends on H^+ or H_3O^+ from dissociation of adsorbed water, rebounding between adjacent hydroxyl groups (C. Wang et al., 2010). Total flow rate of the gases is another influence factor to detect target gases. For example, in literature there are a study that investigate the effect of the rate of the flow on sensitivity. In this study the total flow rate had a significant effect on sensing responses to target gases (Zhou et al., 2014).

Although various gas sensor devices have been developed to date, some problems still remain in the gas sensors, such as poor sensitivity to some gases, few selectivity, small reversibility, and high sensitivity to air humidity. Currently, some approaches to solve all these problems in gas sensors have been developed. Applying an ultraviolet (UV) light to gas sensor is one of the method that can be used to increase the sensitivity of the gas sensor to the gases. UV light can clean the detection material and as a result the detection of very low amounts of gases can be provided (G. Chen et al., 2012). In previous studies that used graphene as gas sensing material show that defects and doping on graphene may affect the

sensitivity of graphene (Terrones et al., 2012). Some researchers investigated the effect of MoS₂ layer number on gas detection and proved that the single layer MoS₂ Nano sheets were not stable when compared to two-layer and five-layer devices. But on the other hand single-layer MoS₂ Nano sheet devices showed sudden and effective response to the gases (Hai Li et al., 2012).

Gas sensing applications of graphene and other layered TMDCs

Graphene and other layered TMDC materials have been mostly used in gas sensing applications because of their functionalized surface area and high adsorption capability (Ko et al., 2016). The gas sensors sensing material, synthesis method, target gas, sensing device, detection limit in the unit of parts-per-million (ppm) and parts-per-billion (ppb) and sensing mechanism are summarized in Table 1.3.

Table 1.2 Gas sensing applications of graphene and TMDC materials

Sensing Material	Synthesis Method	Target Gases	Sensing Device	Detection Limit	Sensing Mechanism
Graphene	Micromechanically exfoliated	NO ₂ , H ₂ O, I ₂ , NH ₃ , CO, ethanol	Chemiresistor	-	Charge transfer (Schedin et al., 2007)
Single- and multi-layer MoS ₂ Film	Micromechanical exfoliation	NO ₂ , NH ₃ , humidity	FET	-	Charge transfer (Late et al., 2013)
Single- and multi-layer MoS ₂ nanosheets	Liquid exfoliation	NH ₃	Chemiresistor	20 ppb	Charge transfer (Yao et al., 2013)

MoS ₂ Film	CVD	NO ₂	FET	120 ppb	Charge transfer (Cho et al., 2015)
Monolayer MoS ₂	CVD	NO ₂ , NH ₃	FET	20 ppm to NO ₂ and 1 ppm to NH ₃	Charge transfer (B. Liu et al., 2014)
Multilayer WS ₂ nanoflakes	Micromechanical exfoliation	Ethanol, NH ₃ , O ₂	FET	-	Charge transfer (Huo et al., 2014)
Single Layer MoSe ₂	Micromechanical exfoliation	NH ₃	Chemiresistor	50 ppm	Charge transfer (Late et al., 2014)

1.7. Motivation of the Thesis

In this thesis, the research focus on the investigation of the production of TMDC materials by CVD method and the gas sensor applications. The motivation behind this research is as follows:

- (1) There are commonly used methods to obtain monolayer TMDC materials, such as the micro-mechanical exfoliation of a single crystal and CVD. The exfoliated materials are limited to micron-sized scale that is not appropriate for production on large scale. In this thesis, CVD method is studied to grow large area monolayer TMDC structures.
- (2) The grown TMDC materials by CVD are commonly existed in a mixture of monolayer and few-layer form. For sensor applications it is important to use the TMDC materials in monolayer form. Thus, a detailed investigation is performed to the grown TMDC materials.

(3) The FET type sensors are easy to manufacture and sensitive to detection. Thus, in this thesis FET fabrication steps are employed.

1.8. Thesis Structure

In Chapter 2, the growth of TMDC materials and the characterization of the TMDC materials by Optical Microscopy, Raman Spectroscopy, Photoluminescence Spectroscopy and Atomic Force Microscopy are explained. In Chapter 3, monolayer TMDC based FET device steps are explained briefly. In Chapter 4, the study results are evaluated and suggestions for future works are discussed.

2. CVD GROWTH AND CHARACTERIZATION OF TMDC MATERIALS

By using CVD method MoS_2 , WS_2 and MoSe_2 flakes can be produced. For gas sensor applications these TMDCs with clean surface, high coverage and large surface area is very necessary.

In the literature there are some studies that proved that using glass as substrate in CVD growth experiments have a positive effect on the growth. For example, it is reported that the growth of monolayer MoSe_2 flakes with millimeter-size on molten glass (Chen et al., 2017). In that study millimeter size monolayer MoSe_2 flakes were produced and it is claimed that molten glass was getting appropriate for large domain growth. There is a study about the growth of uniform monolayer MoS_2 film on soda-lime glass. For investigating the effect of dopants of the glass as, calcium and sodium on the growth of TMDCs, they tested the sodium and calcium-containing solutions and proved that sodium had a positive effect on growth, but the effect of calcium on growth was negligible (P. Yang et al., 2018).

We used glass as a catalyst during CVD experiments because the use of glass in CVD experiments facilitates the growth of TMDC structures with clean surfaces and large area which is very important property of TMDC materials for gas sensor applications and by using piece of glass the repeatability problem of the CVD method has been overcome, due to the dopants of the glasses. To clarify the effects of the compositions of the glasses on the growth of TMDC materials, two different glasses with different compositions were used. The glass used in our experiments are chosen as it is low-cost and easy to access. According to the energy dispersive spectroscopy (EDS) analysis, the composition of these two types of glasses (Glass-1 and Glass-2) shown in Table 2.1. As listed in the Table 2.2, Glass-1 contains higher sodium concentration compared to Glass-2, which is the most important catalytic parameter according to the previous works.

Table 2.1 EDS analysis results of the Glass-1 and Glass-2

Glass-1			Glass-2		
Element	Percentage of Weight	Percentage of Composition	Element	Percentage of Weight	Percentage of Composition
O	51.58	64.65	O	60.53	73.55
Na	9.56	8.34	Na	5.61	4.74
Mg	2.16	1.78	Al	1.92	1.39
Al	0.38	0.29	Si	25.22	17.46
Si	31.71	22.64	K	3.62	1.80
Ca	4.61	2.31	Ti	1.33	0.54
			Zn	1.77	0.53
Total	100.00	100.00	Total	100.00	100.00

After growth of MoS₂, MoSe₂ and WS₂ flakes, the surface morphology of these grown TMDC materials were characterized by optical microscopy and dark field feature of the optical microscope system. The optical microscope was Nikon Eclipse LV100NDA microscope. Nanomagnetic Instruments atomic force microscope (ez-AFM) in the tapping mode was used to measure the thickness of the grown structures. The phonon behaviors of these TMDC structures were analyzed by Raman and photoluminescence spectroscopy. The system that we used was Witec Alpha 300 R μ -Raman and photoluminescence spectroscopy system with a Zeiss 50X microscope objective having a numerical aperture (NA) of 0.8. We also used a 532 nm continuous wave laser with 300 nm spot size and 0.5 miliwatt laser power and 1 s integration time at room temperature.

This chapter consist of three main parts. In these parts, the growth of MoS₂, WS₂ and MoSe₂ materials by CVD method with help of glass assistance and characterization of theses materials are explained, respectively.

2.1. MoS₂

Monolayer MoS₂ is a layered 2D semiconductor material which can be used in various applications (H. S. Lee et al., 2012; Buscema et al., 2013; Lopez-Sanchez et al., 2013). The bulk form of the MoS₂ have an indirect bandgap (1.2 eV), while the bandgap of monolayer MoS₂ changes as direct (1.8 eV) (Splendiani et al., 2010; Gatensby et al., 2014). Single- or few-layer MoS₂ materials can be produced by exfoliation method or be grown by chemical vapor deposition (CVD) method (S. Yang et al., 2014). By using CVD method, monolayer MoS₂ flakes can be produced easily.

2.1.1. Experimental details

Before starting the experiments, the Si/SiO₂ substrates and glass pieces were cleaned by ultrasonic vibrational tool in three solvents (acetone, isopropanol, deionized water). The Si/SiO₂ substrates and glass pieces were kept in each solvent for 5 minutes. The Si/SiO₂ substrates were annealed at 120°C for 5 minutes. In that experiment a piece of glass (2 cm x 2 cm) and two pieces of Si/SiO₂ substrates were used named as S-1 and S-2. 500 mg Sulphur powder (Sigma-Aldrich, 99.98%) and 4 mg molybdenum trioxide (MoO₃) powder (Sigma-Aldrich, 99.995%) were used in that experiment as precursor. The Sulphur powder is placed on a quartz boat and the MoO₃ powder is placed on the S-1 substrate. The S-1 substrate with MoO₃ powder on it and the glass piece are positioned on the S-2 substrate side by side. The distance between sulfur powder and S-2 substrate is set to 16 cm, shown in Figure 2.1.

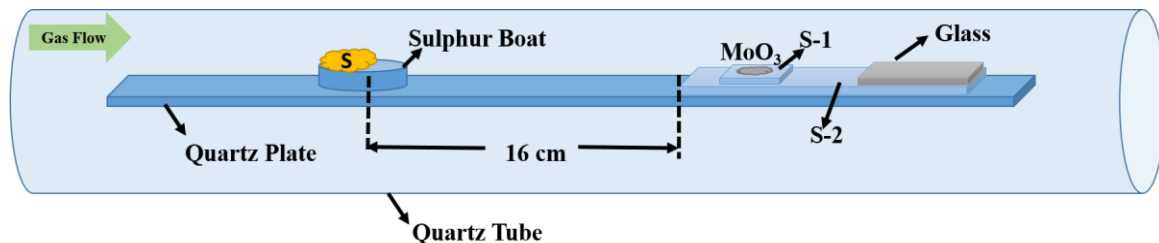


Figure 2.1 Schematic illustration of MoS_2 growth experiment by CVD

As the carrier gases, hydrogen and argon were used. MFC of the argon gas was set to 95 standard cubic centimeters per minute (sccm) and the MFC of the hydrogen gas was set to 5 sccm. Hydrogen gas was included as a carrier gas because of its promoting effect to obtain monolayer TMDC structures with high-quality (Yorulmaz et al., 2019). Growth temperature of that experiment was set to 700°C and pressure was set to 740 Torr, listed in Table 2.2.

Table 2.2 MoS_2 growth parameters

Amount of MoO_3 powder	4 mg
Amount of Sulphur powder	500 mg
Amount of Ar gas	95 sccm
Amount of H_2 gas	5 sccm
Pressure Value	740 Torr
Temperature of the Furnace	700°C
Distance Between Powders	16 cm

Additionally, split furnace has the tracks which makes the system mobile and allowed to shift the furnace towards or away from the Sulphur to control the Sulphur evaporation rate and growth time. Sulfur powder was located at 14 cm away from the entrance of the quartz tube where the furnace location was for the beginning of the experiment. After starting the experiment, Sulphur completely melted when the temperature of the furnace reached to 400°C

and at this point the furnace was shifted right (4 cm away from the quartz boat) and left there until the furnace inner temperature reached to 700°C. Afterwards, at the growth temperature, 700°C, the furnace was shifted to left side by 6 cm. All of the Sulphur was in almost 6 min, which was growth time of the experiment. Growth of MoS₂ flakes occurred on the S-2 substrate. It has been observed that the MoS₂ flakes, which are observed more intensively and bigger in the vicinity of the glass, have decreased and their sizes become small as they moved away from the glass.

2.1.1.1. Optimization of MoS₂ growth parameters by CVD

In our experimental study to find the optimum MoS₂ growth experiment we have done a number of experiments. Amount of the powder used as precursor in these experiments, temperature value of the furnace, the types of the glasses used as catalyzer in these experiments and the value of the pressure were the growth parameters of these experiments. By doing these experiments, the growth parameters changed one at a time to understand the effect of each. In these experiments distance between powders and amount of the gases are keep in a constant value same as the results of the experiments we know were successful. The experimental set ups are listed in Table 2.3. After these set of experiments the optimum growth parameters for MoS₂ were found.

Table 2.3 *Experimental parameters for MoS₂ growth*

Experimental Setups	Amount of MoO ₃	Amount of Sulphur	Temperature Value of Furnace	Types of Glass	The Pressure Value	Results
Different Deposition Processes	From 1.5 mg to 4 mg	From 250 mg to 400 mg	From 700°C to 750°C	Glass-1	From 730 Torr to 740 Torr	Nearly 25 μm flakes

Different Deposition Processes	From 1.5 mg to 4 mg	From 250 mg to 400 mg	From 700°C to 750°C	Glass-2	From 730 Torr to 740 Torr	Nearly 40 μm flakes
Different Deposition Processes	From 1.5 mg to 4 mg	From 250 mg to 400 mg	From 700°C to 750°C	Without any Glass	From 730 Torr to 740 Torr	No Growth

2.1.2. Results and discussions for MoS₂ structures

Optical microscopy images as bright field and as dark field of the growth MoS₂ with Glass-1 flakes shown in Figure 2.2. Grown MoS₂ flakes with Glass-1 have homogenous surfaces with the edge length of nearly 22.35 μm .

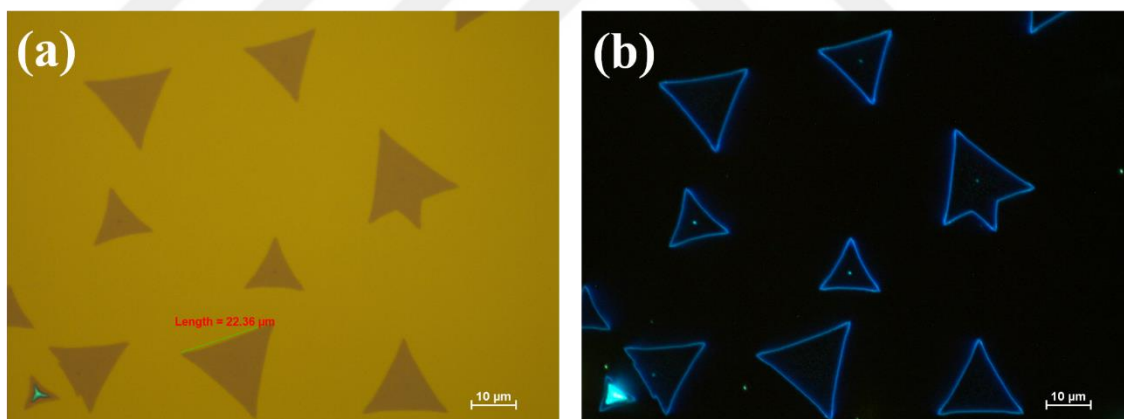


Figure 2.2 OM images of MoS₂ with Glass-1 (a) as bright (b) dark Field

In Figure 2.3, optical microscopy images as bright field and as dark field of the growth MoS₂ with Glass-2 flakes shown. The MoS₂ flakes grown with Glass-2 have nonhomogeneous surfaces. There are bulk MoS₂ formations on the edges and smaller flake structures at the centers of these flakes which are seen in the dark field images. The growth MoS₂ flakes with Glass-1 have longer edge length than Glass-2.

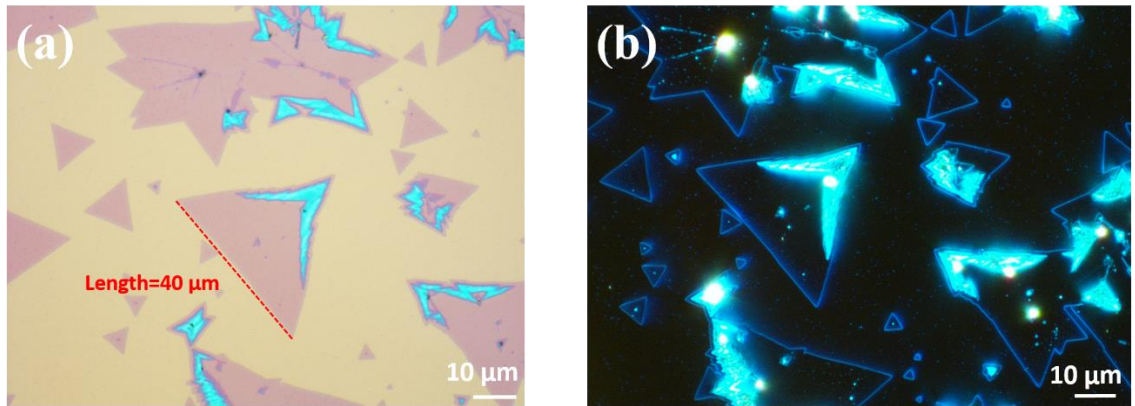


Figure 2.3 OM images of MoS₂ with Glass-2 (a) as bright (b) dark field

In Figure 2.4, Raman spectra analysis result of the monolayer MoS₂ growth flake with Glass-1 shown. According to literature MoS₂ have two characteristic peaks as E¹_{2g} and A_{1g} (Hong Li et al., 2012). The characteristic peaks are identified and deconvoluted to indicate the individual Raman modes using Lorentzian curves. Raman shift differences between A and E modes gives information of the layer number of MoS₂. The Raman shift differences between E and A modes found as $21 \pm 0.1 \text{ cm}^{-1}$. This result proved that the MoS₂ with Glass-1 is monolayer (Hong Li et al., 2012). In the experiment done with Glass-1, no additional peak is observed in Raman peaks of MoS₂.

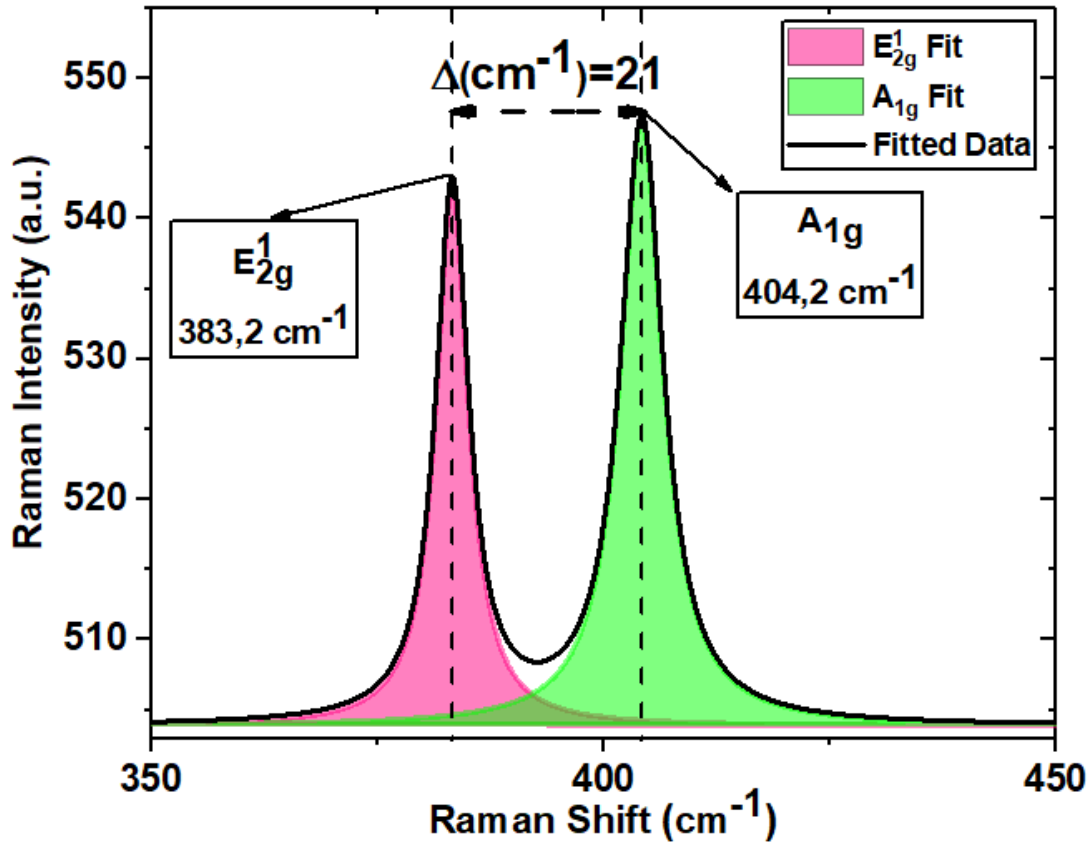


Figure 2.4 Raman spectra of MoS₂ with Glass-1

Raman spectra analysis result of monolayer MoS₂ flakes which was grown by using Glass-2 as catalyzer in CVD experiment is show in Figure 2.5. In this results it is seen that the Raman shifts of E mode and A mode of this monolayer MoS₂ is lying around 382.48 cm⁻¹ and 403.76 cm⁻¹, respectively. According to this characteristic peaks values, the difference between A and E modes found as 21.28 cm⁻¹. This result indicates the MoS₂ growth with Glass-2 shows monolayer feature (Hong Li et al., 2012). In that experiment no additional peak observed.

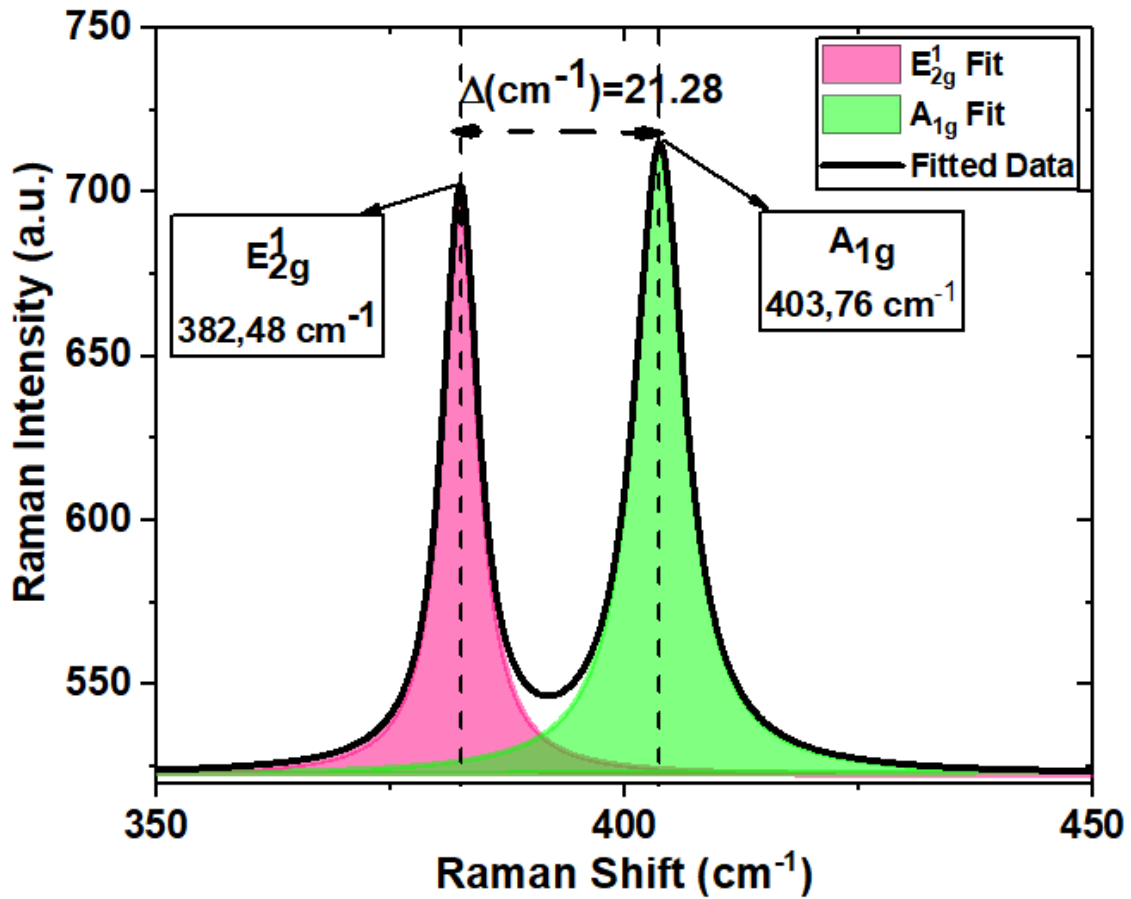


Figure 2.5 Raman spectra of MoS₂ with Glass-2

In Figure 2.6, PL spectra result of MoS₂ growth with Glass-1 shown. In this measurements 532 nm excitation wavelength laser is used at room temperature. Measured PL spectra of the MoS₂ material is deconvulated according to Gaussian curves. According to literature MoS₂ has three different radiative recombination mechanisms such as, A, B and trion (A⁻) which are based on exciton (Özden et al., 2016). MoS₂ growth with Glass-1 PL centers are observed as follows, A-exciton at 679.14 nm (1.83 eV), B-exciton at 637.24 nm (1.95 eV), A⁻-trion at 684.6 nm (1.81 eV). According to the PL centers of the MoS₂ growth with Glass-1, the growth structures shows monolayer feature (Zheng and Chen, 2017).

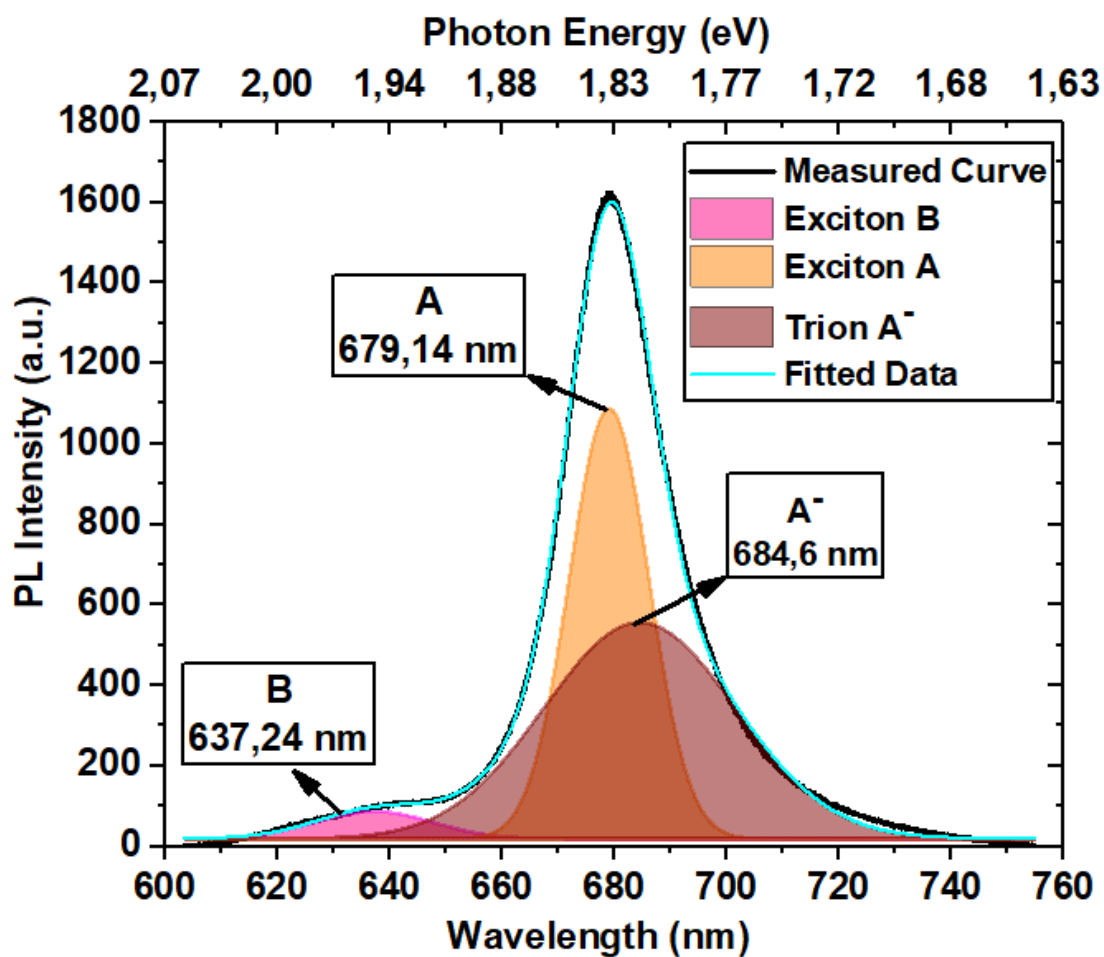


Figure 2.6 PL spectra of MoS₂ with Glass-1

The PL spectra centers of the grown MoS₂ material by using Glass-2 in CVD experiment are located as follows, A-exciton at 660.05 nm (1.88 eV), B-exciton at 618.6 nm (2 eV), A⁻-trion at 665.83 nm (1.86 eV), shown in Figure 2.7. According to these PL centers it can be said that the grown structure is a monolayer (Zheng and Chen, 2017).

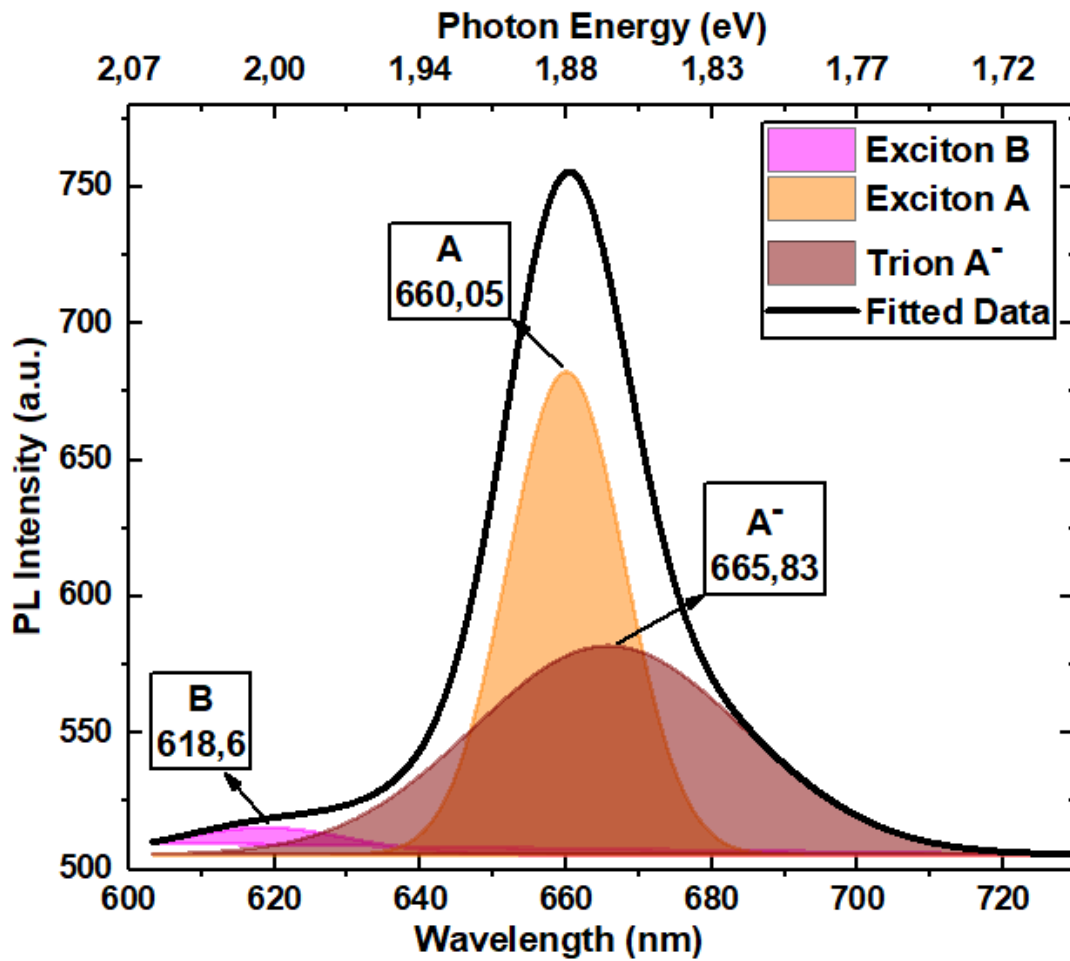
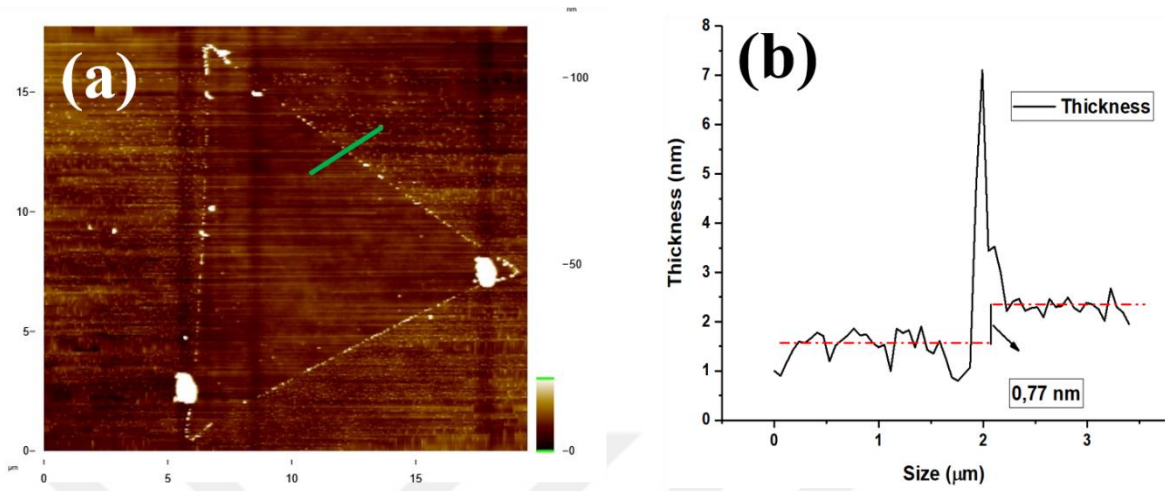
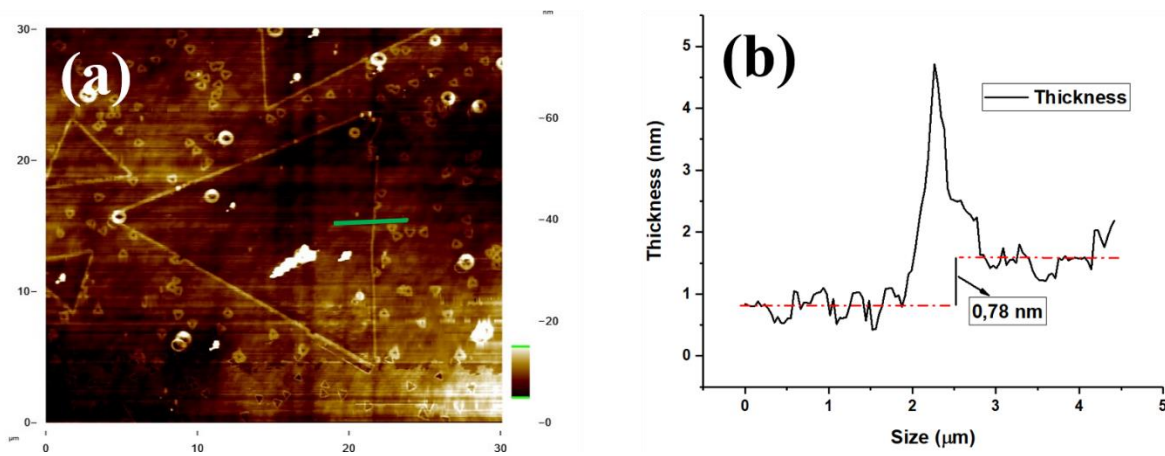


Figure 2.7 PL spectra of MoS₂ with Glass-2

AFM images and step high profiles of the growth MoS₂ with Glass-1 shown in the Figure 2.8. The thickness of the growth MoS₂ triangles are found to be 0.77 nm. This result show that the growth triangles are monolayer (Oh et al., 2016).



AFM image and the high profile of MoS₂ flake growth with Glass-2 shown on Figure 2.9. The thickness of the MoS₂ flake found as 0.78 nm which is indicating monolayer structure (Oh et al., 2016).



2.2. WS₂

Monolayer WS₂ consist of a tungsten layer sandwiched between two sulfur layers (Pawbake et al., 2016). Because of its layer dependent features monolayer WS₂ can be used in different applications (Georgiou et al., 2013; Rout et al., 2013; Huo et al., 2014). WS₂ can be produced by CVD method (Yorulmaz et al., 2019). In this thesis, WS₂ growth experiments were held by using piece of glass as catalyzer. By using piece of glass production of WS₂ with large surface area with CVD method has been possible, due to the dopants of the glasses. Our growth experiments showed that the dopants of the glasses have positive effect on producing large, homogenous and uniformly distributed flakes.

2.2.1. Experimental details

Before starting the experiments, the Si/SiO₂ substrates and glass pieces were cleaned by ultrasonic vibrational tool in three solvents. The Si/SiO₂ substrates and glass pieces were kept in each solvent for 5 minutes. The Si/SiO₂ substrates were annealed at 120°C for 5 minutes. In that experiment a piece of glass (2 cm x 2 cm) and two pieces of Si/SiO₂ substrates were used named as S-1 and S-2. 500 mg Sulphur powder (Sigma-Aldrich, 99.98%) and 4 mg tungsten trioxide (WO₃) powder (Sigma-Aldrich, 99.995%) were used in that experiment as precursor. The sulphur powder is placed on a quartz boat and the WO₃ powder is placed on the S-1 substrate. The S-1 substrate with WO₃ powder on it and the glass piece are positioned on the S-2 substrate side by side. The distance between sulfur powder and S-2 substrate is set to 18 cm, shown in Figure 2.10.

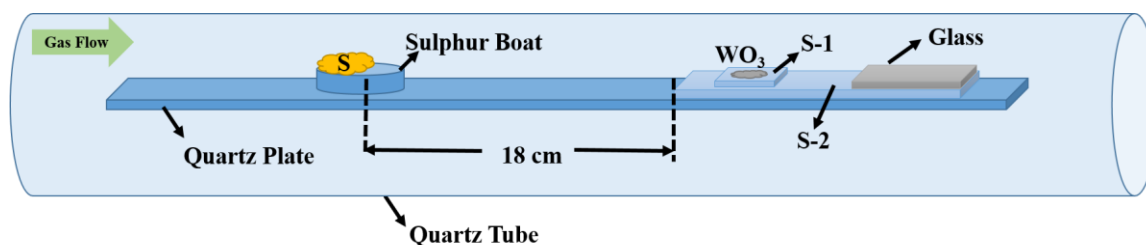


Figure 2.10 Schematic illustration of WS₂ growth experiment by CVD

As the carrier gases, hydrogen and argon were used. The MFC of the argon gas is set to 95 sccm and the MFC of the hydrogen gas is set to 5 sccm. Growth temperature of that experiment was set to 900°C and pressure was set to 740 Torr, listed in the below Table 2.4.

Table 2.4 *WS₂ growth parameters*

Amount of WO ₃ powder	4 mg
Amount of Sulphur powder	500 mg
Amount of Ar gas	95 sccm
Amount of H ₂ gas	5 sccm
Pressure Value	740 Torr
Temperature of the Furnace	900°C
Distance Between Powders	18 cm

Sulfur powder was located at 14 cm away from the entrance of the quartz tube where the furnace location was for the beginning of the experiment. After starting the experiment, Sulphur completely melted when the temperature of the furnace reached to 400°C and at this point the furnace was shifted right (8 cm away from the quartz boat) and left there until the furnace temperature reached to 900°C (corresponds to 900°C inner temperature). Afterwards, at the growth temperature, 900°C, the furnace was shifted to left side by 10 cm. All of the sulphur was evaporated in almost 3 min, which was the growth time of the experiment. The growth of WS₂ flakes occurred on the S-1 substrate. It was observed that the substrate was completely covered with WS₂ thin film and flakes. Because the diffusion rate of WO₃ is low, growth has only been realized on small substrate, which WO₃ powder was putted on.

2.2.1.1. Optimization of WS₂ growth parameters by CVD

Growth of WS₂ by CVD was a challenging process, because the WO₃ powder had very low diffusion rate therefore it was very difficult to react with Sulfur vapor to form WS₂ flake structures. In order to achieve optimum growth experiment values, many experimental setups were established and the parameters used during the experiments were changed in each experiment and the effects of the variables on flake formation were examined. From the previous experiments which made by our group members it is known that the appropriate temperature and pressure for WS₂ growth is 900°C and 740 Torr, respectively (Yorulmaz et al., 2019), so at these experimental setups the temperature and the vacuum pump values did not change. The experiment sets are listed in Table 2.5. After these set of experiments the optimum growth parameters for WS₂ were found as Experiment Set-5.

Table 2.5 Experimental parameters for WS₂ Growth

Experimental Setups	Amount of WO ₃	Amount of Sulphur	Temperature Value of Furnace	Types of Glass	The Pressure Value	Results
Different Deposition Processes	From 1.5 mg to 4 mg	From 250 mg to 400 mg	From 700°C to 750°C	Glass-1	From 730 Torr to 740 Torr	Nearly 20 µm flakes
Different Deposition Processes	From 1.5 mg to 4 mg	From 250 mg to 400 mg	From 700°C to 750°C	Glass-2	From 730 Torr to 740 Torr	Nearly 75 µm flakes
Different Deposition Processes	From 1.5 mg to 4 mg	From 250 mg to 400 mg	From 700°C to 750°C	Without any Glass	From 730 Torr to 740 Torr	No Growth

2.2.2. Results and discussions for WS₂ structures

Optical microscopy images and dark field images of the monolayer WS₂ flakes growth with Glass-1, shown in Figure 2.11. The WS₂ triangles have nearly 15.03 μm edge length and they have clean and homogenous surfaces.

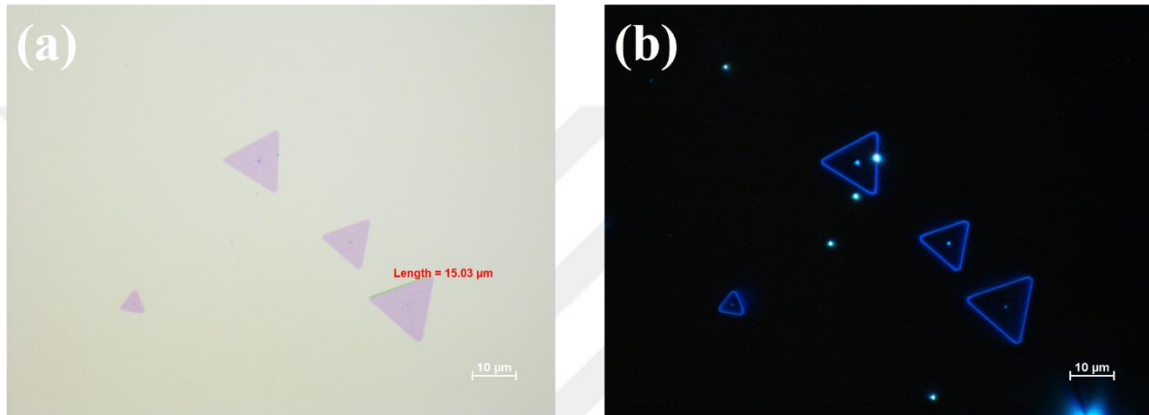


Figure 2.11 OM images of WS₂ with Glass-1 (a) as bright and (b) dark Field

In Figure 2.12, WS₂ growth with Glass-2 shown. As shown in the figures the WS₂ flake structures have bulk formations and small flakes on their surfaces. Their edge sizes of the WS₂ growth with Glass-2 are nearly 72.16 μm . These results show that the WS₂ flakes growth with Glass-2 have longer edge lengths than the WS₂ flakes growth with Glass-1. On the other hand, the WS₂ flakes growth with Glass-1 have more homogenous surfaces than the WS₂ flakes growth with Glass-2.

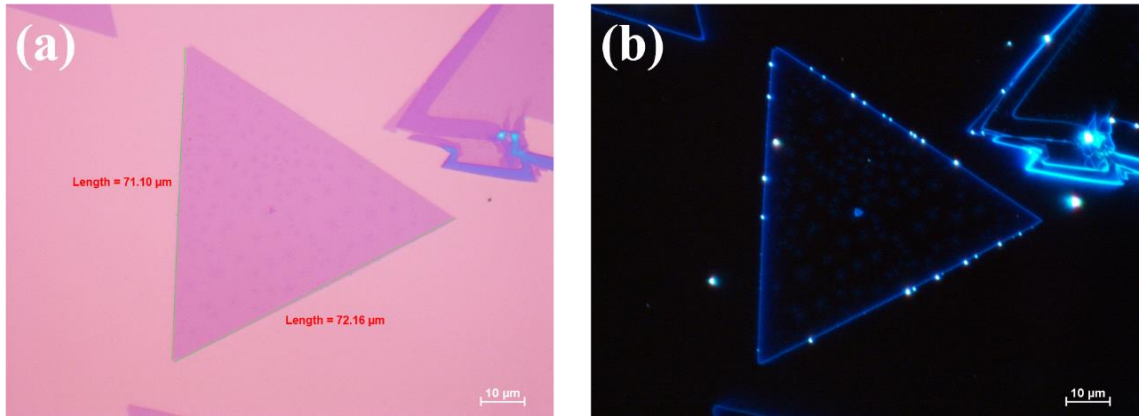


Figure 2.12 OM images of WS₂ with Glass-2 (a) as bright and (b) dark field

In Figure 2.13, the Raman spectrum of the experiment results of the Glass-1 with the characteristic peaks of WS₂ shown. The characteristic peaks are deconvoluted using Lorentzian curves to show the individual Raman modes (Shi et al., 2016). The WS₂ number of layers is estimated from Raman shift differences of E' and A₁ modes. Raman shift difference of the WS₂ growth with Glass-1 is found as $64.56 \pm 0.1 \text{ cm}^{-1}$. This result indicates that the WS₂ growth with Glass-1 is a monolayer structure (Shi et al., 2016). In the Raman spectrum analysis of the WS₂ growth with Glass-1 has not additional Raman peak due to the glass used in that growth experiment so WS₂ growth with Glass-1 is free of doping due to glass.

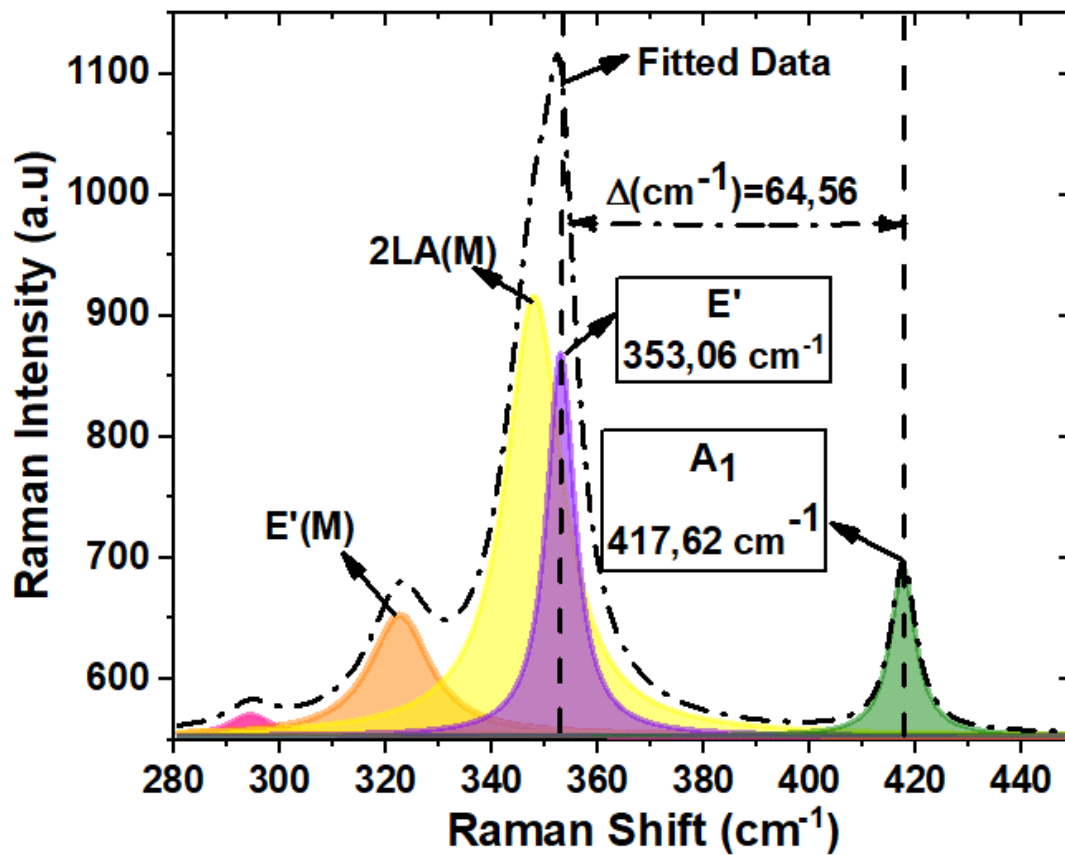


Figure 2.13 Raman spectra of WS₂ with Glass-1

The Raman spectrum of the WS₂ growth with Glass-2 shown in Figure 2.14. The E' Raman mode and the A₁ Raman mode are $351.95 \pm 0.1 \text{ cm}^{-1}$ and $417.30 \pm 0.1 \text{ cm}^{-1}$, respectively. The Raman shift differences between A and E modes is found as $65.35 \pm 0.1 \text{ cm}^{-1}$, which indicate that the WS₂ growth with Glass-2 is monolayer (Shi et al., 2016). The growth WS₂ flakes with Glass-2 have no additional Raman peaks.

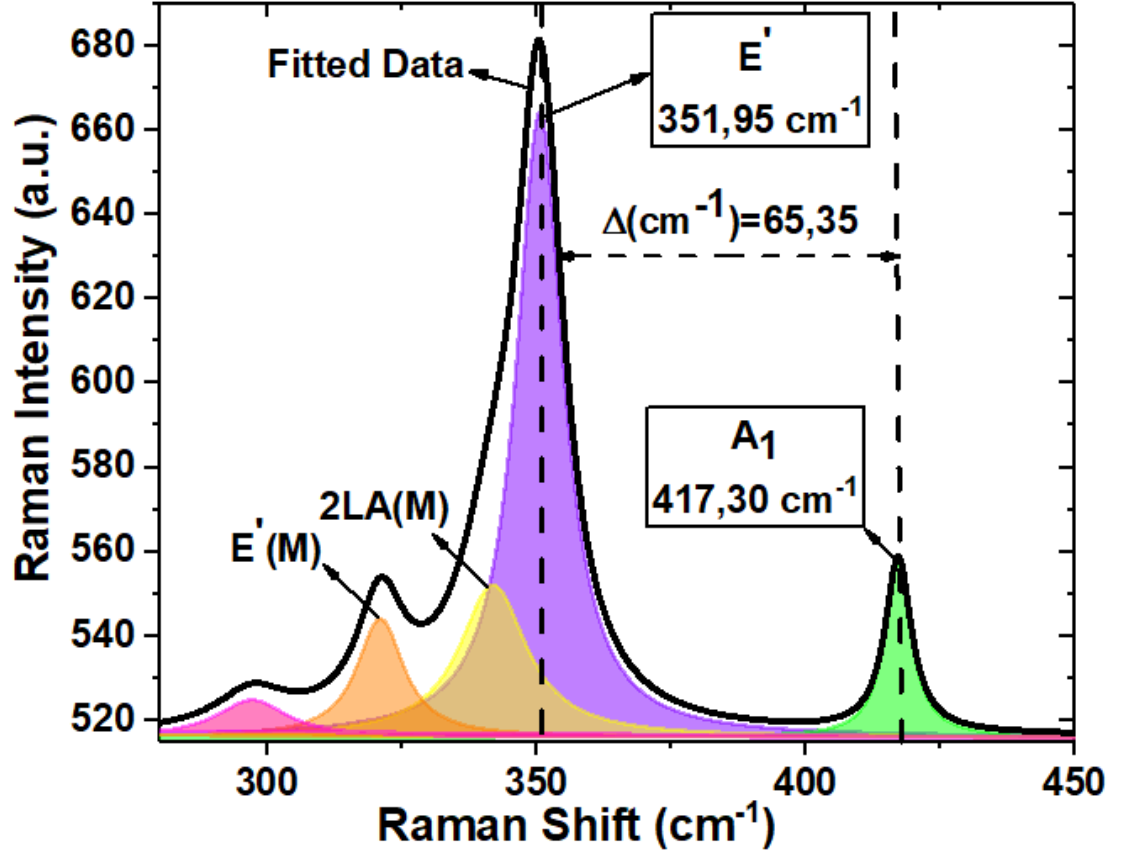


Figure 2.14 Raman spectra of WS₂ with Glass-2

PL spectra of the monolayer WS₂ growth with Glass-1 shown in Figure 2.15. Measurements are taken by 532 nm excitation wavelength laser at room temperature and the measured PL spectra of materials are deconvoluted according to Gaussian curves. The PL spectra of WS₂ structures have three different radiative recombination mechanisms that are based on neutral exciton (A⁰), trion (A⁻) or biexciton (AA). The PL spectral centers of the WS₂ growth with Glass-1 are located as follows, neutral exciton at 629 nm (1.97 eV), trion at 635 nm (1.95 eV), biexciton at 670 nm (1.85 eV). These results show that the WS₂ growth with Glass-1 is monolayer (B. Zhu et al., 2015).

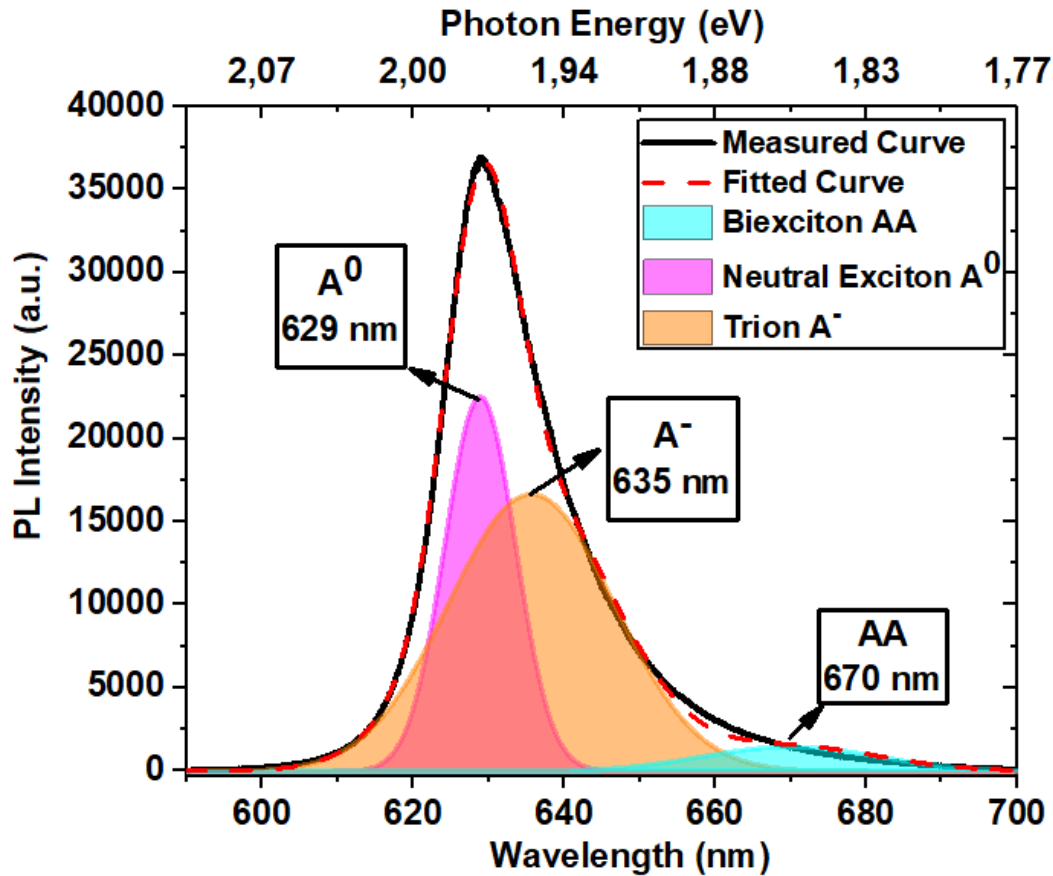


Figure 2.15 PL spectra of WS₂ with Glass-1

PL spectra of the monolayer WS₂ growth with Glass-1 shown in Figure 2.16. Measurements are taken by 532 nm excitation wavelength laser at room temperature and the measured PL spectra of materials are deconvoluted according to Gaussian curves. The PL spectra of WS₂ structures show three different radiative recombination mechanisms that are neutral exciton (A⁰), trion (A⁻) or biexciton (AA). The photo luminance spectral centers of the WS₂ growth with Glass-2 are located as follows, neutral exciton at 629 nm (1.97 eV), trion at 635 nm (1.95 eV), biexciton at 668 nm (1.85 eV). These results show that the WS₂ growth with Glass-2 is monolayer, too (B. Zhu et al., 2015).

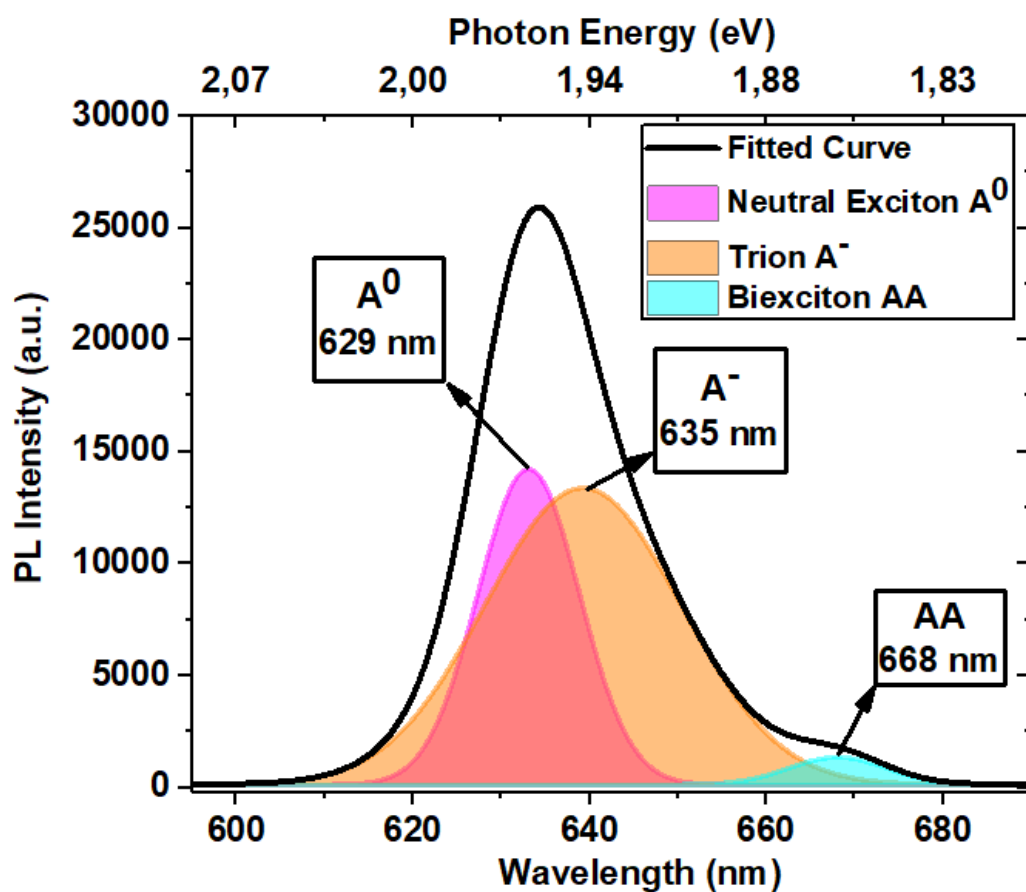
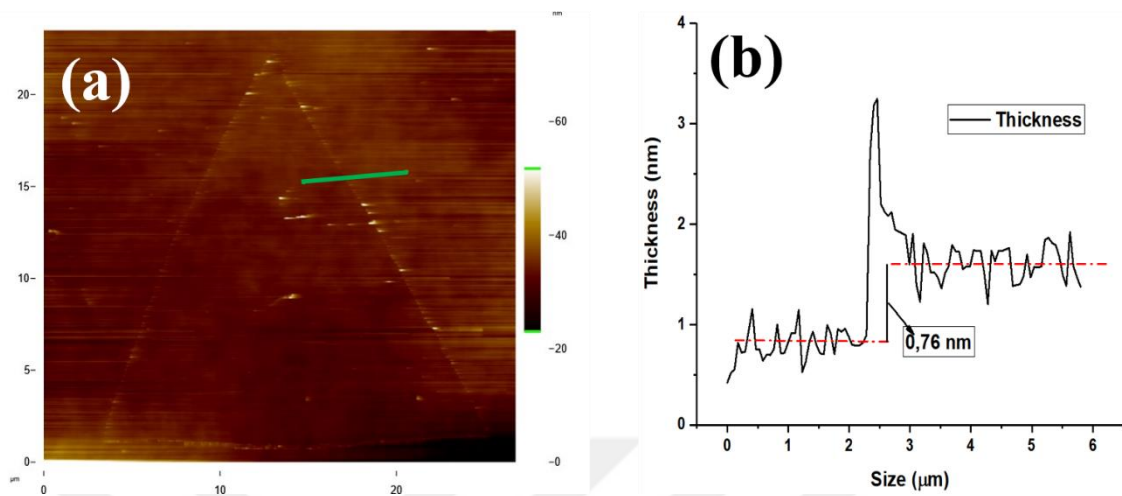
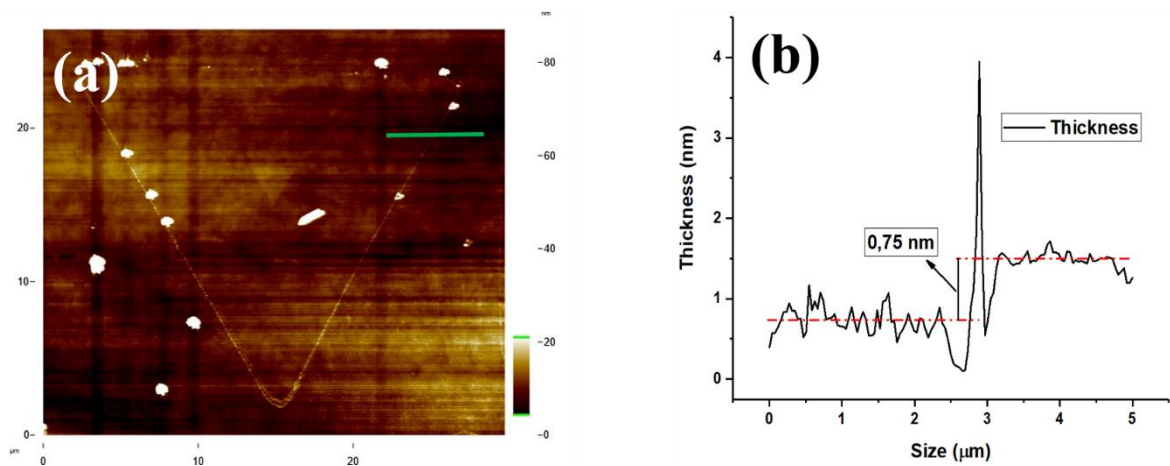


Figure 2.16 PL spectra of WS₂ with Glass-2

Figure 2.17 depicts an AFM image and the step high profile of the WS₂ flake growth with help of Glass-1. According to the step high profile measurement the thickness of the WS₂ flake is found as 0.76 nm. The result of the step high profile of the WS₂ gives an evidence of monolayer growth (Kang et al., 2015).



In the Figure 2.18 the AFM image and the step high profile taken from the AFM image of the WS₂ flake growth with Glass-2 shown. In that step high profile, it is seen that the thickness of the WS₂ flake growth with Glass-2 is found as 0.75 nm so the WS₂ flake is monolayer (Kang et al., 2015).



2.3. MoSe₂

Monolayer MoSe₂ is also one of TMDCs (X. Wang et al., 2014). As changing from bulk to monolayer the band structure of MoSe₂ is changing from indirect (1.1 eV) to direct (1.5 eV), getting appropriate for the fabrication of transistors and photodetectors devices (Xia et al., 2014). In this thesis for the purpose of obtaining MoSe₂ with large area and homogeneously distributed on the substrate glass was used in CVD experiments as catalyzer.

2.3.1. Experimental details

Before starting the experiments, the Si/SiO₂ substrates and glass pieces were cleaned by ultrasonic vibrational tool in three solvents. The Si/SiO₂ substrates and glass pieces were kept in each solvent for 5 minutes. The Si/SiO₂ substrates were annealed at 120°C for 5 minutes. In that experiment a piece of glass (2 cm x 2 cm) and two pieces of Si/SiO₂ substrates were used named as S-1 and S-2. 500 mg selenium powder (Sigma-Aldrich, 99.5%) and 4 mg MoO₃ powder (Sigma-Aldrich, 99.995%) were used in that experiment as precursor. The selenium powder is placed on a quartz boat and the MoO₃ powder is placed on the S-1 substrate. The S-1 substrate with MoO₃ powder on it and the glass piece are positioned on the S-2 substrate side by side. The distance between selenium powder and S-2 substrate is set to 16 cm, shown in Figure 2.19.

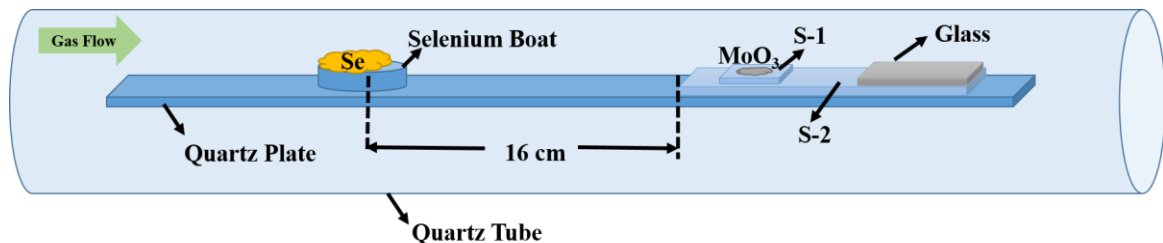


Figure 2.19 Schematic illustration of MoSe₂ growth experiment by CVD

As the carrier gases, hydrogen and argon were used. The mass flow controller (MFC) of the argon gas is set to 95 sccm and the MFC of the hydrogen gas is set to 5 sccm. Growth temperature of that experiment was set to 900°C and pressure was set to 730 Torr, listed in Table 2.6.

Table 2.6 *MoSe₂ growth parameters*

Amount of MoO ₃ powder	4 mg
Amount of Selenium powder	500 mg
Amount of Ar gas	95 sccm
Amount of H ₂ gas	5 sccm
Pressure Value	730 Torr
Temperature of the Furnace	900°C
Distance Between Powders	16 cm

Selenium powder was located at 14 cm away from the entrance of the quartz tube where the furnace location was for the beginning of the experiment. After starting the experiment, selenium completely melted when the temperature of the furnace reached to 450°C and at this conditions the furnace was shifted right (4 cm away from the quartz boat) and left there until the furnace temperature reached to 900°C. Afterwards, at the growth temperature, 900°C, the furnace was shifted to left side by 6 cm. All of the selenium was evaporated from the quartz boat within almost 6 min, which was the growth time of the experiment. The growth of MoSe₂ flakes occurred on the S-2 substrate. It has been observed that the MoSe₂ flakes, which are observed more intensively and bigger in the vicinity of the glass, have decreased and their sizes become small as they moved away from the glass.

2.3.1.1. Optimization of MoSe₂ growth parameters by CVD

In order to achieve optimum growth experiment values, many experimental setups were utilized and the parameters used during the experiments were changed in each experiment

and the effects of the variables on flake formation were examined. From the previous experiments which made by our group members it is known that the appropriate temperature and pressure for MoSe₂ growth is 900°C and 730 Torr, respectively, so at these experimental setups the temperature and the vacuum pump values did not change. The experiment sets are listed in Table 2.7. After these set of experiments the optimum growth parameters for MoSe₂ were found as Experiment Set-5.

Table 2.7 Experimental parameters for MoSe₂ growth

Experimental Setups	Amount of MoO ₃	Amount of Selenium	Temperature Value of Furnace	Types of Glass	The Pressure Value	Results
Different Deposition Processes	From 1.5 mg to 4 mg	From 250 mg to 400 mg	900°C	Glass-1	730 Torr	Nearly 25 μm flakes
Different Deposition Processes	From 1.5 mg to 4 mg	From 250 mg to 400 mg	900°C	Glass-2	730 Torr	Nearly 70 μm flakes
Different Deposition Processes	From 1.5 mg to 4 mg	From 250 mg to 400 mg	900°C	Without any glass	730 Torr	No growth

2.3.2. Results and discussions for MoSe₂ structures

In Figure 2.20 optical microscopy images and the dark field images of MoSe₂ growth with Glass-1 shown. This optical microscopy images show that the grown MoSe₂ have nearly 22.3 μm and homogenous surfaces.

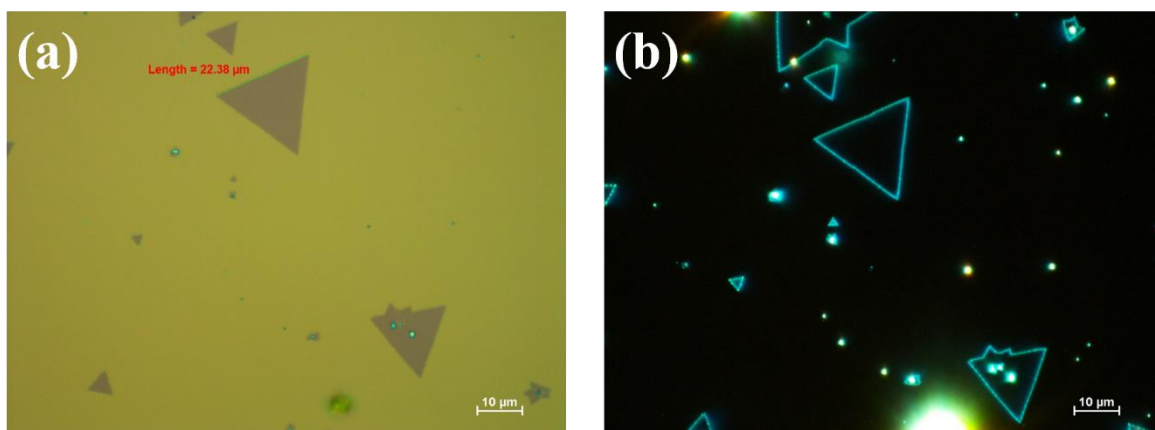


Figure 2.20 OM images of MoSe₂ with Glass-1 (a) as bright and (b) dark field

In Figure 2.21 the optical microscopy images and the dark field images of MoSe₂ growth with Glass-2 shown. In the bright field image, it is shown that the edge length of the MoSe₂ is nearly 68.74 μm. In the dark field image, the surface of the MoSe₂ flake is shown and it is seen that the surface of the flake is nonhomogeneous. According to these results it can be said that the MoSe₂ flakes growth with Glass-1 have more homogenous surfaces than the MoSe₂ flakes growth with Glass-2 and the MoSe₂ flakes growth with Glass-2 have longer edge length than the MoSe₂ flakes growth with Glass-1.

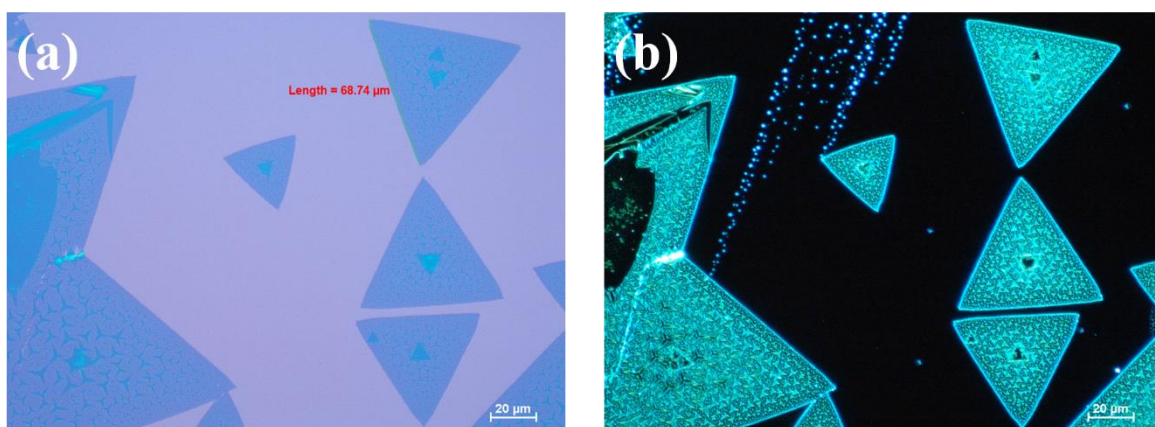


Figure 2.21 OM images of MoSe₂ with Glass-2 (a) as bright and (b) dark field

Figure 2.22 depicts Raman spectra analysis of MoSe₂ flakes growth with Glass-1 with the characteristic peaks of MoSe₂ (A_{1g} and E_{2g}¹). For indicating individual Raman modes the peaks are identified and deconvoluted using Lorentzian curves. For MoSe₂ the number of layer is estimated from the location of the A_{1g} mode (Gong et al., 2016; Zheng and Chen, 2017). A_{1g} and E_{2g}¹ modes of MoSe₂ are located at $240 \pm 0.1 \text{ cm}^{-1}$ and $285 \pm 0.1 \text{ cm}^{-1}$, respectively. These results indicate that MoSe₂ flakes are monolayer for the experiments with Glass-1 (Gong et al., 2016).

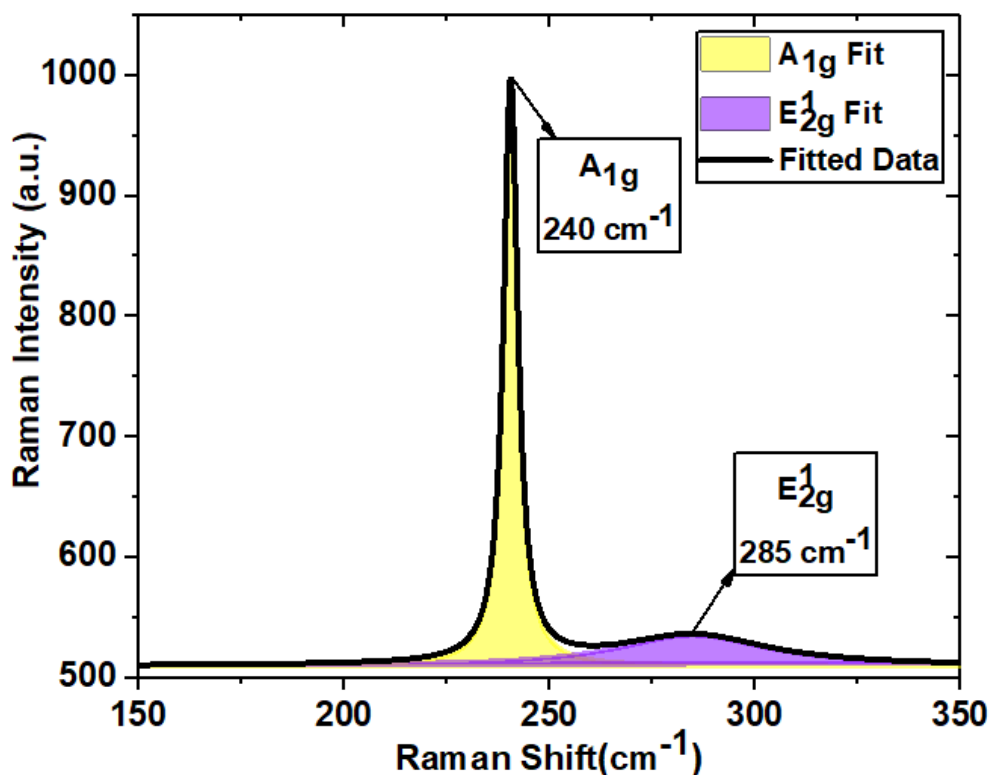


Figure 2.22 Raman spectra of MoSe₂ with Glass-1

Figure 2.23 shows Raman spectra analysis of MoSe₂ flakes growth with Glass-2 with the characteristic peaks of MoSe₂ (A_{1g} and E_{2g}¹). For indicating individual Raman modes the peaks are identified and deconvoluted using Lorentzian curves. A_{1g} and E_{2g}¹ modes of MoSe₂

growth with Glass-2 are located at $239 \pm 0.1 \text{ cm}^{-1}$ and $293 \pm 0.1 \text{ cm}^{-1}$, respectively. These results indicate that MoSe₂ flakes growth with Glass-2 are monolayer (Gong et al., 2016).

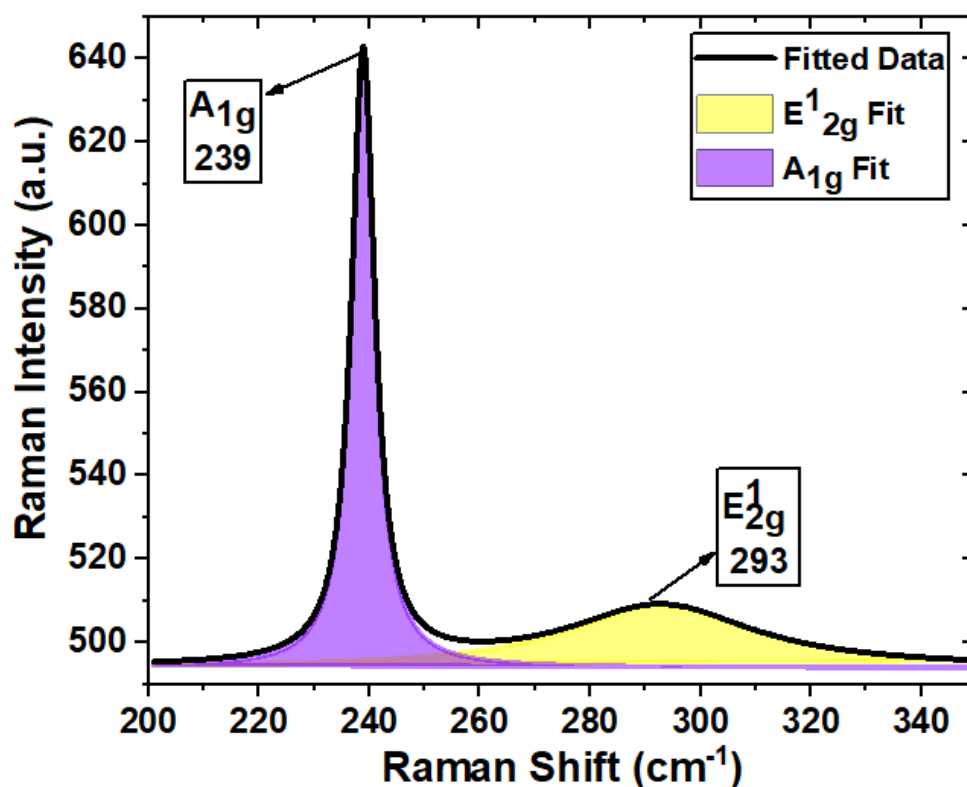


Figure 2.23 Raman spectra of MoSe₂ with Glass-2

In the Figure 2.24 the PL spectra of MoSe₂ flakes growth with Glass-1 shown. The measurements are taken at room temperature by 532 nm excitation wavelength laser. The measured photoluminescence spectra of materials are deconvoluted according to Gaussian curves. The PL centers of MoSe₂, produced by help of Glass-1, are located as follows, A-exciton at 823 nm (1.51 eV) and B-exciton at 720 nm (1.72 eV). These PL centers prove that the MoSe₂ growth with Glass-1 is monolayer (Shim et al., 2014).

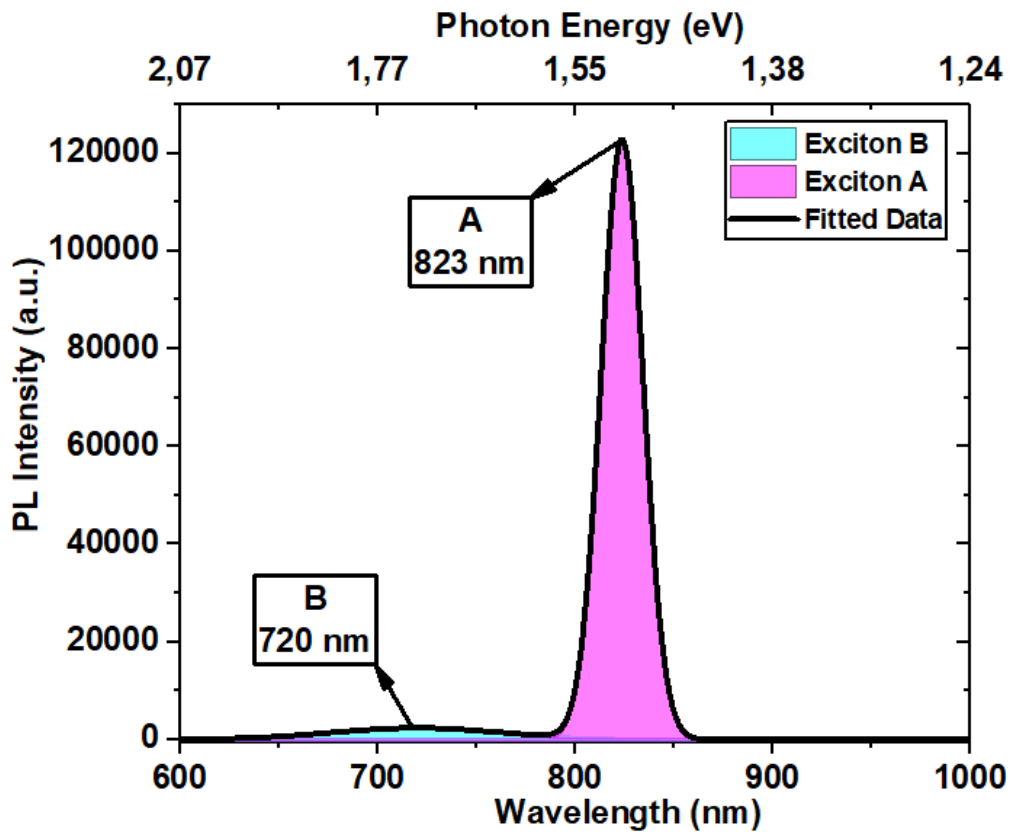


Figure 2.24 PL spectra of MoSe₂ with Glass-1

In the Figure 2.25 the PL spectra of MoSe₂ flakes growth with Glass-2 shown. The measurements are taken at the same conditions as before, at room temperature by using 532 nm excitation wavelength laser. The measured photoluminescence spectra of materials are deconvoluted according to Gaussian curves. The PL centers of MoSe₂, produced by help of Glass-2, are located as follows, A-exciton at 825 nm (1,50 eV) and B-exciton at 720 nm (1.72 eV). These PL centers prove that the MoSe₂ growth with Glass-2 is monolayer, too (Shim et al., 2014).

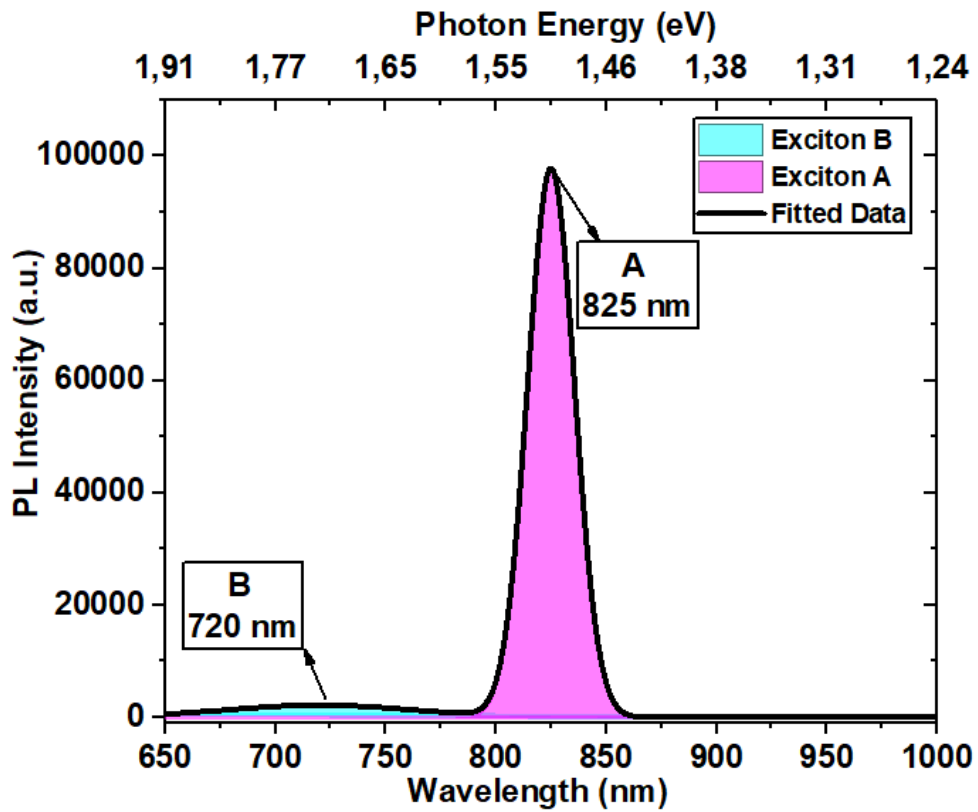
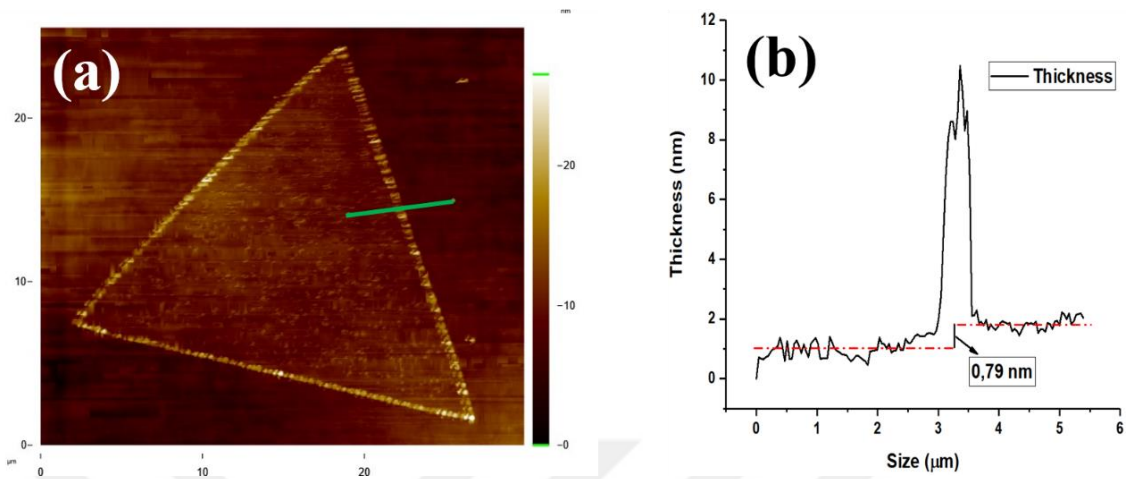
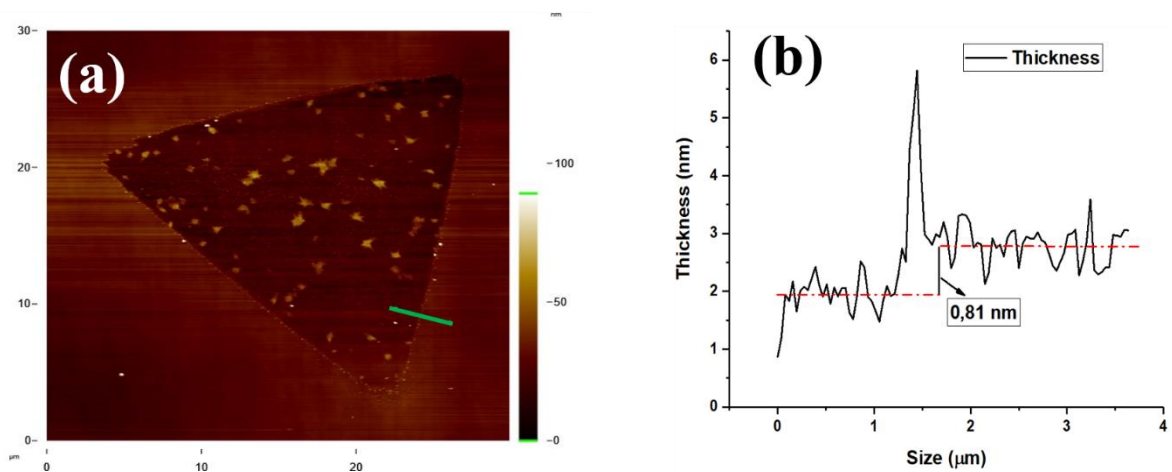


Figure 2.25 PL spectra of MoSe₂ with Glass-2

Figure 2.26 depicts an AFM image and the step high profile of the MoSe₂ flake growth with help of Glass-1. According to the step high profile measurement the thickness of the MoSe₂ flake is found as 0.79 nm. The result of the step high profile of the MoSe₂ gives an evidence of monolayer growth (Tongay et al., 2013).



In the Figure 2.27 the AFM image and the step high profile taken from the AFM image of the MoSe₂ flake growth with Glass-2 is shown. In that step high profile, it is seen that the thickness of the MoSe₂ flake growth with Glass-2 is found as 0.81 nm so the MoSe₂ flake is monolayer (Tongay et al., 2013).



By using a piece of glass in CVD chamber when doing growth experiments, the challenge of growing large-area transition metal dichalcogenide (TMDC) monolayers with a high-coverage has been overcome. By using two types of glass in the MoS₂, WS₂ and MoSe₂ growth experiments the effect of the glass dopants on growth experiments is studied. Our results show that although the uniformity and flake sizes change with the composition of the glasses, MoS₂, WS₂ and MoSe₂ monolayer flakes have been grown successfully for both of the glass types. So, the catalytic effect of using a glass in the CVD process has been confirmed. The growth is realized on Si/SiO₂ substrate and thus the transfer requirement has been eliminated. For gas sensor applications FET is fabricated from the growth samples. In the following section FET fabrication steps are described.

3. DEVICE FABRICATION

In Chapter 1, TMDC materials and their applications were described in details. As mentioned in Chapter 1, TMDC materials based FET devices can be used as gas sensor. In Chapter 2 monolayer TMDC materials produced during this thesis and their properties were elaborated. By using these produced monolayer TMDC materials FET device was designed and fabricated for the purpose of detecting gas. The fabrication of the FET device consists of mask design, transferring of the produced flake structures, photolithography, metal coating and lift off processes.

First of all, monolayer TMDC flakes to be used in the production of FET device are produced by using CVD method. After producing the flake structures, if the flake structures need to be transferred, then the transfer process takes place. Then, the photoresist is coated with the help of the spin coater and then annealing process is performed to allow the photoresist material to dry on the substrate. After that, photolithography process is performed to transfer an image from the mask to a substrate. If FET patterns on the mask do not coincide with the TMDC flake structures and the FET device with TMDC flake as semiconductor layer is not formed, the photoresist coating on the substrate is cleaned with acetone and the process is repeated. After photolithography process is finished, metal coating, lift off and baking are done. Flow chart of all these production processes shown in Fig.3.1.

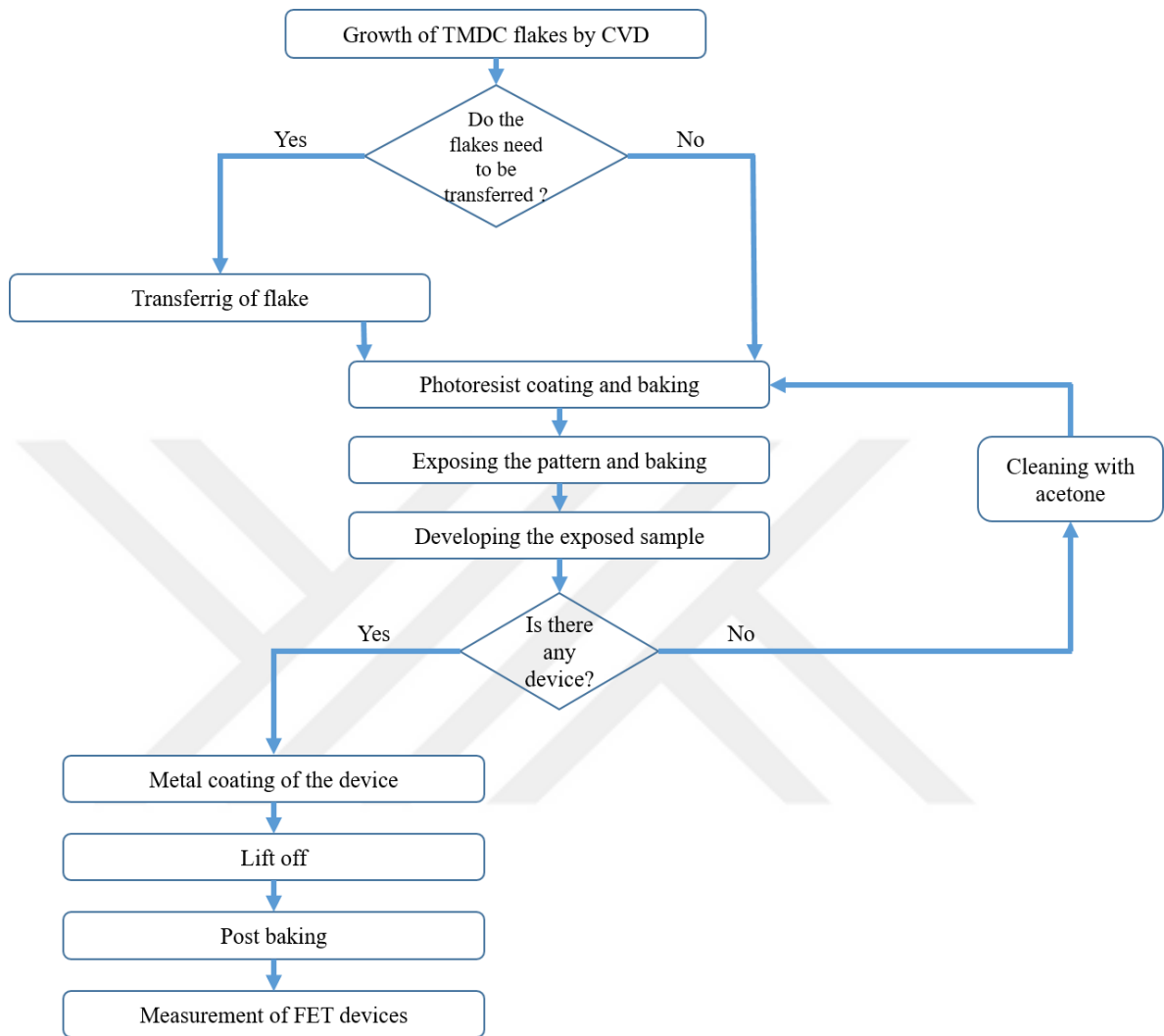


Figure 3.1 Flow chart of the FET device fabrication processes

As per the fabrication steps, this chapter is divided into five sections. Section 3.1 describes the detail process of mask design adopted in gas sensor fabrication. Transfer process is explaining in section 3.2. Photolithography is performed for the transfer of mask pattern and discussed in detail in sections 3.3. Finally, the metal coating process and the lift off processes and measurement of the FET devices are discussed in sections 3.4 and 3.5, respectively.

3.1. Mask Design for Gas Sensor Applications

When designing a layout mask there are some important and useful things to ensure that the correct mask is used for the appropriate step in a process sequence. When designing a mask layout first of all, the patterns of the mask should be designed according to the material to be used in FET construction and the purpose of using the FET device to be produced. Then, the layout should include the name of the designer and the date when it is designed. This makes it easier to find the owner of a mask when it is misplaced, and it is beneficial to know how old it is if there are several similar masks. When the mask is used for multi-layer lithography alignment marks have to be included.

In this thesis designing the layout was the process that the patterns were transferred to the mask which were defined as the geometry of the devices. The layout is generally performed in a graphical editing tool L-Edit because L-Edit support GDSII file format and this is the format that is needed when the mask is ordered from a manufacturer. In this thesis L-Edit was used to design the layout.

There are some important issues to be considered in TMDC-based FET devices which were designed as gas sensors. The most important consideration was that the gas could react as much as possible with the TMDC material acting as a semiconductor in the FET devices and using interdigitated electrodes (IDEs) pattern provides expansion of the semiconductor surface in contact with gas. There were many examples in the literature for TMDC based gas sensors. Most gas sensors in the literature were designed as IDEs. For example, MoS₂ film based FET device was used to detect NH₃, the interdigitated electrode (IDE) pattern used for the contacts (Gatensby et al., 2014). A chemiresistor device by using MoS₂ film was designed to detect NH₃ with the pattern of IDE (K. Lee et al., 2013). WS₂ based chemiresistor was used to detect NH₃ with the patterning of IDE, shown in Figure 3.2 (O'Brien et al., 2014). WSe₂ based FET device was patterned as IDE and used to detect NO₂ gas (Ko et al., 2018).

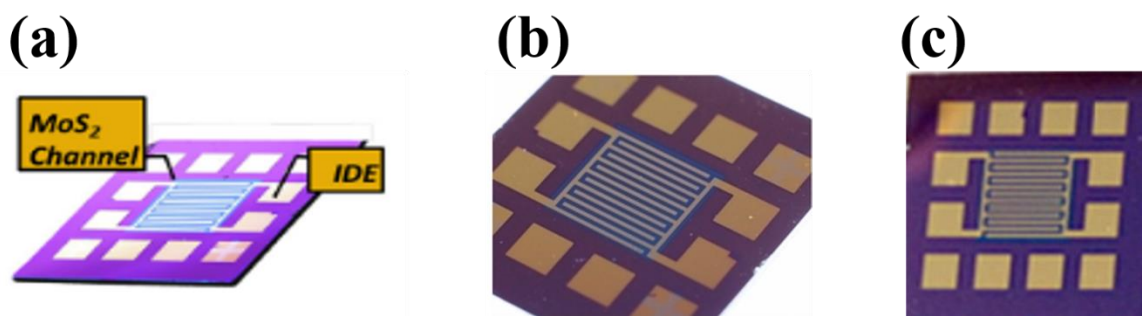


Figure 3.2 IDE patterned (a) MoS₂ (b) MoS₂ (c) WS₂ based devices for gas detection

In this thesis study the mask was designed as a 4-inch square plate, dark field mask by using L-Edit program. Because in general bright field masks are used with negative resists and dark field masks with positive resists. Dark field means that the mask looks like the negative of the layout (the space left open in layout is opaque). The overall picture of the mask shown in Figure 3.3.

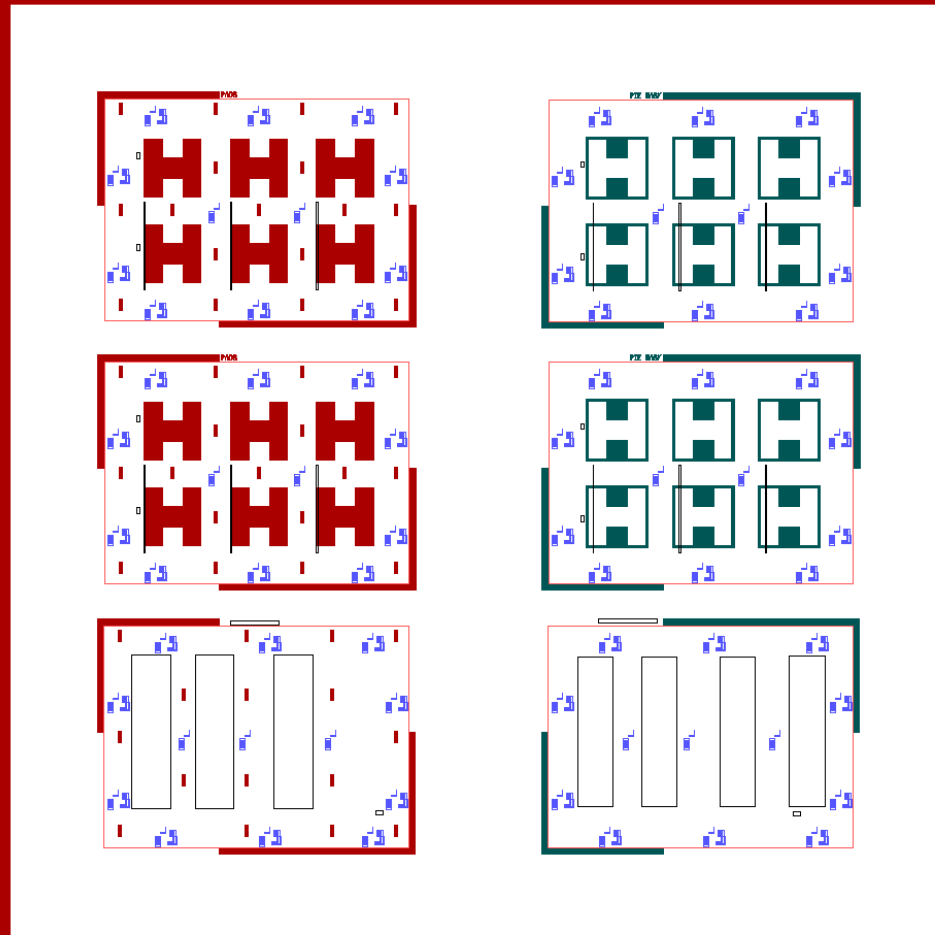


Figure 3.3 Overall view of the designed gas sensor device mask

For the purpose of gas sensor FET device design IDE patterns were used in this designing study. The contact pads were designed to be easy to see clearly while taking measurements in a gas sensing test set-up. The dimensions of the TMDC flake structures that we produce while deciding the dimensions of the IDE designs are taken into consideration. The TMDC flake size produced by CVD in that study was changing from nearly $10\ \mu\text{m}$ to $120\ \mu\text{m}$ so three different IDE patterns with the gaps between two fingers as $10\ \mu\text{m}$, $50\ \mu\text{m}$

and 100 μm were designed named as IDE-1, IDE-2 and IDE-3, respectively and shown in Figure 3.4. The dimensions for each proposal IDE pattern are listed in Table 3.1.

Table 3.1 *Dimensions of IDE patterns used in the design*

	IDE-1	IDE-2	IDE-3
Gaps between two electrodes	10 μm	50 μm	100 μm
Width of electrodes	50 μm	50 μm	50 μm
Length of electrodes	1.39 mm	1.35 mm	1.3 mm
Contact pads dimensions	1.6 mm x 1.6 mm	1.6 mm x 1.6 mm	1.6 mm x 1.6 mm
Active area	$1.1895 \times 10^{-6} \text{ m}^2$	$3.6225 \times 10^{-6} \text{ m}^2$	$4.79 \times 10^{-6} \text{ m}^2$
Total IDE size	5 mm x 4.97 mm	5 mm x 4.95 mm	5 mm x 5 mm

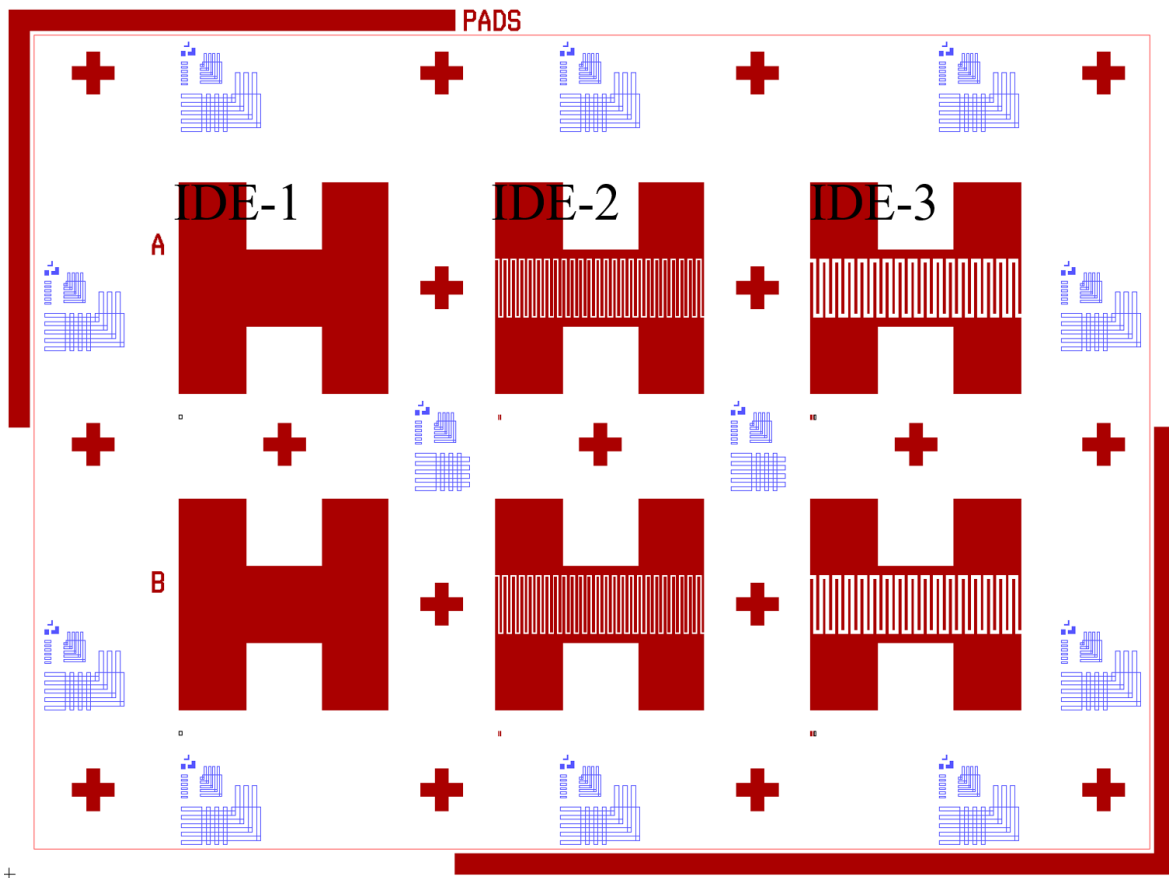


Figure 3.4 *Designed IDE patterns of the metal mask for gas sensor applications*

This mask contains metal mask named as PADS and RIE etching mask named as RIE MASK, shown in Figure 3.5. The metal mask layout and the etching mask layout will be used as sequential.

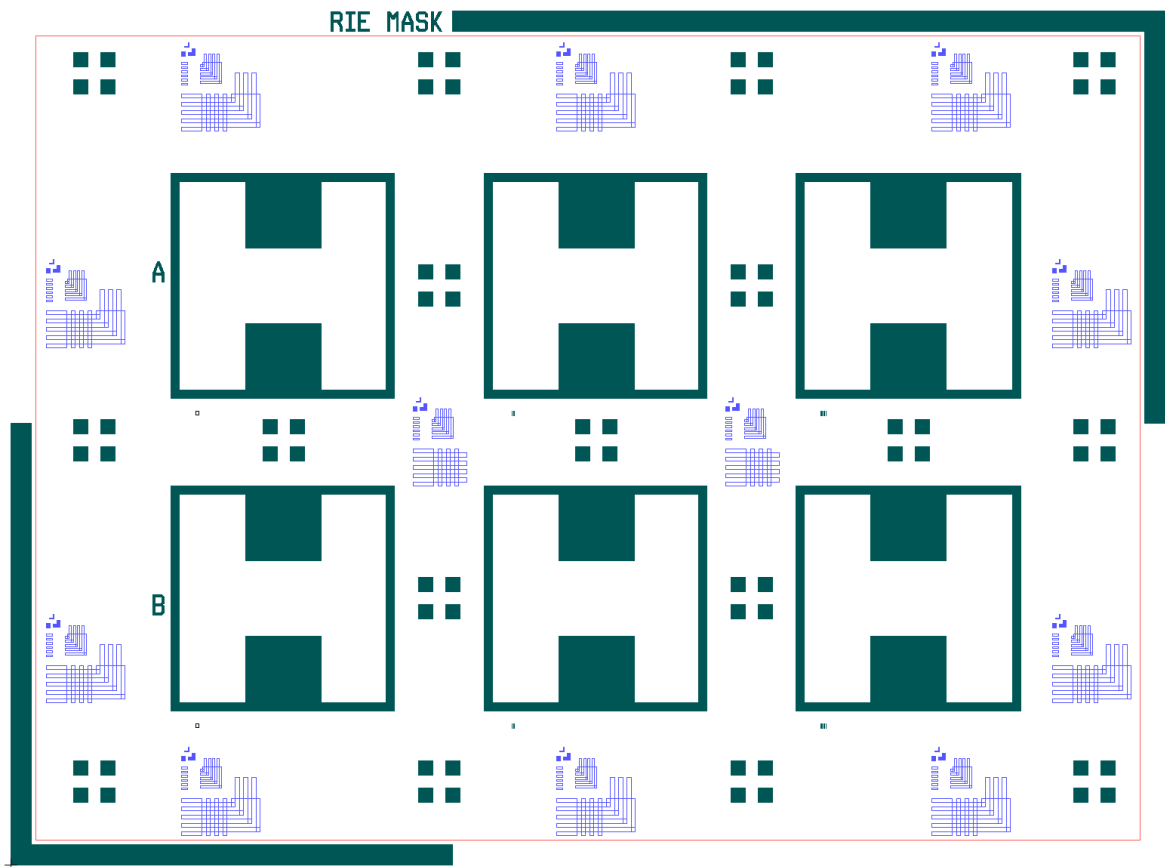


Figure 3.5 *Designed etching layout patterns*

The two of the layout contain alignment marks and name of them top of the designs. The mask also contains resolution test patterns as shown in blue color in Figure 3.6. The resolution test patterns are used to measure the resolution limits can be customized and scaled to the size range of interest to the application.

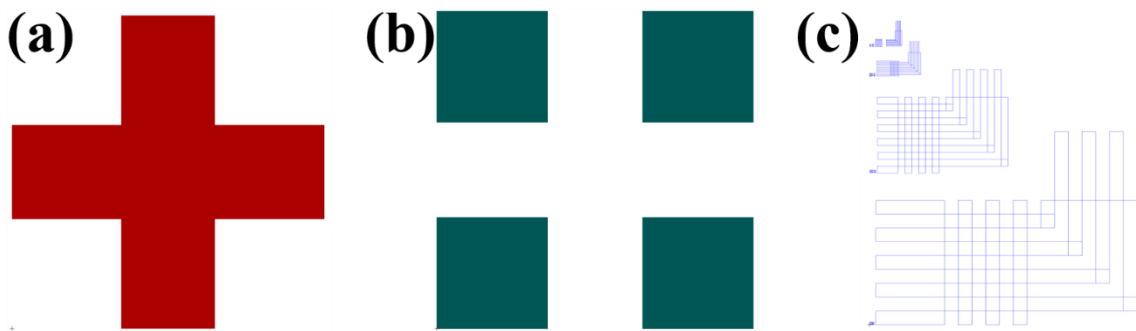


Figure 3.6 Alignment marks of the (a)metal (b)etching (c)resolution test patterns

3.2. Transfer of the TMDC Flakes

Transfer of the TMDC flake from the grown substrate to another substrate is an important process while fabricating a device. The most important thing to consider when transferring flake structures from one substrate to another is the fact that the flake structures can remain intact. The transfer of the TMDC flake is necessary when the flakes are grown on glass, sapphire, etc. For example, when TMDC flakes grown on glass the transfer of the TMDC flakes from glass to Si/SiO₂ is done step by step as follows;

- Si/SiO₂ wafer is diced with the glass dimensions and cleaned with three solvents as acetone, propanol-alcohol and DI water.
- The glass is coated with poly (methyl methacrylate) (PMMA) with help of spin coater. The maximum speed, spin time and the acceleration of the spin coater are set to 750 revolutions per minute (rpm), 40 seconds and 500 rpm/s, respectively.
- The coated glass is baked at 130°C for 2 minutes.
- After baking, the PMMA coated glass is slowly inserted into deionized water (DI water) until glass and PMMA separated from each other.
- TMDC flakes are now on PMMA material after separation has taken place. The PMMA separated from the glass is fished out of the DI water using Si/SiO₂.
- The Si/SiO₂ is baked at 70°C until the PMMA adhere to the Si/SiO₂ surface.

- After Si/SiO₂ and PMMA are bonded together, Si/SiO₂ is heated at 50°C in acetone bath. The purpose of this process is to make the PMMA material melt away from the surface of Si/SiO₂.
- The TMDC/Si/SiO₂ is taken out, washed with acetone and isopropanol.

But in this thesis the TMDC flakes were grown on Si/SiO₂ substrate so the flakes were not transferred on another substrate. By using the TMDC flakes on the Si/SiO₂ substrate a device can be produced.

3.3. Photolithography

The lithography is defined as the transfer of an image from a mask to a substrate by using a photosensitive material (Shie and Yang, 2008). There are two types of photoresist can be used in lithography process as negative and positive photo resist. Positive photo resist contains three compounds as, a photosensitive, a base resin and an organic solvent. Before exposure process, the photosensitive material is insoluble in the developer solution. After exposure process, the photosensitive material absorbs radiation in the exposed pattern areas then changes its chemical structure and becomes soluble in the developer solution. After developer solution, the exposed areas can be removed.

In this thesis study positive photo resist process was utilized. Figure 3.7 shows the flow chart of photolithography process in the FET fabrication. First the photo-resist (AZ5215E) was coated on the Si/SiO₂ substrate with 1.4 μm thickness by using a spin coater of 6000 rpm. The processed substrate was annealed at 110°C for 50 seconds on a hot plate device. After the annealing, the substrate was employed in the mask aligner (KARL SUSS MJB4 Mask Aligner) for the exposure of UV radiation for 10 seconds. After UV radiation treatment, the exposed substrate in UV radiation is then treated with a developer (AZ351B developer) solution for 50 seconds to dissolve the photo resist. The developer solution was prepared with the ratio of 1:4, 1 part of concentrate and 4 parts of DI-water. After lithography process, the Si/SiO₂ wafer was coated with metal. The metal coating process will be described in the following section.

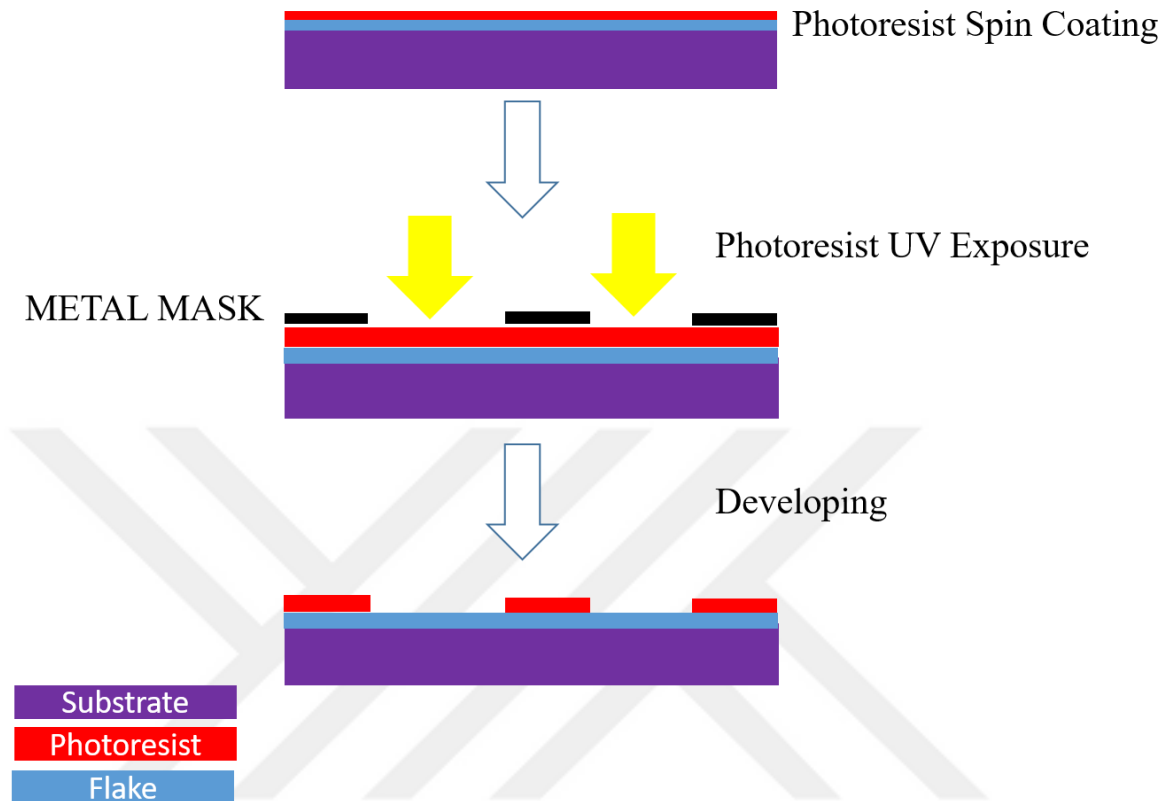


Figure 3.7 Schematic view of the mechanism of positive photo resist

3.4. Metal Coating and Lift-off Processes

During the metal coating process electron-beam physical vapor deposition (EBPVD) apparatus was used. EBPVD, is the form of physical vapor deposition method. A target anode is bombarded by an electron beam given off by a charged tungsten filament under high vacuum conditions. Metal atoms transform into the gaseous phase caused by the electron beam. These atoms then turn into solid form, coating everything in the vacuum chamber with a thin layer of the anode material.

The TMDC flake based device was fabricated as back-gated configuration FET device. The device was fabricated on as-grown substrate. Source and drain electrodes were patterned by optical lithography. Firstly, 10 nm titanium (Ti) was deposited. Secondly, 90 nm of gold (Au) was deposited by EBPVD, shown in Figure 3.8.

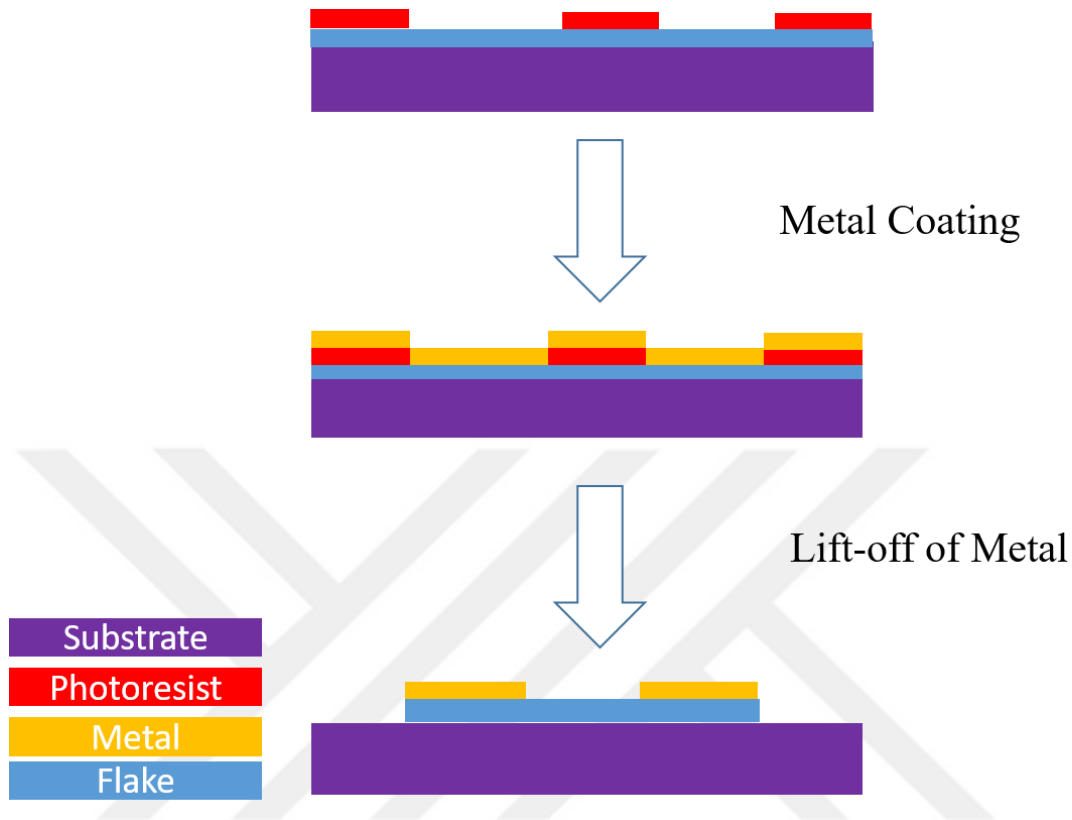


Figure 3.8 Schematic view of the metal coating and lift-off process

After the metal coating process, the device was put into acetone to remove metal from the area outside the contact pads. After the fabrication process the FET device was baked in the CVD furnace for 120 min at 200°C under the pressure of the 200 Torr and with 500 sccm of N₂ gas to remove any solvents introduced during the fabrication. Highly doped n-type 500 μm-thick silicon wafer (1–10 Ω cm) with 270 ± 35 nm SiO₂ dielectric layer was used as the back gate electrode and gate dielectric, respectively.

3.5. Measurement of FET Devices

The cross-sectional view of the fabricated device with electrical connections shown in Figure 3.9. FET is fabricated on a 270 ± 35 nm thick gate oxide layer on top of a highly doped 525 nm thick Si substrate. Gate bias voltage was applied to the Si substrate for modulating the FET device. Electrical measurement of the device was handled in ambient

atmosphere condition, under dark illumination at room temperature by a grounded probe station with a Keysight B2902a source/measure unit.

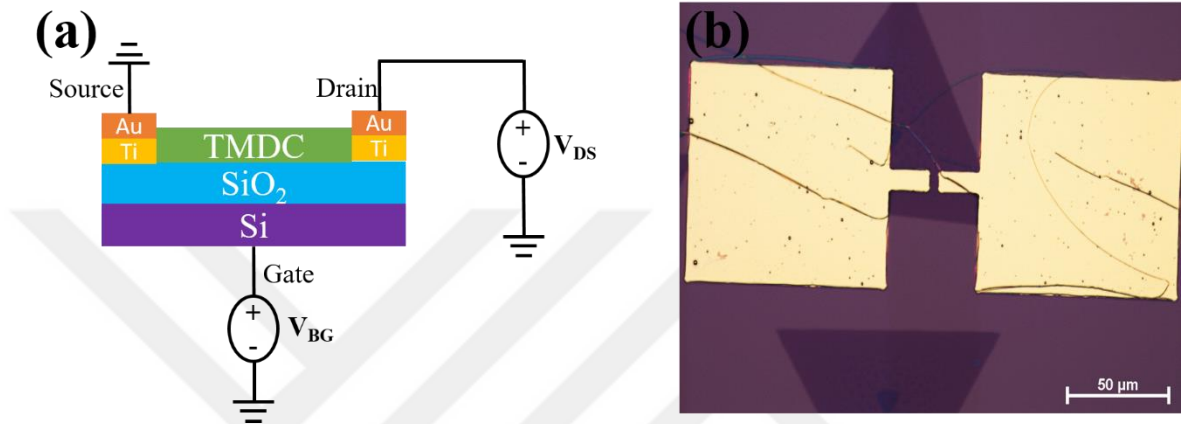


Figure 3.9 (a) The cross-sectional view (b) the optical image of the device

According to the measured transfer curves, shown in Figure 3.10, MoSe₂ based FET shows n-type behavior. The threshold voltages (V_{TH}) was determined from the linear regime of the on-state conduction. The tangent line with maximum slope to $I_{DS}-V_{BG}$ curve at the peak trans conductance (g_m) was linearly extrapolated to V_{BG} (axis) to extract V_{TH} . The extracted V_{TH} value of MoSe₂ based FET device was ~ 110 V. Field effect mobility calculated from estimated trans conductance $g_m = \frac{\partial I_{DS}}{\partial V_{BG}}$ using:

$$\mu_{FE} = \frac{L_{CH}}{W_{CH}} \frac{1}{V_{DS} C_g} g_m \quad (3.1)$$

where μ_{FE} is the field effective carrier mobility, I_{DS} is drain source current, L_{CH}/W_{CH} is the ratio of channel length to channel width, V_{DS} is bias voltage and C_g is the gate capacitance per unit area $C_g = \epsilon_g/t_g \cdot \epsilon_g$ and t_g is the dielectric constant and the thickness of gate oxide, respectively. The FET of MoSe₂ showed μ_{FE} of $1.15 \text{ cm}^2 \text{ V}^{-1} \text{ s}^{-1}$. The contact resistance effect was not accounted for mobility estimation which may result in degraded mobility.

Furthermore, the current ON/OFF ratio of device was obtained as $\sim 10^4$ for monolayer MoSe₂.

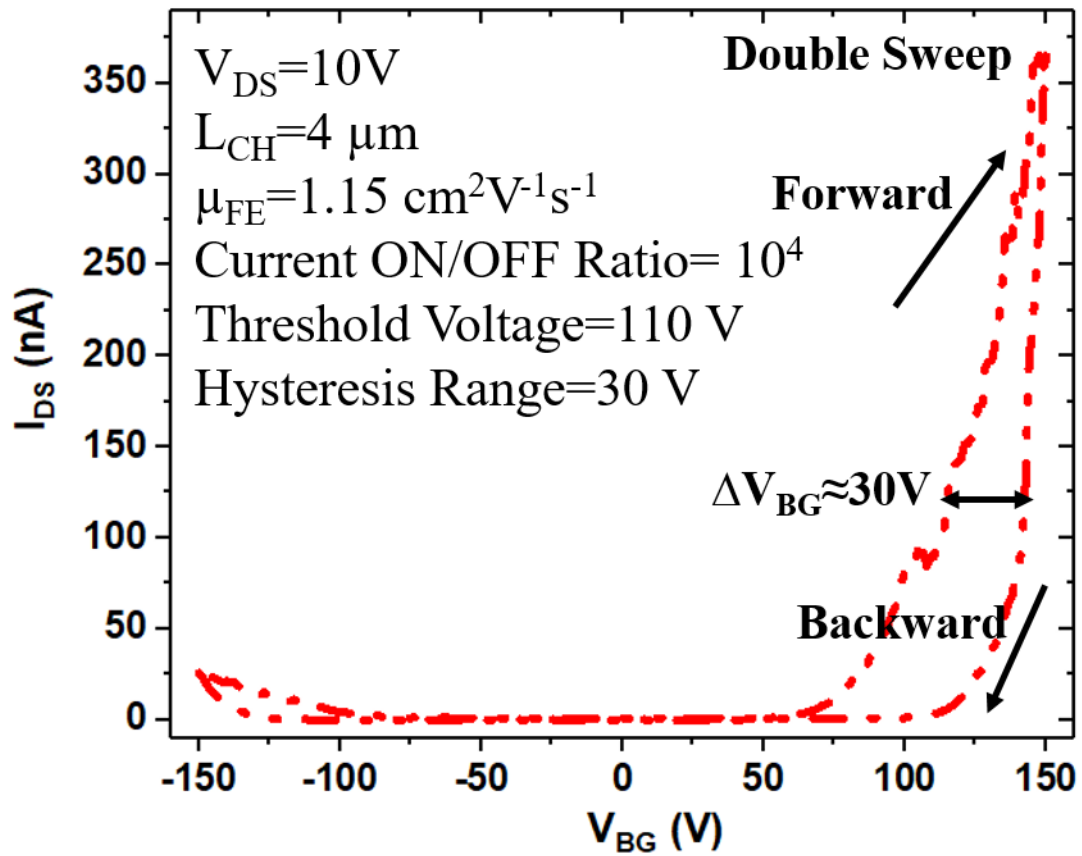


Figure 3.10 Transfer Curve of the MoSe₂ with Glass-2 Based FET Device

4. CONCLUSIONS AND SUGGESTIONS FOR FUTURE WORK

The conclusions of this thesis and the suggestions for the future works will be discussed in the next sections of this chapter.

4.1. Conclusions

2D TMDC materials have layer dependent properties and in addition to these monolayer TMDC materials have high surface area. These layer dependent and physical properties make 2D TMDC materials attractive for electronic, optoelectronic and sensing applications. There are several methods to fabricate monolayer TMDC materials and CVD method is one of them. By using CVD method large scale, monolayer TMDC materials can be produced. Using the catalyst during the CVD growth experiments, TMDC flake structures with large surface area can be produced.

In this thesis study two different type of glasses as their dopants were used in CVD chamber during MoS₂, MoSe₂ and WS₂ growth. All growth experiments were done by using nearly the same configuration. The same growth experiments were done by using any piece of glass and as results of these glassless experiment no flake formation was occurred. The glassless experiments showed that the dopants of the glasses show a catalytic effect on the growth. One of the glass contains more sodium concentration, named Glass-1 than the other, named Glass-2. By using Glass-1 monolayer TMDC materials were grown with more homogenous surfaces than the monolayer TMDC materials grown by using Glass-2. The grown monolayer TMDC materials with Glass-2 have longer edge lengths than with Glass-1. The growth structures, MoS₂, WS₂ and MoSe₂, are characterized and analyzed by using optical microscopy, Raman spectroscopy, PL measurement and AFM thickness measurement techniques. According to the measurements it was observed that the growth structures, MoS₂, MoSe₂ and WS₂, by using glasses are monolayer.

The presence of TMDC materials that act as semiconductor layers in FET devices, which will come into contact with gas in FET device structures used for gas sensor applications. For increasing the gas sensor sensitivity of the FET devices a mask was designed by using

L-Edit program. This mask was designed to provide maximum benefit as a gas sensor from the growth flake structures.

Monolayer MoS₂, WS₂ and MoSe₂ have fewer dangling bonds and this feature makes these monolayer TMDC materials attractive for use as channel layers in FET devices. In this thesis the growth of the monolayer TMDCs occurred on the Si/SiO₂ substrate so needing of the transfer of the flakes and the transfer caused effects on the flakes can be eliminated. The FET device fabricated on the as grown substrate. The FET fabrication steps such as, lithography, metal coating and lift-off were utilized.

By using MoSe₂ with Glass-2 a FET device was fabricated. According to the transfer curve of this device current ON/OFF ratio, mobility, threshold voltage and hysteresis voltage are found as, nearly 10⁴, 1.15 cm² V⁻¹ s⁻¹, 110V and 30V, respectively.

2D materials includes all necessary materials for fabricating 2D devices, such as graphene as conductor material, hexagonal boron nitride as dielectric material and 2D TMDCs as semiconductor material. The 2D devices are promising research area for the next generation devices because the 2D materials have advantages such as, thickness dependent band gap variation, thickness dependent performance variation, interface variations, controllable thickness dependence and therefore controllable band gaps, fast circuit speed and low power consumption. In the future 2D materials certainly will be used in electronics such as, sensor applications, energy harvesting applications, displays etc.

4.2. Suggestions for Future Work

In-depth studies of 2D TMDC growth and 2D TMDC based FET devices for gas sensor applications are still needed to further improvement. The followings are some up-and-coming research topics and directions for future works.

1. Growth of hetero-structures by using glass in CVD chamber. Hetero-structures can be used as p-n junctions.

2. Doping monolayer TMDC materials with elements such as silver etc. Doping with metal elements increase the sensitivity of gas sensors by enabling it to interact faster with gases.
3. Developing a system to read data from 2D TMDC based gas sensors. The currently used 2D TMDC based gas sensors can only show changes in current when exposed gas. With a display system, it is possible to use the gas sensors more widely by determining the voltage and current values of gas levels.



REFERENCES

- Ammu, S., Dua, V., Agnihotra, S. R., Surwade, S. P., Phulgirkar, A., Patel, S., Manohar, S. K. (2012). Flexible, all-organic chemiresistor for detecting chemically aggressive vapors. *Journal of the American Chemical Society*, 134(10), 4553-4556.
- Ayari, A., Cobas, E., Ogundadegbe, O., Fuhrer, M. S. (2007). Realization and electrical characterization of ultrathin crystals of layered transition-metal dichalcogenides. *Journal of Applied Physics*, 101(1), 014507.
- Balasingam, S. K. , Lee, J. S. and Jun, Y. (2015). Few-layered MoSe₂ nanosheets as an advanced electrode material for supercapacitors. *Dalton Transactions*, 44(35), 15491-15498.
- Barsan, N. and Weimar, U. (2001). Conduction model of metal oxide gas sensors. *Journal of electroceramics*, 7(3), 143-167.
- Bilgin, I., Liu, F., Vargas, A., Winchester, A., Man, M. K., Upmanyu, M., . . . Mohite, A. D. (2015). Chemical vapor deposition synthesized atomically thin molybdenum disulfide with optoelectronic-grade crystalline quality. *Acs Nano*, 9(9), 8822-8832.
- Binnig, G. , Quate, C. F. and Gerber, C. (1986). Atomic force microscope. *Physical review letters*, 56(9), 930.
- Bosi, M. (2015). Growth and synthesis of mono and few-layers transition metal dichalcogenides by vapour techniques: a review. *RSC Advances*, 5(92), 75500-75518.
- Braga, D., Gutiérrez Lezama, I., Berger, H., Morpurgo, A. F. (2012). Quantitative determination of the band gap of WS₂ with ambipolar ionic liquid-gated transistors. *Nano letters*, 12(10), 5218-5223.
- Brent, J. R. , Savjani, N. and O'Brien, P. (2017). Synthetic approaches to two-dimensional transition metal dichalcogenide nanosheets. *Progress in Materials Science*, 89, 411-478. doi:10.1016/j.pmatsci.2017.06.002
- Brinkman, W. F. , Haggan, D. E. and Troutman, W. W. (1997). A history of the invention of the transistor and where it will lead us. *IEEE Journal of Solid-State Circuits*, 32(12), 1858-1865.
- Bruch, L. (2005). Evaluation of the van der Waals force for atomic force microscopy. *Physical Review B*, 72(3), 033410.
- Buscema, M., Barkelid, M., Zwiller, V., van der Zant, H. S., Steele, G. A., Castellanos-Gomez, A. (2013). Large and tunable photothermoelectric effect in single-layer MoS₂. *Nano letters*, 13(2), 358-363.

- Carladous, A., Coratger, R., Ajustron, F., Seine, G., Péchou, R., Beauvillain, J. (2001). Light emission from spectral analysis of Au/MoS₂ nanocontacts stimulated by scanning tunneling microscopy. *Physical Review B-Condensed Matter and Materials Physics*, 66(4), 454011-454018.
- Chen, B., Liu, H., Li, X., Lu, C., Ding, Y., Lu, B. (2012). Fabrication of a graphene field effect transistor array on microchannels for ethanol sensing. *Applied Surface Science*, 258(6), 1971-1975.
- Chen, G., Paronyan, T. M., Pigos, E. M., Harutyunyan, A. R. (2012). Enhanced gas sensing in pristine carbon nanotubes under continuous ultraviolet light illumination. *Scientific reports*, 2, 343.
- Chen, J., Zhao, X., Tan, S. J., Xu, H., Wu, B., Liu, B., . . . Liu, Y. (2017). Chemical vapor deposition of large-size monolayer MoSe₂ crystals on molten glass. *Journal of the American Chemical Society*, 139(3), 1073-1076.
- Cho, B., Kim, A. R., Park, Y., Yoon, J., Lee, Y.-J., Lee, S., . . . Ko, H. C. (2015). Bifunctional sensing characteristics of chemical vapor deposition synthesized atomic-layered MoS₂. *ACS applied materials & interfaces*, 7(4), 2952-2959.
- Chow, P. K., Jacobs-Gedrim, R. B., Gao, J., Lu, T.-M., Yu, B., Terrones, H., Koratkar, N. (2015). Defect-induced photoluminescence in monolayer semiconducting transition metal dichalcogenides. *Acs Nano*, 9(2), 1520-1527.
- Coleman, J. N., Lotya, M., O'Neill, A., Bergin, S. D., King, P. J., Khan, U., . . . Smith, R. J. (2011). Two-dimensional nanosheets produced by liquid exfoliation of layered materials. *Science*, 331(6017), 568-571.
- Dan, Y., Lu, Y., Kybert, N. J., Luo, Z., Johnson, A. C. (2009). Intrinsic response of graphene vapor sensors. *Nano letters*, 9(4), 1472-1475.
- Davis, C., Ho, C., Hughes, R., Thomas, M. (2005). Enhanced detection of m-xylene using a preconcentrator with a chemiresistor sensor. *Sensors and Actuators B: Chemical*, 104(2), 207-216.
- Di Francia, G. , Alfano, B. and La Ferrara, V. (2009). Conductometric gas nanosensors. *Journal of Sensors*, 2009.
- Drobek, M., Kim, J.-H., Bechelany, M., Vallicari, C., Julbe, A., Kim, S. S. (2016). MOF-based membrane encapsulated ZnO nanowires for enhanced gas sensor selectivity. *ACS applied materials & interfaces*, 8(13), 8323-8328.
- Du, J., Liang, D., Tang, H., Gao, X. P. (2009). InAs nanowire transistors as gas sensor and the response mechanism. *Nano letters*, 9(12), 4348-4351.
- Eaton, P. and West, P. (2010). *Atomic force microscopy*: Oxford university press.

- Eda, G., Yamaguchi, H., Voiry, D., Fujita, T., Chen, M., Chhowalla, M. (2011). Photoluminescence from chemically exfoliated MoS₂. *Nano letters*, 11(12), 5111-5116.
- Fang, H., Chuang, S., Chang, T. C., Takei, K., Takahashi, T., Javey, A. (2012). High-performance single layered WSe₂ p-FETs with chemically doped contacts. *Nano letters*, 12(7), 3788-3792.
- Fang, H., Yang, Z., Wang, Y., Dai, T., Sang, L., Zhao, L., . . . Zhang, G. (2008). Analysis of mass transport mechanism in InGaN epitaxy on ridge shaped selective area growth GaN by metal organic chemical vapor deposition. *Journal of Applied Physics*, 103(1), 014908.
- Fontana, M., Deppe, T., Boyd, A. K., Rinzan, M., Liu, A. Y., Paranjape, M., Barbara, P. (2013). Electron-hole transport and photovoltaic effect in gated MoS₂ Schottky junctions. *Scientific reports*, 3, 1634.
- Ganapathi, K. L., Bhattacharjee, S., Mohan, S., Bhat, N. (2016). High-performance HfO₂ back gated multilayer MoS₂ transistors. *IEEE Electron Device Letters*, 37(6), 797-800.
- Gardeniers, J. G. , Tilmans, H. and Visser, C. (1996). LPCVD silicon-rich silicon nitride films for applications in micromechanics, studied with statistical experimental design. *Journal of Vacuum Science & Technology A: Vacuum, Surfaces, and Films*, 14(5), 2879-2892.
- Gatensby, R., McEvoy, N., Lee, K., Hallam, T., Berner, N. C., Rezvani, E., . . . Duesberg, G. S. (2014). Controlled synthesis of transition metal dichalcogenide thin films for electronic applications. *Applied Surface Science*, 297, 139-146.
- Geim, A. K. and Grigorieva, I. V. (2013). Van der Waals heterostructures. *Nature*, 499(7459), 419.
- Geim, A. K. and Novoselov, K. S. (2010). The rise of graphene *Nanoscience and Technology: A Collection of Reviews from Nature Journals* (pp. 11-19): World Scientific.
- Georgiou, T., Jalil, R., Belle, B. D., Britnell, L., Gorbachev, R. V., Morozov, S. V., . . . Makarovskiy, O. (2013). Vertical field-effect transistor based on graphene–WS₂ heterostructures for flexible and transparent electronics. *Nature nanotechnology*, 8(2), 100.
- Gong, Y., Ye, G., Lei, S., Shi, G., He, Y., Lin, J., . . . Zhou, W. (2016). Synthesis of Millimeter-Scale Transition Metal Dichalcogenides Single Crystals. *Advanced Functional Materials*, 26(12), 2009-2015.

- Haynes, C. L. , McFarland, A. D. and Van Duyne, R. P. (2005). Surface-enhanced Raman spectroscopy: ACS Publications.
- He, Q., Wu, S., Yin, Z., Zhang, H. (2012). Graphene-based electronic sensors. *Chemical Science*, 3(6), 1764-1772.
- Huang, S., Ling, X., Liang, L., Kong, J., Terrones, H., Meunier, V., Dresselhaus, M. S. (2014). Probing the interlayer coupling of twisted bilayer MoS₂ using photoluminescence spectroscopy. *Nano letters*, 14(10), 5500-5508.
- Hubble, L. J., Cooper, J. S., Sosa-Pintos, A., Kiiveri, H., Chow, E., Webster, M. S., . . . Raguse, B. (2015). High-Throughput Fabrication and Screening Improves Gold Nanoparticle Chemiresistor Sensor Performance. *ACS combinatorial science*, 17(2), 120-129.
- Huo, N., Yang, S., Wei, Z., Li, S.-S., Xia, J.-B., Li, J. (2014). Photoresponsive and gas sensing field-effect transistors based on multilayer WS₂ nanoflakes. *Scientific reports*, 4, srep05209.
- Jariwala, D., Sangwan, V. K., Lauhon, L. J., Marks, T. J., Hersam, M. C. (2014). Emerging device applications for semiconducting two-dimensional transition metal dichalcogenides. *Acs Nano*, 8(2), 1102-1120.
- Johnson, J. L., Behnam, A., Pearton, S., Ural, A. (2010). Hydrogen sensing using Pd-functionalized multi-layer graphene nanoribbon networks. *Advanced materials*, 22(43), 4877-4880.
- Joseph, Y., Guse, B., Vossmeier, T., Yasuda, A. (2008). Gold nanoparticle/organic networks as chemiresistor coatings: the effect of film morphology on vapor sensitivity. *The Journal of Physical Chemistry C*, 112(32), 12507-12514.
- Kang, K. N. , Godin, K. and Yang, E.-H. (2015). The growth scale and kinetics of WS₂ monolayers under varying H₂ concentration. *Scientific reports*, 5, 13205.
- Kannan, P. K., Late, D. J., Morgan, H., Rout, C. S. (2015). Recent developments in 2D layered inorganic nanomaterials for sensing. *Nanoscale*, 7(32), 13293-13312.
- Ketchum, J. M. (1995). Apparatus and method for removing deposits from an APCVD system: Google Patents.
- Ko, K. Y., Park, K., Lee, S., Kim, Y., Woo, W. J., Kim, D., . . . Kim, H. (2018). Recovery Improvement for Large-Area Tungsten Diselenide Gas Sensor. *ACS applied materials & interfaces*.
- Ko, K. Y., Song, J.-G., Kim, Y., Choi, T., Shin, S., Lee, C. W., . . . Kim, J. (2016). Improvement of gas-sensing performance of large-area tungsten disulfide nanosheets by surface functionalization. *Acs Nano*, 10(10), 9287-9296.

- Kong, D., Wang, H., Cha, J. J., Pasta, M., Koski, K. J., Yao, J., Cui, Y. (2013). Synthesis of MoS₂ and MoSe₂ films with vertically aligned layers. *Nano letters*, 13(3), 1341-1347.
- Korotcenkov, G. and Cho, B. (2013). Engineering approaches for the improvement of conductometric gas sensor parameters: Part 1. Improvement of sensor sensitivity and selectivity (short survey). *Sensors and Actuators B: Chemical*, 188, 709-728.
- Kuc, A. , Zibouche, N. and Heine, T. (2011). Influence of quantum confinement on the electronic structure of the transition metal sulfide T S 2. *Physical Review B*, 83(24), 245213.
- Kuzminykh, Y., Dabirian, A., Reinke, M., Hoffmann, P. (2013). High vacuum chemical vapour deposition of oxides:: A review of technique development and precursor selection. *Surface and Coatings Technology*, 230, 13-21.
- Late, D. J. , Doneux, T. and Bougouma, M. (2014). Single-layer MoSe₂ based NH₃ gas sensor. *Applied physics letters*, 105(23), 233103.
- Late, D. J., Huang, Y.-K., Liu, B., Acharya, J., Shirodkar, S. N., Luo, J., . . . Dravid, V. P. (2013). Sensing behavior of atomically thin-layered MoS₂ transistors. *Acs Nano*, 7(6), 4879-4891.
- Lee, H. S., Min, S.-W., Chang, Y.-G., Park, M. K., Nam, T., Kim, H., . . . Im, S. (2012). MoS₂ nanosheet phototransistors with thickness-modulated optical energy gap. *Nano letters*, 12(7), 3695-3700.
- Lee, K., Gatensby, R., McEvoy, N., Hallam, T., Duesberg, G. S. (2013). High-performance sensors based on molybdenum disulfide thin films. *Advanced materials*, 25(46), 6699-6702.
- Lee, S., Kim, W.-G., Rhee, S.-W., Yong, K. (2008). Resistance switching behaviors of hafnium oxide films grown by MOCVD for nonvolatile memory applications. *Journal of The Electrochemical Society*, 155(2), H92-H96.
- Li, H., Yin, Z., He, Q., Li, H., Huang, X., Lu, G., . . . Zhang, H. (2012). Fabrication of single- and multilayer MoS₂ film-based field-effect transistors for sensing NO at room temperature. *small*, 8(1), 63-67.
- Li, H., Zhang, Q., Yap, C. C. R., Tay, B. K., Edwin, T. H. T., Olivier, A., Baillargeat, D. (2012). From bulk to monolayer MoS₂: evolution of Raman scattering. *Advanced Functional Materials*, 22(7), 1385-1390.
- Li, X., Cai, W., An, J., Kim, S., Nah, J., Yang, D., . . . Tutuc, E. (2009). Large-area synthesis of high-quality and uniform graphene films on copper foils. *Science*, 324(5932), 1312-1314.

- Lin, Y.-M. and Avouris, P. (2008). Strong suppression of electrical noise in bilayer graphene nanodevices. *Nano letters*, 8(8), 2119-2125.
- Liu, B., Chen, L., Liu, G., Abbas, A. N., Fathi, M., Zhou, C. (2014). High-performance chemical sensing using Schottky-contacted chemical vapor deposition grown monolayer MoS₂ transistors. *Acs Nano*, 8(5), 5304-5314.
- Liu, N., Kim, P., Kim, J. H., Ye, J. H., Kim, S., Lee, C. J. (2014). Large-area atomically thin MoS₂ nanosheets prepared using electrochemical exfoliation. *Acs Nano*, 8(7), 6902-6910.
- Liu, Y., Parisi, J., Sun, X., Lei, Y. (2014). Solid-state gas sensors for high temperature applications—a review. *Journal of Materials Chemistry A*, 2(26), 9919-9943.
- Long, D. A. (1977). Raman spectroscopy. *New York*, 1-12.
- Lopez-Sanchez, O., Lembke, D., Kayci, M., Radenovic, A., Kis, A. (2013). Ultrasensitive photodetectors based on monolayer MoS₂. *Nature nanotechnology*, 8(7), 497.
- Losurdo, M., Giangregorio, M. M., Capezzuto, P., Bruno, G. (2011). Graphene CVD growth on copper and nickel: role of hydrogen in kinetics and structure. *Physical Chemistry Chemical Physics*, 13(46), 20836-20843.
- Mak, K. F., Lee, C., Hone, J., Shan, J., Heinz, T. F. (2010). Atomically thin MoS₂: a new direct-gap semiconductor. *Physical review letters*, 105(13), 136805.
- Meyyappan, M., Delzeit, L., Cassell, A., Hash, D. (2003). Carbon nanotube growth by PECVD: a review. *Plasma Sources Science and Technology*, 12(2), 205.
- Morrison, S. R. (1987). Selectivity in semiconductor gas sensors. *Sensors and actuators*, 12(4), 425-440.
- Mouri, S., Miyauchi, Y. and Matsuda, K. (2013). Tunable photoluminescence of monolayer MoS₂ via chemical doping. *Nano letters*, 13(12), 5944-5948.
- Nallon, E. C., Schnee, V. P., Bright, C., Polcha, M. P., Li, Q. (2015). Chemical discrimination with an unmodified graphene chemical sensor. *ACS sensors*, 1(1), 26-31.
- Nayak, A. P., Pandey, T., Voiry, D., Liu, J., Moran, S. T., Sharma, A., . . . Chhowalla, M. (2014). Pressure-dependent optical and vibrational properties of monolayer molybdenum disulfide. *Nano letters*, 15(1), 346-353.
- Newaz, A., Prasai, D., Ziegler, J., Caudel, D., Robinson, S., Haglund Jr, R., Bolotin, K. (2013). Electrical control of optical properties of monolayer MoS₂. *Solid State Communications*, 155, 49-52.

- Nicolosi, V., Chhowalla, M., Kanatzidis, M. G., Strano, M. S., Coleman, J. N. (2013). Liquid exfoliation of layered materials. *Science*, 340(6139), 1226419.
- Nie, S. and Emory, S. R. (1997). Probing single molecules and single nanoparticles by surface-enhanced Raman scattering. *Science*, 275(5303), 1102-1106.
- Novoselov, K., Jiang, D., Schedin, F., Booth, T., Khotkevich, V., Morozov, S., Geim, A. (2005). Two-dimensional atomic crystals. *Proceedings of the National Academy of Sciences of the United States of America*, 102(30), 10451-10453.
- Novoselov, K. S., Geim, A. K., Morozov, S. V., Jiang, D., Zhang, Y., Dubonos, S. V., . . . Firsov, A. A. (2004). Electric field effect in atomically thin carbon films. *Science*, 306(5696), 666-669.
- O'Brien, M., Lee, K., Morrish, R., Berner, N. C., McEvoy, N., Wolden, C. A., Duesberg, G. S. (2014). Plasma assisted synthesis of WS₂ for gas sensing applications. *Chemical Physics Letters*, 615, 6-10.
- O'Neill, A. , Khan, U. and Coleman, J. N. (2012). Preparation of high concentration dispersions of exfoliated MoS₂ with increased flake size. *Chemistry of Materials*, 24(12), 2414-2421.
- Oh, H. M., Han, G. H., Kim, H., Bae, J. J., Jeong, M. S., Lee, Y. H. (2016). Photochemical reaction in monolayer MoS₂ via correlated photoluminescence, Raman spectroscopy, and atomic force microscopy. *Acs Nano*, 10(5), 5230-5236.
- Özden, A., Ay, F., Sevik, C., Perkgöz, N. K. (2017). CVD growth of monolayer MoS₂: Role of growth zone configuration and precursors ratio. *Japanese Journal of Applied Physics*, 56(6S1), 06GG05.
- Özden, A., Şar, H., Yeltik, A., Madenoğlu, B., Sevik, C., Ay, F., Perkgöz, N. K. (2016). CVD grown 2D MoS₂ layers: A photoluminescence and fluorescence lifetime imaging study. *physica status solidi (RRL)–Rapid Research Letters*, 10(11), 792-796.
- Pawbake, A. S., Waykar, R. G., Late, D. J., Jadkar, S. R. (2016). Highly transparent wafer-scale synthesis of crystalline WS₂ nanoparticle thin film for photodetector and humidity-sensing applications. *ACS applied materials & interfaces*, 8(5), 3359-3365.
- Perea-López, N., Elías, A. L., Berkdemir, A., Castro-Beltran, A., Gutiérrez, H. R., Feng, S., . . . Ghosh, S. (2013). Photosensor device based on few-layered WS₂ films. *Advanced Functional Materials*, 23(44), 5511-5517.
- Podzorov, V., Gershenson, M., Kloc, C., Zeis, R., Bucher, E. (2004). High-mobility field-effect transistors based on transition metal dichalcogenides. *Applied physics letters*, 84(17), 3301-3303.

- Pu, H., Rhim, S., Gajdardziska-Josifovska, M., Hirschmugl, C., Weinert, M., Chen, J. (2014). A statistical thermodynamics model for monolayer gas adsorption on graphene-based materials: implications for gas sensing applications. *RSC Advances*, 4(88), 47481-47487.
- Radisavljevic, B., Radenovic, A., Brivio, J., Giacometti, i. V., Kis, A. (2011). Single-layer MoS₂ transistors. *Nature nanotechnology*, 6(3), 147.
- Radisavljevic, B. , Whitwick, M. B. and Kis, A. (2011). Integrated circuits and logic operations based on single-layer MoS₂. *Acs Nano*, 5(12), 9934-9938.
- Radisavljevic, B. , Whitwick, M. B. and Kis, A. (2012). Small-signal amplifier based on single-layer MoS₂. *Applied physics letters*, 101(4), 043103.
- Raguse, B., Chow, E., Barton, C. S., Wieczorek, L. (2007). Gold nanoparticle chemiresistor sensors: direct sensing of organics in aqueous electrolyte solution. *Analytical chemistry*, 79(19), 7333-7339.
- Rao, C. , Ramakrishna Matte, H. and Maitra, U. (2013). Graphene analogues of inorganic layered materials. *Angewandte Chemie International Edition*, 52(50), 13162-13185.
- Roldán, R., Silva-Guillén, J. A., López-Sancho, M. P., Guinea, F., Cappelluti, E., Ordejón, P. (2014). Electronic properties of single-layer and multilayer transition metal dichalcogenides MX₂ (M= Mo, W and X= S, Se). *Annalen der Physik*, 526(9-10), 347-357.
- Rout, C. S., Joshi, P. D., Kashid, R. V., Joag, D. S., More, M. A., Simbeck, A. J., . . . Late, D. J. (2013). Superior field emission properties of layered WS₂-RGO nanocomposites. *Scientific reports*, 3, 3282.
- Saint Jean, M., Hudlet, S., Guthmann, C., Berger, J. (1999). Van der Waals and capacitive forces in atomic force microscopies. *Journal of Applied Physics*, 86(9), 5245-5248.
- Sarkar, D., Liu, W., Xie, X., Anselmo, A. C., Mitragotri, S., Banerjee, K. (2014). MoS₂ field-effect transistor for next-generation label-free biosensors. *Acs Nano*, 8(4), 3992-4003.
- Schedin, F., Geim, A., Morozov, S., Hill, E., Blake, P., Katsnelson, M., Novoselov, K. (2007). Detection of individual gas molecules adsorbed on graphene. *Nature materials*, 6(9), 652.
- Seong, W. K., Huh, J. Y., Kang, W. N., Kim, J. W., Kwon, Y. S., Yang, N. K., Park, J. G. (2007). Growth of epitaxial MgB₂ thick films with columnar structures by using HPCVD. *Chemical Vapor Deposition*, 13(12), 680-683.

- Shanmugam, M., Bansal, T., Durcan, C. A., Yu, B. (2012a). Molybdenum disulphide/titanium dioxide nanocomposite-poly 3-hexylthiophene bulk heterojunction solar cell. *Applied physics letters*, 100(15), 153901.
- Shanmugam, M., Bansal, T., Durcan, C. A., Yu, B. (2012b). Schottky-barrier solar cell based on layered semiconductor tungsten disulfide nanofilm. *Applied physics letters*, 101(26), 263902.
- Shi, W., Lin, M.-L., Tan, Q.-H., Qiao, X.-F., Zhang, J., Tan, P.-H. (2016). Raman and photoluminescence spectra of two-dimensional nanocrystallites of monolayer WS₂ and WSe₂. *2D Materials*, 3(2), 025016.
- Shie, J.-R. and Yang, Y.-K. (2008). Optimizations of a photoresist coating process for photolithography in wafer manufacture via a radial basis neural network: A case study. *Microelectronic Engineering*, 85(7), 1664-1670.
- Shim, G. W., Yoo, K., Seo, S.-B., Shin, J., Jung, D. Y., Kang, I.-S., . . . Choi, S.-Y. (2014). Large-area single-layer MoSe₂ and its van der Waals heterostructures. *Acs Nano*, 8(7), 6655-6662.
- Simpkins, P., Greenberg-Kosinski, S. and MacChesney, J. (1979). Thermophoresis: the mass transfer mechanism in modified chemical vapor deposition. *Journal of Applied Physics*, 50(9), 5676-5681.
- Sorkin, V., Pan, H., Shi, H., Quek, S., Zhang, Y. (2014). Nanoscale transition metal dichalcogenides: structures, properties, and applications. *Critical Reviews in Solid State and Materials Sciences*, 39(5), 319-367.
- Splendiani, A., Sun, L., Zhang, Y., Li, T., Kim, J., Chim, C.-Y., . . . Wang, F. (2010). Emerging photoluminescence in monolayer MoS₂. *Nano letters*, 10(4), 1271-1275.
- Srivastava, V. K., Quinlan, R. A., Agapov, A. L., Dunlap, J. R., Nelson, K. M., Duranty, E., . . . Mays, J. W. (2014). Macroscopic Properties of Restacked, Redox-Liquid Exfoliated Graphite and Graphite Mimics Produced in Bulk Quantities. *Advanced Functional Materials*, 24(31), 4969-4977.
- Stephenson, T., Li, Z., Olsen, B., Mitlin, D. (2014). Lithium ion battery applications of molybdenum disulfide (MoS₂) nanocomposites. *Energy & Environmental Science*, 7(1), 209-231.
- Tarasov, A., Campbell, P. M., Tsai, M. Y., Hesabi, Z. R., Feirer, J., Graham, S., . . . Vogel, E. M. (2014). Highly Uniform Trilayer Molybdenum Disulfide for Wafer-Scale Device Fabrication. *Advanced Functional Materials*, 24(40), 6389-6400.
- Terrones, H., Lv, R., Terrones, M., Dresselhaus, M. S. (2012). The role of defects and doping in 2D graphene sheets and 1D nanoribbons. *Reports on Progress in Physics*, 75(6), 062501.

- Tian, H., Chin, M. L., Najmaei, S., Guo, Q., Xia, F., Wang, H., Dubey, M. (2016). Optoelectronic devices based on two-dimensional transition metal dichalcogenides. *Nano Research*, 9(6), 1543-1560.
- Tongay, S., Suh, J., Ataca, C., Fan, W., Luce, A., Kang, J. S., . . . Zhou, J. (2013). Defects activated photoluminescence in two-dimensional semiconductors: interplay between bound, charged, and free excitons. *Scientific reports*, 3, 2657.
- Vossen, J. L. , Kern, W. and Kern, W. (1991). *Thin film processes II* (Vol. 2): Gulf Professional Publishing.
- Wang, C., Yin, L., Zhang, L., Xiang, D., Gao, R. (2010). Metal oxide gas sensors: sensitivity and influencing factors. *Sensors*, 10(3), 2088-2106.
- Wang, H., Yu, L., Lee, Y.-H., Shi, Y., Hsu, A., Chin, M. L., . . . Palacios, T. (2012). Integrated circuits based on bilayer MoS₂ transistors. *Nano letters*, 12(9), 4674-4680.
- Wang, Q. H., Kalantar-Zadeh, K., Kis, A., Coleman, J. N., Strano, M. S. (2012). Electronics and optoelectronics of two-dimensional transition metal dichalcogenides. *Nature nanotechnology*, 7(11), 699.
- Wang, X., Gong, Y., Shi, G., Chow, W. L., Keyshar, K., Ye, G., . . . Ringe, E. (2014). Chemical vapor deposition growth of crystalline monolayer MoSe₂. *Acs Nano*, 8(5), 5125-5131.
- Xi, Q., Zhou, D.-M., Kan, Y.-Y., Ge, J., Wu, Z.-K., Yu, R.-Q., Jiang, J.-H. (2014). Highly sensitive and selective strategy for microRNA detection based on WS₂ nanosheet mediated fluorescence quenching and duplex-specific nuclease signal amplification. *Analytical chemistry*, 86(3), 1361-1365.
- Xia, J., Huang, X., Liu, L.-Z., Wang, M., Wang, L., Huang, B., . . . Meng, X.-M. (2014). CVD synthesis of large-area, highly crystalline MoSe₂ atomic layers on diverse substrates and application to photodetectors. *Nanoscale*, 6(15), 8949-8955.
- Xu, K., Yin, L., Huang, Y., Shifa, T. A., Chu, J., Wang, F., . . . He, J. (2016). Synthesis, properties and applications of 2d layered mⁱⁱⁱ x vi (m= ga, in; x= s, se, te) materials. *Nanoscale*, 8(38), 16802-16818.
- Yamazoe, N. and Shimano, K. (2011). Theoretical approach to the gas response of oxide semiconductor film devices under control of gas diffusion and reaction effects. *Sensors and Actuators B: Chemical*, 154(2), 277-282.
- Yang, P., Zou, X., Zhang, Z., Hong, M., Shi, J., Chen, S., . . . Zhou, X. (2018). Batch production of 6-inch uniform monolayer molybdenum disulfide catalyzed by sodium in glass. *Nature communications*, 9(1), 979.

- Yang, S., Kang, J., Yue, Q., Yao, K. (2014). Vapor phase growth and imaging stacking order of bilayer molybdenum disulfide. *The Journal of Physical Chemistry C*, 118(17), 9203-9208.
- Yao, Y., Tolentino, L., Yang, Z., Song, X., Zhang, W., Chen, Y., Wong, C. p. (2013). High-Concentration Aqueous Dispersions of MoS₂. *Advanced Functional Materials*, 23(28), 3577-3583.
- Yavari, F. and Koratkar, N. (2012). Graphene-based chemical sensors. *The journal of physical chemistry letters*, 3(13), 1746-1753.
- Yin, Z., Li, H., Li, H., Jiang, L., Shi, Y., Sun, Y., . . . Zhang, H. (2011). Single-layer MoS₂ phototransistors. *Acs Nano*, 6(1), 74-80.
- Yorulmaz, B., Özden, A., Şar, H., Ay, F., Sevik, C., Perkgöz, N. K. (2019). CVD growth of monolayer WS₂ through controlled seed formation and vapor density. *Materials Science in Semiconductor Processing*, 93, 158-163.
- Yu, W. J., Li, Z., Zhou, H., Chen, Y., Wang, Y., Huang, Y., Duan, X. (2013). Vertically stacked multi-heterostructures of layered materials for logic transistors and complementary inverters. *Nature materials*, 12(3), 246.
- Yuan, W. and Shi, G. (2013). Graphene-based gas sensors. *Journal of Materials Chemistry A*, 1(35), 10078-10091.
- Yuan, Y. , Li, R. and Liu, Z. (2014). Establishing water-soluble layered WS₂ nanosheet as a platform for biosensing. *Analytical chemistry*, 86(7), 3610-3615.
- Yue, Q., Shao, Z., Chang, S., Li, J. (2013). Adsorption of gas molecules on monolayer MoS₂ and effect of applied electric field. *Nanoscale research letters*, 8(1), 425.
- Zhan, B., Li, C., Yang, J., Jenkins, G., Huang, W., Dong, X. (2014). Graphene Field-Effect Transistor and Its Application for Electronic Sensing. *small*, 10(20), 4042-4065.
- Zhan, Y., Liu, Z., Najmaei, S., Ajayan, P. M., Lou, J. (2012). Large-area vapor-phase growth and characterization of MoS₂ atomic layers on a SiO₂ substrate. *small*, 8(7), 966-971.
- Zhang, S.-L., Choi, H.-H., Yue, H.-Y., Yang, W.-C. (2014). Controlled exfoliation of molybdenum disulfide for developing thin film humidity sensor. *Current Applied Physics*, 14(3), 264-268.
- Zhang, W., Huang, J. K., Chen, C. H., Chang, Y. H., Cheng, Y. J., Li, L. J. (2013). High-gain phototransistors based on a CVD MoS₂ monolayer. *Advanced materials*, 25(25), 3456-3461.

- Zheng, B. and Chen, Y. (2017). *Controllable Growth of Monolayer MoS₂ and MoSe₂ Crystals Using Three-temperature-zone Furnace*. Paper presented at the IOP Conference Series: Materials Science and Engineering.
- Zhou, Y., Jiang, Y., Xie, T., Tai, H., Xie, G. (2014). A novel sensing mechanism for resistive gas sensors based on layered reduced graphene oxide thin films at room temperature. *Sensors and Actuators B: Chemical*, 203, 135-142.
- Zhu, B. , Chen, X. and Cui, X. (2015). Exciton binding energy of monolayer WS₂. *Scientific reports*, 5, 9218.
- Zhu, C., Zeng, Z., Li, H., Li, F., Fan, C., Zhang, H. (2013). Single-layer MoS₂-based nanoprobe for homogeneous detection of biomolecules. *Journal of the American Chemical Society*, 135(16), 5998-6001.
- Zou, X., Wang, J., Chiu, C. H., Wu, Y., Xiao, X., Jiang, C., . . . Li, J. (2014). Interface engineering for high-performance top-gated MoS₂ field-effect transistors. *Advanced materials*, 26(36), 6255-6261.

CURRICULUM VITAE

Name Surname : Gonca USLU ÖZKÜÇÜK

Language : English

Birth Place and Date : Burdur/1990

Email Adress : goncausluozkucuk@eskisehir.edu.tr

Educational:

- 2017-2019 : Eskisehir Technical University (Graduate) Electrical and Electronics Engineering Department GPA: 3.63/ 4.00
- 2009-2015 : Dokuz Eylül University (Undergraduate) Electrical and Electronics Engineering Department GPA: 2.20 / 4.00

Professional:

- 2017-2019: Research Assitant at Eskisehir Technical University Electrical and Electronics Engineering Department
- July 2017- Sepetember 2017: Research Assitant at Niğde Ömer Halisdemir University Electrical and Electronics Engineering Department

Fields of Interest:

- Electronics, Nanotechnology.